NANO-ENGINEERING OF CONDUCTING POLYMERS

by
MÜGE AÇIK

Submitted to the Graduate School of Engineering and Natural Sciences
in partial fulfillment of
the requirements for the degree of
Master of Science

Sabancı University
Fall 2005

NANO-ENGINEERING OF CONDUCTING POLYMERS

APPROVED BY:

Asst. Prof. Dr. Gürsel Sönmez …….

(Dissertation Supervisor)

Prof. Dr. Yuda Yürüm …….

Assoc. Prof. Dr. Orhan Güney ……

Assoc. Prof. Dr. Yusuf Z. Menceloğlu …….

Asst. Prof. Dr. Hikmet Budak …….

DATE OF APPROVAL: …….

ABSTRACT

Oxidative interfacial and template polymerization approaches were developed to synthesize conducting polymer nanostructures for possible applications of these materials in charge storage devices like supercapacitors. Resulting nano-structured materials were characterized using scanning electron microscopy (SEM), fourier transform infrared coupled with attenuated total reflectance (FTIR-ATR), cyclic voltammeter, ultraviolet-visible-near infrared (UV-vis-NIR) spectrophotometer, multimeter and Brunaur-Emmett-Teller (BET) analyses.

Two different methods were used to obtain desired nano-structured conducting polymers. In the first method, a homogeneous polypyrrole (PPy) nano-network structure was produced. Optimization results indicated that mole ratios of oxidant to monomer should be kept as 4:1 and surfactant to monomer as 3:1, 4:1 and 5:1 for the production of PPy nanofibers in networks. The average size of fibers and beads were measured as *ca.* 150 and 300 nm, respectively. The electrical conductivity measurements and electrochemical studies with cyclic voltammetry resulted in reasonable electroactivity of these PPy nano-networks. BET analyses resulted in a surface area greater than 500 m^2/g.

In the latter method, conductive nano-arrays of polypyrrole (PPy) **(1)**, poly(N-methylpyrrole) (P(NMPy)) **(2)**, poly(thiophene) (PTh) **(3)** and poly(3,4-ethylenedioxythiophene) (PEDOT) **(4)** were aligned in one dimension (1D). Reaction conditions; such as, monomer concentrations, types of membranes and solvents for the synthesis of each polymer nanostructure were optimized. SEM images revealed that fiber diameters were in a range of 80-350 nm with 10-30 μm length for conducting polymer nanotubules aligned unidirectionally. Characterization of P(NMPy) nanotubules with cyclic voltammetry indicated that template-synthesized materials are electroactive as desired.

ÖZET

Süperkapasitörlerde elektrot malzemesi olarak kullanım amaçlı nano yapılı iletken polimerlerin sentezi için, oksidatif ara yüzey ve template polimerleşme tekniklerinden yararlanıldı. Elde edilen nano yapılı malzemeler, taramalı elektron mikroskobu (SEM), fourier transform infrared coupled with attenuated total reflectance (FTIR-ATR), ultraviolet-visible-near infrared (UV-vis-NIR) spectrofotometresi, siklik voltametre, multimetre ve Brunaur-Emmett-Teller (BET) analizleri kullanılarak karakterize edildi.

Arzu edilen nano yapılı iletken polimerleri elde etmek için iki farkli metot kullanıldı. Birinci metotta ara yüzey polimerizasyon tekniği kullanılarak, homojen poli(pirol) (PPy) nano-ağ yapıları üretildi. Optimizasyon sonuçları, PPy nano-ağlarının üretimi için, oksidanin monomere mol oranının 4:1 ve yüzey aktif maddenin monomere mol oranının 3:1, 4:1 ve 5:1'te tutulması gerektiğini gösterdi. Fiber ve boncukların ortalama boyutları sırasıyla 150 ve 300 nm olarak ölçüldü. Elektriksel iletkenlik ölçümleri ve siklik voltametre ile elektrokimyasal çalışmalar, sentezlenen PPy nano-ağlarının elektroaktif olduğunu gösterdi. BET analizleri, malzemenin yüzey alanının 500 m^2/g'dan daha yüksek olduğu sonucunu verdi.

Poli(pirol) (PPy) **(1)**, poli(N-metilpirol) (P(NMPy)) **(2)**, poli(tiyofen) (PTh) **(3)** ve poli(3,4-etilendioksitiyofen) (PEDOT) **(4)** iletken nanofiberleri, ikinci metot olan template polimerizasyon metoduyla tek yönde sıralandı. Monomer konsantrasyonları, membran ve çözücü çeşitleri gibi kullanılan tepkime şartları, nano yapılı iletken polimerlerin sentezi için optimize edildi. SEM resimleri, tek bir yönde dizilmiş iletken tüplerin çaplarının 80-350 nm ve uzunluklarının 10-30 μm aralığında olduğunu gösterdi. Sentezlenen P(NMPy) nanotüplerinin siklik voltametre ile karakterizasyonu, template polimerizasyon yöntemiyle sentezlenmiş malzemelerin elektiksel aktifliklerinin oldugunu gösterdi.

Bana olan güvenini ve destegini daima yanımda hissettigim,
Prof. Dr. Levent Artok'a ...

ACKNOWLEDGMENTS

I would like to give my special thanks to my thesis advisor, Asst. Prof. Dr. Gürsel Sönmez, for his support and guidance throughout the work and creation of the thesis. I am very greatful to him for his proposing this research to me.

I would like to thank to Asst. Prof. Dr. Alpay Taralp for his being a great leader to help me choose my research area and my advisor at the early stages of my graduate education. It was impossible to start such a successful work without his support, encouragement and insight.

Special thanks to Assoc. Prof. Mehmet Ali Gülgün for helping me with all the problems I faced in SEM imaging. I am also thankful to him for his great recommendations during my graduate education.

I want to thank to Prof. Dr. Yuda Yürüm, Asst. Prof. Dr. Clewa Ow Yang, Assoc. Prof. Dr. Yusuf Z. Menceloğlu, Asst. Prof. Dr. Canan Baysal for their kindness in my interview, also thanks to Asst. Prof. Dr. Melih Papila for his good intentions to me.

I would like to convey my thanks to Assoc. Prof. Dr. Ahmet Sirkecioğlu for his BET analyses for the first part of my research.

I am also grateful to Mehmet Manyas from Document Supply Department at Information Center for his helping me reach so many references as quick as possible.

I also thank to all my friends both in Sonmez's group and Materials Science and Engineering Program for their help. In particular, I want to thank to my friend, Yeşim Müge Çalık Şahin, for her moral support during difficulties in my research. I also want to thank to my friends: Esen Aksoy for her intelligent ideas and endless friendship, Okan Kurt, Shahzad Khan, Derya Baykal, Sedef Önal for their lovable friendships.

I also thank to my love, Yıldıray, for his everlasting moral support and being always there for me.

Finally, I want to give my deepest thanks to my family, especially to my sister and my uncle for their endless love and support throughout my life.

TABLE OF CONTENTS

Page No

LIST OF TABLES

LIST OF SCHEMES

LIST OF FIGURES

LIST OF SYMBOLS

σ	:	Conductivity
n	:	Number of charge carriers
μ	:	Mobility of charge carriers
R	:	Resistivity
I	:	Current
V	:	Potential
L	:	Thickness of sample layer
σ	:	Electrical conductivity
V_i^L	:	Lower bound
V_i^U	:	Upper bound
$E_{1/2}$	:	Half-wave potential
cm^{-1}	:	Wavenumber

LIST OF ABBREVIATIONS

(PA)	:	Poly(acetylene)
(PPy)	:	Poly(pyrrole)
(P(NMPy))	:	Poly(N-methylpyrrole)
(PTh)	:	Poly(thiophene)
(PEDOT)	:	Poly(3,4- ethylenedioxythiophene)
(PPP)	:	Poly(p-phenylene)
(PPV)	:	Poly(p-phenylenevinylene)
(PPS)	:	Poly(phenylenesulfide)
(PAN)	:	Poly(aniline)
(PF)	:	Poly(furan)
(PSe)	:	Poly(selenophene)
(PAz)	:	Poly(azulene)
(OLEDs)	:	Organic Light Emitting Diodes
(PC)	:	Poly(carbonate)
P(3-MTh)	:	Poly(3-methylthiophene)
(PSS)	:	Polystyrene sulfonic acid
(MIMIC)	:	Micromolding in cappilaries
(TEOS/MTES)	:	Tetraethyl orthosilicate/methyltriethoxysilane
(DBSA)	:	Dodecylbenzenesulfonic acid
(PMVP)	:	Poly(N-methyl-4-pyridine)
(EDOT)	:	3,4-ethylenedioxythiophene
(MeCN)	:	Acetonitrile
(HF)	:	Hydrofluoric acid
(DSA)	:	Sodium dodecyl (lauryl) sulfonate
(SEM)	:	Scanning Electron Microscopy
(FTIR-ATR)	:	Fourier Transform Infrared-Attenuated Total Reflectance
(UV-vis-NIR)	:	Ultraviolet-Visible-Near Infrared

(BET)	:	Brunaur-Emmett-Teller
(HOMO)	:	Highest occupied molecular orbitals
(LUMO)	:	Lowest unoccupied molecular orbitals
(TBAP)	:	Tetrabutylammoniumperchlorate
(CB)	:	Conduction Band
(VB)	:	Valence Band

1. INTRODUCTION

1.1 Conjugated Polymers

Conjugated polymers- polyunsaturated compounds, in which all backbone atoms are sp- or sp^2- hybridized, are either insulators or wide-gap semiconductors in their neutral states. The discovery of poly(acetylene) (PA) in 1977 [1] prompted future designs of polymers with conjugated π-systems such as poly(pyrrole) (PPy, 1979) [2], poly(p-phenylene) (PPP, 1979) [3], poly(p-phenylenevinylene) (PPV, 1979) [4], poly(phenylenesulfide) (PPS, 1980) [5], poly(aniline) (PAN, 1980) [6], poly(thiophene) (PTh, 1981) [7], poly(furan) (PF, 1981) [7], poly(selenophene) (PSe, 1984) [8], poly(azulene) (PAz, 1983) [9], etc. from academic world with a contribution to their industrial applications. In recent years, many synthetic methods have been applied to obtain materials made of conjugated polymers with high molecular weight, high levels of purity, and processability [10].

At its most basic, interesting electrical and optical properties of π-conjugated polymers are due to the presence of a delocalized electronic structure, which results in a strong absorption in the UV-vis region (related to π-π* transition) as well as the stabilization. Moreover, upon doping, the efficient transport of various charge carriers (radical cations, dications) also helps manufacturing of conjugated polymers. Of further interest is that utility of conjugated polymers is generally realized in complex chemical systems, created by adding functional groups to the conjugated backbone. The presence of various substituents on polymer backbone can not only modify processability but can also modulate electrical, electrochemical and optical properties of resulting conjugated polymers. Such modified polymers typically include side groups to modify conductivity of backbone by doping in either electrons or holes.

The diagram below demonstrates conductivity of conjugated polymers in a scale comparing with materials that are considered as insulators, semiconductors or conductors (Scheme 1.1).

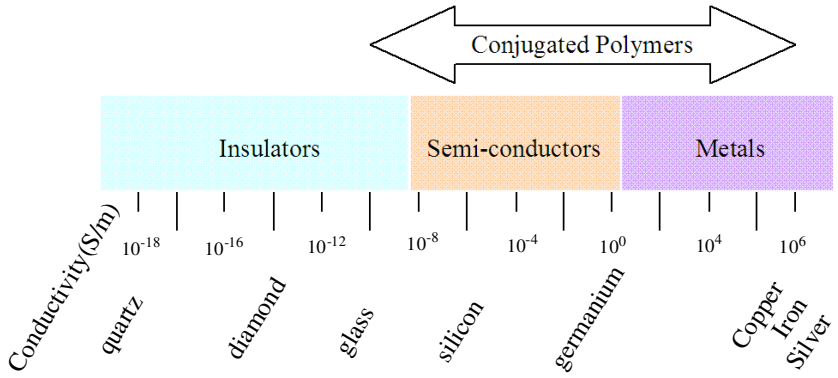

Scheme 1.1 Conductivity chart of various substances [11]

Conducting Polymers are conjugated polymers, having extended delocalized π-π* orbital system, through which electrons can move from one end of the polymer to the other. Furthermore, conductive polymers are also plastics (which are organic polymers) and therefore can combine the mechanical properties (flexibility, toughness, elasticity, etc.) of plastics with high electrical conductivities of a doped conjugated polymer. In addition, conductive polymeric materials are light in weight, inexpensive, air-stable, processable and flexible [12]. As analysis of their possessions, novel properties of conducting polymers are given below.

- Ability to tune properties from same building blocks
- Ability to dope, implant
- Large dimensional changes in going from doped/dedoped
- Ability to pattern, shape
- Ability to process in thin film form
- One D processability
- High and low frequency properties
- Surfaces and bulk effects

1.1.1 How Polymers Conduct Electricity?

Electrical conductivity dramatically increases as soon as charge carriers are introduced into the conduction or valence bands (known as band gaps) (Scheme 2).

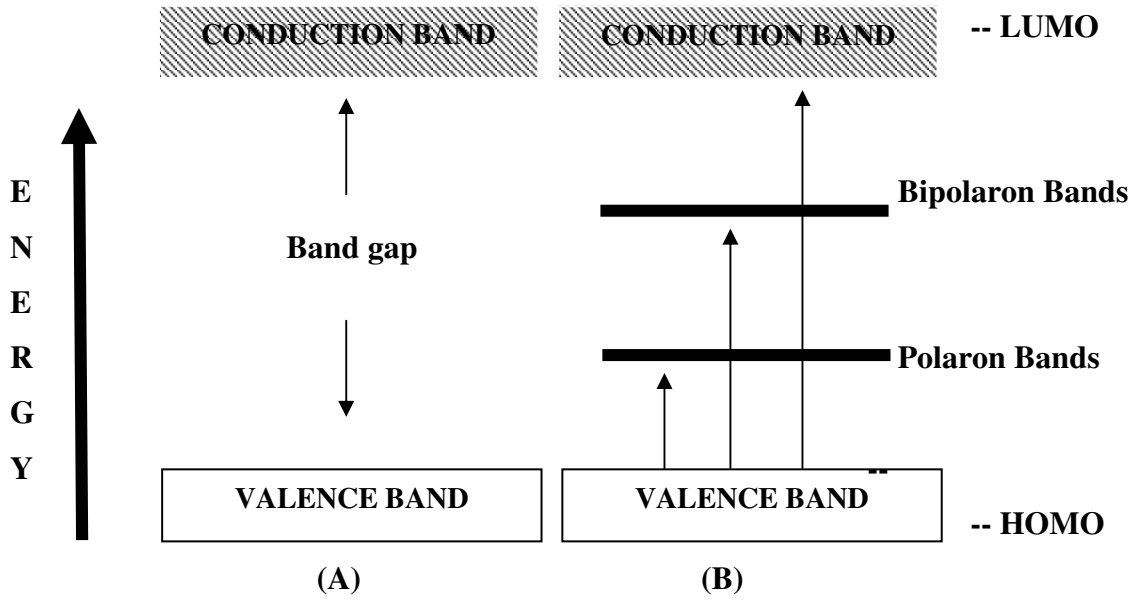

Scheme 1.2 Undoped conducting polymer (A), Oxidatively doped conducting polymer (B) [13]

Because of the band structure, almost all known commercial or man-made conductive polymers are semiconductors. Taking semiconductors into account, the only effect in differentiating the conductive polymers from inorganic semiconductors is the mobility, which was dramatically lower in conductive polymers than their inorganic counterparts in its past attempts.

The conductivity, σ of a conducting polymer is related to the number of charge carriers *n* and their mobility μ.

$$\sigma \alpha (n, \mu) \tag{1.1}$$

In delocalizing a conjugated backbone (e.g., alternating single and double carbon-carbon bonds), a continuous path of overlapping π-orbitals is formed. This continuous

string of orbitals creates degeneracy in the frontier molecular orbitals (the highest occupied and the lowest unoccupied molecular orbitals named HOMO and LUMO, respectively) (Scheme 1.2). As a result, filled (electron containing) and unfilled bands (valence and conduction bands, respectively) are built.

The term ‘doping’ can be classified as ‘p-doping’ and ‘n-doping’ to describe polymer oxidation and reduction, respectively. Once doping has occurred, the electrons in the π-bonds are able to "jump" around the polymer chain. As the electrons are moving along the molecule, an electric current occurs.

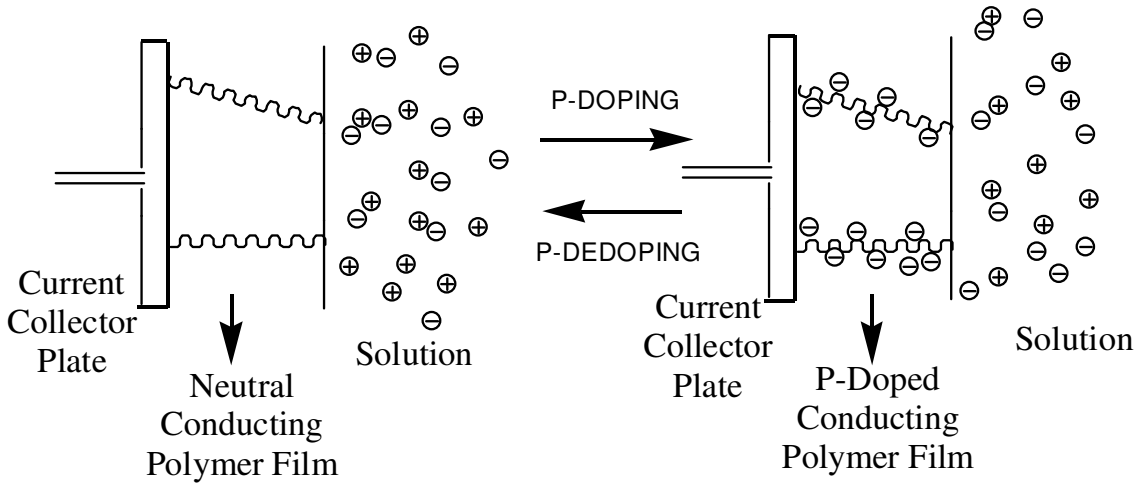

Scheme 1.3 Mechanism of p-doping and p-dedoping processes

In their neutral form, conductive polymers exhibit very low conductivities. It is not until an electron is added to the valence band (occupied band) resulting an empty conduction band, which generates charge carriers moving in an electric field. In this sense, injection of positive charges (holes) or negative charges (electrons) into polymer chains by p-type (Scheme 1.3) or n-type doping, respectively, does a conducting polymer become highly conductive. This movement of charge is actually responsible for electrical conductivity due to the creation of soliton or polaron states in the gap [14]. In fact, the conductivity of these polymers can easily be tuned by chemical manipulation of the polymer backbone, by the nature of the dopant, by the degree of doping and by blending with other polymers.

There are two primary methods of doping a conductive polymer, both through an oxidation-reduction (redox) process. The first method, chemical doping, involves exposing a polymer to an oxidant or reductant. The second is electrochemical doping in which a polymer-coated, working electrode is suspended in an electrolyte solution in

which the polymer is insoluble along with separate counter and reference electrodes. In the latter case, a potential difference is created between the electrodes which causes a charge (and the appropriate counter ion from the electrolyte) to enter the polymer in the form of electron addition (n-doping) or removal (p-doping).

Taking both advantages and disadvantages of these two fields into account, an electron-rich n-doped polymer will react immediately with elemental oxygen to de-dope the polymer (re-oxidize to the neutral state). Thus, chemical n-doping has to be done in an environment of an inert gas (e.g., argon). In comparison, electrochemical n-doping is far more common in research, because it is easier to exclude oxygen from a solvent in a sealed flask; however, there are likely no commercialized n-doped conductive polymers.

1.1.1.1 Polarons and Bipolarons

When one electron per level is removed, oxidation generates a radical cation with both spin and charge, which is referred to as a polaron. This species comprises both the hole site and the structural distortion, which accompanies it and remained an unpaired electron removed by yielding a dicationic species (bipolarons) in the following oxidation (Scheme 1.4). When the polymer is lightly doped, polaron levels are created between valence and conduction bands, thereafter bipolaron bands as doping goes on as shown in Scheme 1.4. In comparison, one bipolaron is more stable than two polarons despite the coulombic repulsion of the two ions.

While PA has degenerate states as solitons, other conducting polymers have non-degenarate ground states (i.e. without two equivalent resonance forms). When it is doped with a dopant ion, a hole is created on the π-conjugated chain (polaron). Thereafter, the negatively charged ion remains associated with the polymer. Another type of excitation can exist in PA backbone structure, which occurs after the reversal of the bond alternation pattern. Therefore, it is believed, when oxidized, that most of conducting polymers indicates destabilization of the orbital raising of the energy.

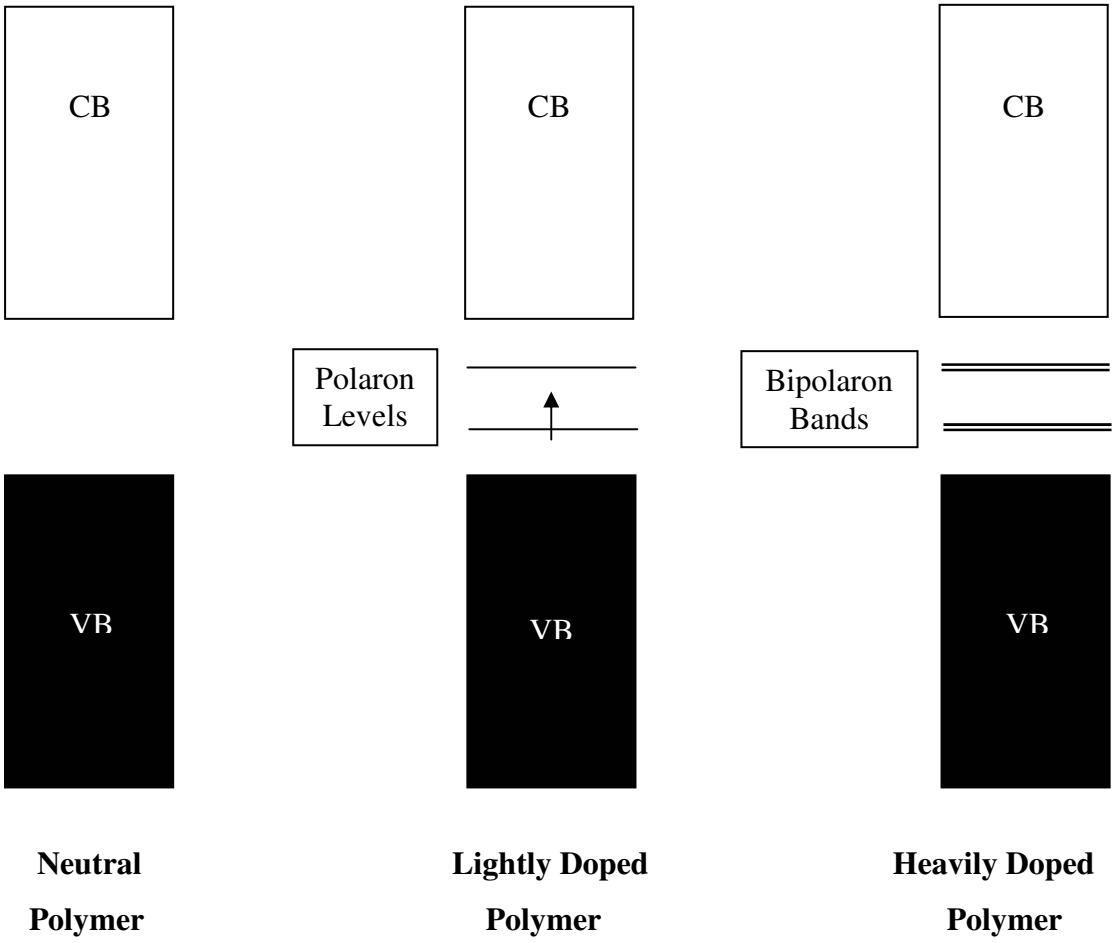

Scheme 1.4 Neutral and doped polymers as charged species [15]

1.1.2 Optical Properties of Conducting Polymers

A broad variety of structurally controlled color changes for conducting polymers can be observed between their redox states as a result of polaronic levels and bipolaron bands residing in the band gap. Several transitions to the orbitals in the bipolaronic state may decrease the energy yielding polymers with red-shifted absorptions though the neutral polymer only has its characteristic π-π^* transition. This change in a conducting polymer's optical properties provides a new family of polymeric materials, called electrochromic polymers. PEDOT and its derivatives are ideal electrochromic materials of conducting polymers, especially for electronic materials due to their good color, mechanical stabilities and facile fabrication properties [16].

1.1.3 Applications of Conducting Polymers

Conducting polymers are organic semiconductors (and can be organic conductors) in a wide variety of optical, electronic, optoelectronic, and sensor applications. Many successful commercial applications of these polymers have been available for more than fifteen years in the area of electrolytic capacitors, 'coin' batteries, magnetic storage media, electrostatic loudspeakers and anti-static bags. The first product of conducting organic materials was commercialized in 1983, which were electrolytic capacitors. These capacitors are not only reliable but also long-lived, since the electrolyte is a solid and cannot dry out. Possible applications of them can be found in high technologies of video cameras, automobile power supplies, FM car stereos, telephone exchanges, digital controllers for air conditioners and washing machines, displays for computers and TV power circuits. In pursue of these electrolytic capacitors, capacitors based on PPy from Panasonic, antistatic protective films and bags of PTh, under the trade name of Hostaphan, by Hoechst AG and PPy based batteries by Varta Batterie/BASF have recently been developed [17].

In today's developments, it is all aimed to put conducting polymers into use as thin televisions and sensors like chemical-weapons detectors, cell phone displays, computer monitors. One of the latest applications of these materials has been demonstrated in the medical field of nerve regeneration [18]. Certainly, conductive polymers are present in most mammal tissues where electrical conduction or transduction from light or sound are necessary, including the skin, eye, inner ear and brain.

Other present and potential commercial applications of conducting polymers can be categorized on a large scale in many groups according to their utilization as: photovoltaics, non-linear optics, microlithography, EMI shielding, anti-static fabrics, corrosion prevention in metals, rechargeable batteries, gas separation membranes, corrosion inhibitors, compact capacitors, electromagnetic shielding for computers, smart windows, transistors, organic light emitting diodes (OLEDs), lasers used in flat televisions and solar cells, etc.

1.1.3.1 Conducting Polymers for Supercapacitor Applications

Supercapacitors (also called electrochemical capacitors, electric double layer capacitors, or ultracapacitors) are electrochemical devices. They are all capable of very fast charges and discharges, able to store and deliver high power electricity for numerous repeated cycles without any appreciable decay of performances. When a supercapacitor is charged, there is no chemical reaction. Instead, the energy is stored as a charge or concentration of electrons on the surface of a material. Apparently, an electrochemical capacitor works on a principle that when an electrode material with large specific surface area is combined with a material that can be reversibly oxidized or reduced over a wide potential range.

They all can incorporate conductive polymer electrodes, which store electrical charge faradaically in a three dimensional system. Therefore, it is important to design useful electrode materials for supercapacitor applications by controlling the shape, size and morphology of materials on the nanometer length scale [19]. This control can be achieved using templates of the appropriate size scale and topology [20]. There are three types of electrode materials suitable for the supercapacitors: high surface area activated carbons, metal oxides and conducting polymers.

Compared to the secondary batteries, supercapacitors have many advantages; for instance long cycle life (> 100 000 cycles), simple principle and mode of construction, short charging time, safety and high power density [21]. Being related to its use for many purposes, the characteristics of electrode materials for supercapacitors include high cyclability, long-term stability, high surface area, low impedance and resistance to electrochemical oxidation/reduction [22].

Commercialized common applications of supercapacitors include starting with diesel trucks, railroad locomotives, actuators and in electric/hybrid-electric and fuel-cell powered vehicles, mobile phones, digital cameras, laptops and radio tuners, UPS, memory protection, automotive subsystems and military systems, etc.

In the past few years, many works have been devoted to materials for electrochemical supercapacitors. Recently, a variety of methods have been reported for producing composites of redox pseudocapacitive materials (PPy, PAN, PPV) and

ruthenium oxide) and double-layer capacitive materials (activated carbon black, carbon aerogels and carbon nanotubes) [23]. PPy electrodes containing polysulfonated aromatic anions are also investigated [24] or, alternatively, PPys were activated for use in electrochemical supercapacitors [25]. Especially, newer designs allow higher capacities in a smaller size. Because of their small size, nanostructures provide a huge surface area on which to store and release energy.

1.2 Conducting Polymers of Interest

Since the late 1970s, after H. Shirakawa, A. McDiarmid, A. J. Heeger *et. al* made the first discovery with PA for the field of conducting polymers, combining known advantageous properties of these polymers with high electrical conductivity initiated a revolution in technology [1].

In comparison of this positively charged PA with doped PPy or PTh, the origin of the higher stability on the latter polymers is dependent on the stabilizing effect on the positive charges by nitrogen or sulfur. Consequently, incorporating more substituents by reducing steric effects on unsaturated polymer backbone could result more stable polymers [26]. Among this substituted or unsubstituted field of conducting polymers, this thesis mainly focuses on the synthesis of PPys and PThs together with their performance as nanostructures for their effective use in supercapacitor applications (Scheme 1.5).

On a weight basis, for PPys and PThs, there exist a positive charge on every third or fourth pyrrole or thiophene unit along the polymer chain for their optical conductivities. In the light of this knowledge, these materials can be prepared either by chemical oxidation or they can be deposited electrochemically.

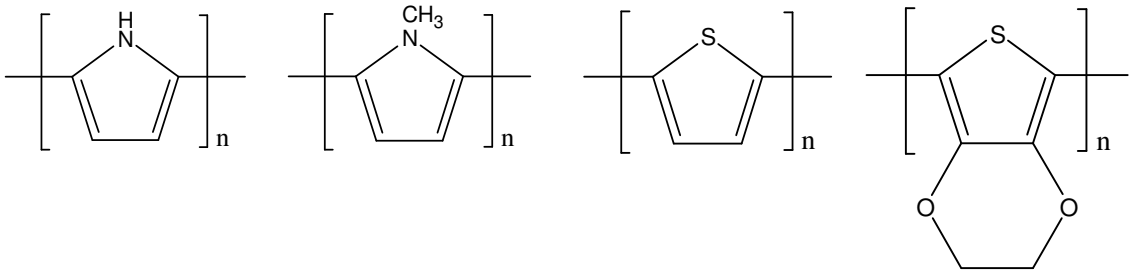

1 **2** **3** **4**

Scheme 1.5 Chemical structures of PPy **(1)**, P(NMPy) **(2)**, PTh **(3)**, PEDOT **(4)**

1.2.1 Polypyrrole (PPy)

PPy **(1)** is a promising conducting polymer for use in various fields because of its good intrinsic properties. The nitrogen on a five-membered heterocyclic ring yields in a molecule with a completely different behaviour when compared with PThs and a great tendency to oxidative polymerization. PPy can be synthesized by chemical reactions including various oxidizing agents, such as nitrous acid, potassium or ammonium persulfate, ferric chloride, etc. that presents high electrical conductivities, good redox properties and high environmental stability [27]. For highly conductive PPy films, at the maximum oxidation level, the anion content ranges between 25% and 30% by weight, corresponding to an oxidation level of 25%-35%, which is low dependent on the nature of the anion. Other than its important properties, PPys have some advantages, such as; easy and controlled processing by electrochemical polymerization [28,29], biocompatibility [30], ease of synthesis [31], stability in air at the oxidized form [32], ability to give high electrical conductivities [33,34], useful electrical and optical properties [35], while the difficulty to dissolve them in any solvent because of their delocalized π-electronic structures may be one of its disadvantages. However, in near future, this difficulty has been eradicated by oxidative polymerization of pyrrole in the presence of anionic polymers [36].

The concept of PPy having high electrical conductivities [37,38] and spectacular film morphologies [39] as heterocyclic conjugated polymers has raised both commercial and technological applications [40]. Hence, PPy has been extensively studied for many

applications, such as; bio- [41,42] and gas- [43,44] sensors, wires [45,46], microactuators [47], coating layers [48], conductive textiles [49], solid-state devices [50], electrochromic windows and displays [51], polymeric batteries [52], electronic devices [53], functional membranes [54,40,55], drug and biomolecule releases [56], corrosion protections [57] and conductive adhesives [58].

Comparing to the other electroactive polymers, PPy has been alluded the researchers for proficient methods of engineering to accomplish high-quality conducting polymers due to the nature of wide application ranges, ease of synthesis and environmental stability in the oxidized state. In these studies, one of the most widely used method for PPy synthesis is the treatment of pyrrole monomer with oxidizing agents in the presence of charge-compensating dopant anions in various organic solvents or in aqueous media [37,59,60]. Obviously, the presence of an anionic surfactant in the reaction media is likely to improve electrical, mechanical, thermo-oxidative and hydrolytic stability due to the interaction of hydrophobic component [61]. Template-guided polymerization is another technique to produce PPy nanofibers. Zeolites [62], alumina [63] or particle track-etched membranes [64] were used in this technique.

1.2.2 N-Substituted Poly(pyrrole) (P(NMPy))

The use of specific substituents opened up new possibilities for several applications of these conducting polymers. In pyrroles, there are two positions, which can be substituted in order to obtain conducting polymers: the 3 position and the N position (e.g., P(NMPy) **(2)**). In general, N-substitution in PPy lowers the conductivity of the material as a result of sterically twisting adjacent rings out of planarity. The quality of the film decreases when a butyl or larger alkyl groups attached from the nitrogen position to the structure. Therefore, these steric effects are essential both in the coupling step of polymerization process and in the degree of coplanarity of the aromatic rings along the polymer chain, which will influence the conductivity of materials.

1.2.3 Poly(thiophene) (PTh)

PThs **(3)** are one of the most important class of conducting polymers due to their high environmental stability in both doped and undoped states, electrical and non-linear optical properties and highly reversible redox switching. Within the family of conducting polymers, thiophene itself has a rich flexibility that allows the incorporation of various side chain functionalities.

In another sense, regioregular PThs have wide range of potential applications, such as dissipating static electrical charges that build up on coated floors or use in disposable devices called radio frequency identification tags. In parallel with these efforts toward functionality of PThs, the superior conducting performance of regioregular PThs is captured in their structures. Simply, each polymer unit is composed of a chemical ring (thiophene) with a chemical branch on one side, where units are attached head to tail, so that all of the branches line up in one direction.

1.2.4 Poly(3,4-ethylenedioxythiophene) (PEDOT)

Several attempts have been made to synthesize PEDOT **(4)** and its derivatives due to the high stability of the oxidized conducting form (doped state), high environmental stability, low band gap, high conductivity, redox switching ability, excellent transparency, facility in both chemical and electrochemical syntheses [65]. Polymerization occurs through the open 2- and 5-positions with the effect of electron donor dioxyethane bridge across the 3, 4-positions raising HOMO and yielding a linear polymer. In comparison with other conductive polymers, PEDOT itself with its outstanding air stability is more valuable and applicable than other PTh derivatives.

In developing PEDOT as a depictive and promising class of conducting polymers, by researchers at BAYER AG, use of some environmentally and thermally stable materials speeded up in recent three decades [66]. Due to PEDOT's high electrical conductivity, and low band gap properties, its applications have gained an increase in industry, such as; sensors, electrical conductors, electrodes, solar cells, nano-electronic

devices, electrochromic displays, conductive textiles, storage batteries, light emitting diodes (LEDs) and etc. Apart from PEDOT synthesis, recent development of its another form PEDOT-PSS, which is a result of complexation of PEDOT with polystyrene sulfonic acid (PSS), has been used for various applications like preparation of a gold-patterned ion track-etched membrane [67]. PEDOT nanorods can also be synthesized by cylindirical micelle-mediated interfacial polymerization technique for sensor applications [68]. Preferably, with the help of cleverly applied soft lithography technique, PEDOT nanorods and nanodots could be obtained by patterning PEDOT or by micromolding in cappilaries (MIMIC) [69].

Meanwhile, not only its ease of polymerization but also its applications to create new materials accelerated studies with PEDOT using new chemical and electrochemical synthetic methods. Solid-state polymerization of PEDOT is one facile chemical synthetic method in well-ordered crystalline state [70]. Moreover, one another urgent electrochemical synthetic technique is the growth of PEDOT in porous tetraethyl orthosilicate/methyltriethoxysilane (TEOS/MTES) sol-gel films used as templates [71] or copolymerization of PEDOT and pyrrole electrochemically through the pores of alumina membrane filter to synthesize nanofibrils [72].

Nanofibers of PEDOT in PC membranes [73], nanotubes of PEDOT in alumina membrane [74], PEDOT-dodecylbenzenesulfonic acid (DBSA) nanotubes and PEDOT-DBSA nanowires [75], PEDOT tubes and wires [76] are a few template-synthesized designs. Another fabrication way of PEDOT by template design can also be materialized inside the pores of a track-etch membrane in the presence of poly(N-methyl-4-pyridine) (PMVP) as a component for amperometric biosensors [77].

1.3 Polymerization Methods

Conjugated polymers, most likely PPy, PTh, PAN, PEDOT and PPV have been synthesized in free-standing films or in bulky powder forms, through either electrochemical or chemical polymerization methods [78].

1.3.1 Electropolymerization

Electropolymerization is an alternative way to synthesize new polymers avoiding polymer isolation and purification. Using electropolymerization, a monomer can be self-coupled with the help of irreversible oxidation (anodic polymerization) or reduction (cathodic polymerization) as a result of exchange of ions with the surrounding solution. In this process, anions necessary for charge compensation, doping and help for their incorporation into the backbone of polymers are provided with an electrolyte in the conductive state [79]. The most important aspect of these conjugated polymers from an electrochemical perspective is their ability to act as electronic conductors as a consequence of reversible redox processes that allow repetitions in switching between their neutral and charged states.

1.3.2 Chemical polymerization: Conductive Nanofiber Synthesis

Keeping in mind that for some applications, it is necessary to fabricate conducting polymers at nano-dimensional level. In this purpose, each of aforementioned conducting polymers (**(1)**, **(2)**, **(3)** and **(4))** may also be produced by chemical oxidation techniques. It is the aim of this thesis to show how these selected conductive polymers can be envisaged as nanostructures in nano-scales using both template or non-template (interfacial oxidative polymerization) routes through chemical polymerization methods. The polymerization involves formation of lower molecular weight oligomers that are further oxidized to form a polymer that eventually precipitates at interfaces of two different media or through the walls of membranes.

1.3.2.1 Interfacial Oxidative Polymerization

Interfacial polymerization method involves a one step chemical polymerization of reactive monomers or dopant anions, which can therefore be regarded as a non-template approach resulting aggregates [80]. These aggregates can act as nucleation sites for

polymerization resulting in powders with fibrillar morphology. Besides, the reaction takes place at interface of the two immiscible liquid phases. Hence, organic solvents, such as benzene, chloroform and toluene are commonly used as the organic phase in interfacial polymerization method.

In this manner, this technique is preferably applied to many fields, ranging from micro-encapsulation of pharmaceutical products to prepare conducting polymers. In an attempt to this approach, conducting polymer nanofibers and nanotubes with diameters in the range of 80-650 nm have been obtained [81].

The interfacial synthesis technique has the following advantages: (1) Both the synthesis and purification are very simple, (2) the diameter of conductive fibers are at nanoscales, which might be an advantage for applications.

Recently, some major perspectives have given a chance to structure PPy thin films made of nanofibers via interfacial polymerization. Lu *et al.* obtained 3-4 μm PPy films by chemical oxidation of pyrrole at interface of chloroform and water using ammonium persulfate as oxidizing agent [82]. Lately, Zhang *et al.* has approached to well-designed PPy nanofibers by seeding route [83]. In another study, large organic dopant anions such as naphthalenesulfonic acid have contributed to PPy to proceed in a fibrillar and tubular morphology [84]. Having these related works in hand, in this study, the success in the synthesis of PPy nano-networks in the presence of an anionic surfactant, sodium dodecyl sulfate, was demonstrated.

1.3.2.2 Template Synthesis

Template synthesis is an elegant approach for fabricating nanostructures with desired size and shapes. This method involves synthesis of a material within the pores of a nanoporous membrane [85]. The outside diameter of nanostructures is determined by the diameter of the pores in the template and the length of nanostructures by the thickness of the template. In taking the dimensions of these nanostructures into account, it is difficult to control the wall thickness [86]. From the point of structural behavior, depending on the membrane and synthetic method used, the shapes of cylindrical nanostructures can be varied [87]. Basically, these nano-template methods involve restricted growth within a porous host structure and thus rely on the shape of the pores

to determine the final morphology of the material. Template synthesis method can be summarized by an imaginary example (Scheme 1.6). Linear pores (white rectangulars) of a membrane (in greys) can be filled gradually, illustrated as black rectangulars after the polymerization starts (Scheme 6A and 6B). As the time increases, polymer was completely deposited through the pores of membrane (Scheme 6B).

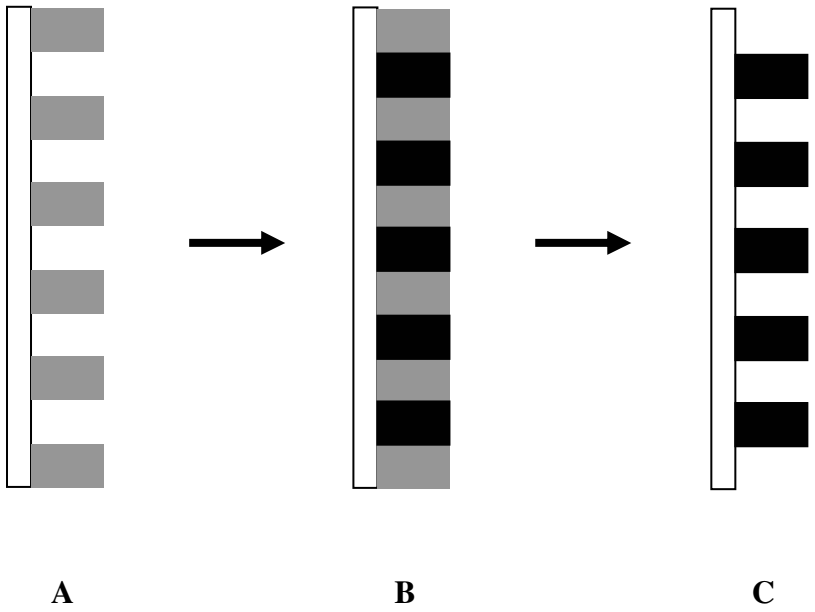

Scheme 1.6 Flowchart of the fabrication process for the assembly of fibrillar conducting polymers with the use of controlled pore size of templates. (A) membrane with linear pores, (B) polymer growth initiates and continues, (C) dissolution of polymer away by removal of template [88]

Among various routes to achieve 1D growth, such as; confined liquid droplet, direction through a template, use of kinetically controlled capping agents, self-assembly, size reduction and crystallographic dictation techniques [89]; template synthesis method, was used for 1D alignment of conducting PPy and PTh derivatives as nanostructures. Channels in porous membranes were first pioneered by C. R. Martin [90], which afford a class of templates for use in the synthesis of 1D nanostructures. Resulting lower dimensional conducting polymer structures have been developed by introducing ‘‘structural directors’’ during their synthesis, including ‘‘hard templates’’ such as an anodized alumina membrane, a track-etched polymer porous membrane and a zeolite channel by Martin *et al.* [91], while ‘‘soft templates’’, such as surfactants and organic dopants, have also been explored by several others [92].

It is generally accepted that template-directed synthesis provides a simple, high-throughput and cost-effective procedure. Recent use of this technique is the preparation of hollow or filled nanocylinders composed of metals, semiconductors and other materials [93].

Alignment of conducting polymers on interior walls of the pores inside templates is possible as a result of polymerization process of monomers (e.g., pyrroles, thiophenes). In relation, the conducting polymer is formed at interface between the two solutions, precipitating on the inner surface of the pores inside the membrane with the diffusion through the pores of the membrane [94]. Attributively, combination of electrostatic interactions between the positively charged polymer that is generated and the anionic sites on the pore walls of the membrane is responsible for a completion in alignment [95].

In literature, both chemical and electrochemical synthetic methods have been applied to the preparation of various template-synthesized polymers. However, most of these studies dealt with template synthesis including electrochemical processes. Gold nano-particled membranes have been successfully applied to the synthesis of 1D conducting polymer assemblies of PPy and P(NMPy) nano-particles prepared in alumina (Al_2O_3) or PC membrane [96]. It is worth noting that PPy nanostructures in alumina membrane pores [97], PPy nano-cylinders within the pores of PC [98] and fibrillar PPys in host membranes [99] could easily be fabricated.

While there are numerous reports on template-synthesized PPys, the reports on template-grown studies for conducting polymer nano-structured materials made of PTh derivatives overweigh in recent years. Poly(3-methylthiophene) P(3-MTh) nanocones in the pores of alumina membranes on carbon cloth [100], polyheterocyclic fibrils of both PPy and P(3-MTh) [101] are a few examples for template-synthesized PThs.

Herein, one of the prime objective was unidirectional alignment of PPy **(1)**, P(NMPy) **(2)**, PTh **(3)** and PEDOT **(4)** to fulfill novel designs of nano-shaped structures from a different chemical perspective. Without any doubt, building their nanostructures of life was possible with an oxidative chemical approach in 1D well-ordered architecture using an easy but powerful synthetic tool: template synthesis. These 1D nanostructures can easily be modified according to pore size of templates in one-step process. Consequently, their morphologies intrinsically change as tubes, arrays or fibers. Therefore, phase purity problem was overcome as one-phase medium was

used. The chemical composition remained the same for each reaction medium, yielding an efficient functionality for all these nanostructures.

1.3.2.2.1 Membrane Types: Tools for Template Synthesis

To date, most of the work on membrane synthesis followed by track-etching and electrochemical techniques other than commercial productions. Two types of porous membranes are commonly used in such synthesis: polymer films containing track-etched channels and alumina films containing anodically etched pores. Commercially, both of them can be obtained from a number of venders that include companies like Nuclepore, Poretics and Whatman.

For track-etching, damaged spots in the surface of a polymer film (6-20 μm thick) are formed as a result of irradiation with heavy ions. Then, uniform and cylindrical pores are generated through chemical etching with amplification of spots by penetrating the membrane film [102]. Randomly scattered pore fabrication across the membrane surface is possible using this method and the pore orientation may also be tilted by as much as 34° with respect to the surface normal.

Anodization of aluminum foils in an acidic medium is one of the techniques to prepare porous alumina membranes [103], which contain a hexagonally packed 2D array of cylindrical pores with a relatively uniform size. When compared with these polymer membranes fabricated by track-etching, the pores in alumina membranes have little or no tilting with respect to the surface normal and the pore density is also much higher. In controlling the potential used, the diameter of the pores in these membranes can be varied during electrochemical preparation [50].

Polycarbonate (PC) filtration membranes can be prepared via track-etch method [104], and micro porous alumina (Al_2O_3) by electrochemical process from aluminum foil [105] as template materials. A few examples to nano-structured material achievement as templates are zeolite synthesis [106,107], layer-by-layer inorganic assembly [108,109], incorporation of a single fullerene nanotube within a synthetic membrane [110,111] and the preparation of gold nano-tubule membranes via electroless deposition of gold onto the pore walls of PC filter [112,113].

1.3.2.2.2 Mechanistic Pathways in Template Synthesis

In addition to electrostatic interactions, a mechanism was proposed for the formation of Cho *et al.*'s PEDOT nanotube synthesis as an overall contribution, which is useful to generalize the mechanistic reality in template polymerizations [16]. As a result of their study, spectroscopic investigations indicated that nanotube growth starts up from the bottom along the pore walls due to the interactions between the polymer and pore walls. Therefore, the wall thickness gets thicker (at the lower part of the pore) with respect to the growth axis of the nanotube. As well, there occurs a consumption of monomers in the pores so that diffusional flux of monomers along the pores causes an inclination in monomer concentration. Then, further polymerization results a thicker lower part of the pore than its upper side.

There is another attribution to understand the pathway inside the pores by Martin *et al.*, which was the first on template synthesis method [52]. In their exploration; depending on the polymerization time, the thickness of the layers inside the pores differs. As a result, alignment of the polymer chains in the outer layer covering the surface of the pores preferentially happens parallel to the axis of the pores. Indeed, the inner layer of the conducting polymer is formed more disorderly due to the lackness in the interaction with the negatively charged membrane.

1.4 The Route from Conducting Polymers to Nanoscience

Polymers formed in a "potential field" can have enhanced conductivity in a specific direction. Therefore, they can be "lined up" in a given orientation by orienting the monomers through template materials. One route to nanoscience is the nanoscale orientation of the conjugated polymers for the development of next-generation electrode materials for supercapacitor applications. In this respect, unidirectional alignment of conjugated polymers through the pores of membranes as templates is a futuristic approach for the synthesis of nano-structured conjugated polymers.

1.4.1 Overview of Nanostructures: Miniaturization

Nanostructures can be defined as structures having at least one dimension between 1 and 100 nm. As a result of their peculiar and fascinating properties and applications superior to their bulk counterpart, they all receive growing interests in recent times [50]. Therefore, there is an increasing trend for miniaturization in favor of the design of devices with critical dimensions.

A few of chemical routes to nano-structured materials and thin films are zeolite synthesis [114], porous membrane template synthesis [115], layer-by-layer inorganic [116], colloidal particle [117], polymer polyelectrolyte assembly [118] and advanced nano-lithographic techniques [46], such as; electron beam or focused-ion-beam writing [47], proximal probe patterning [54] and X-ray or extreme-UV lithography [55]. Although so many techniques have been developed into practical routes to large quantities of diversified 1D nano-structured materials, rapidly and at reasonably, low costs, still requires great ingenuity [50].

1.4.1.1 One Dimensional (1D) Nanostructures

Thanks to the efforts in many research groups that there is a considerable interest for 1D nanostructures (e.g., wires, rods, belts and tubes) composed of conducting polymers [119]. They all gain so much attention for fabrication of nano-scaled devices because of their one-dimensional intrinsic properties and their potential for commercial applications [120], their unique electronic and optical properties, such as; their high surface-to-volume ratio and enhanced current carrying ability, which are a result of their low dimensionality [70]. Especially, conducting polymer nanostructures including nanorods, nanofibers and nanotubes have a high surface area as compared to their conventional bulk counterparts [121].

Exploration of 2D (quantum wells) and 0D (quantum dots) nanostructures in the past two decades is the force that drives the production of 1D nano-processed materials for many chemists and material scientists. Beginning with the design of buckyballs, graphite-like 1D nanostructures, enhancement went on with the invention of 1D

buckytubes (carbon nanotubes). When compared with quantum dots and wells, the innovation of 1D nanostructures has been slow until very recently due to the difficulties in the synthesis and fabrication of these nanostructures with well-controlled dimensions, morphology, phase purity and chemical composition [50].

1.4.2 Applications of Nanostructures

So far, several conducting polymeric nanostructures could successfully be obtained through both template-based with different types of membranes or non-template routes other than interfacial polymerization method. Researchers have developed innovative approaches by bringing about materials with the control of structure at the nano-dimension so that terms of nanopatterns, nanodomains, nanowires, nanocomposites, nanojunctions have been generated and mostly encountered in time. Nanoscale patterning of PPy dot structures was produced in a diameter range of 80 to 180 nm in self-organized arrays via block copolymer surface-micelle templated approach [122]. Conducting polymers in nanodomains were established in high-range order using opal templates [123]. Jerome *et al.* were created PPy nanowires electrochemically using polyacrylate film predeposited on a carbon electrode [124]. Chiral PAN nanocomposites were studied by McCarthy *et al.* via a template-guided synthesis [125]. PPy-iron oxide nanocomposites were prepared for application as a humidity and a gas sensor [126]. A nanojunction was formed by He and co-workers with a technique wherein PAN was deposited between two nanoelectrodes [127]. In 1999, chemical and electrochemical synthesis of PPy nanotubules were obtained with diameters of 15 nm [128]. Dramatic improvements were made in specific capacitance of PTh tubules in nanotube formations [129]. A different model was also described by Kaiser, in which the bulk properties of conducting polymers arose from crystalline nanodomains in a sea of amorphous material [130].

Potentially, the benefits of these highly ordered nanostructures together with a nano-dimensional control yield novel fabrication of electronic, optoelectronic, electrochemical and electromechanical devices at nano-scaled dimensions in all areas of nanotechnology.

In conclusion, in this study, it was aimed to fabricate conducting, nano-structured, highly-surfaced, electroactive materials for the use of them as electrode materials in supercapacitors. Two chemical synthetic methods, interfacial oxidative polymerization and template synthesis techniques, were used to obtain nano-structured materials of PPy, P(NMPy), PTh and PEDOT. The use of a soft template like a surfactant in interfacial oxidative method developed PPy nano-network structures at interface including nanofibers with beads crosslinking to each other, while the use of a hard template like a membrane produced nanotubule structures of both polypyrrole and polythiophene derivatives along the pore walls of the membrane.

2. EXPERIMENTAL

2.1 Materials

All chemicals were purchased as highly pure as possible: pyrrole, N-methyl pyrrole, thiophene, chloroform, methanol, lithium perchlorate (Aldrich Chemical Co.), sodium dodecyl sulfate (Sigma Chemical Co., 99 %), aluminum oxide (Acros, neutral, 50-200 μ), ferric chloride, acetonitrile, hydrofluoric acid (Merck Chemical Co.), (3,4-ethylenedioxythiophene) (EDOT, Bayer A.Ş.), ammonia solution (Riedel-de Haën, 26 %), alumina membrane filter (Whatman Anodics, pore size: 200 nm, 100 nm, 20 nm, pore diameter: 25 mm), polycarbonate membrane filter (Millipore, pore size: *ca* 220 nm).

2.2 Polymer Synthesis

2.2.1 Oxidative Interfacial Polymerization (A)

An interfacial polymerization reaction was performed in a glass bottle including two phases: pyrrole in chloroform phase and oxidant with surfactant in aqua [131]. A certain amount of pyrrole (0.6 M) was dissolved in the organic phase (3 ml) (Figure 2.1A). Here, the chloroform subphase was chosen as an organic phase to force the polymer formation at interface due to its complete immiscibility and higher density than that of water phase. Ferric chloride (0.24 M) and sodium dodecyl sulfate (0.18 M) were dissolved in bidistilled water (18.2 Mohm, 3ml) (Figure 2.1B).

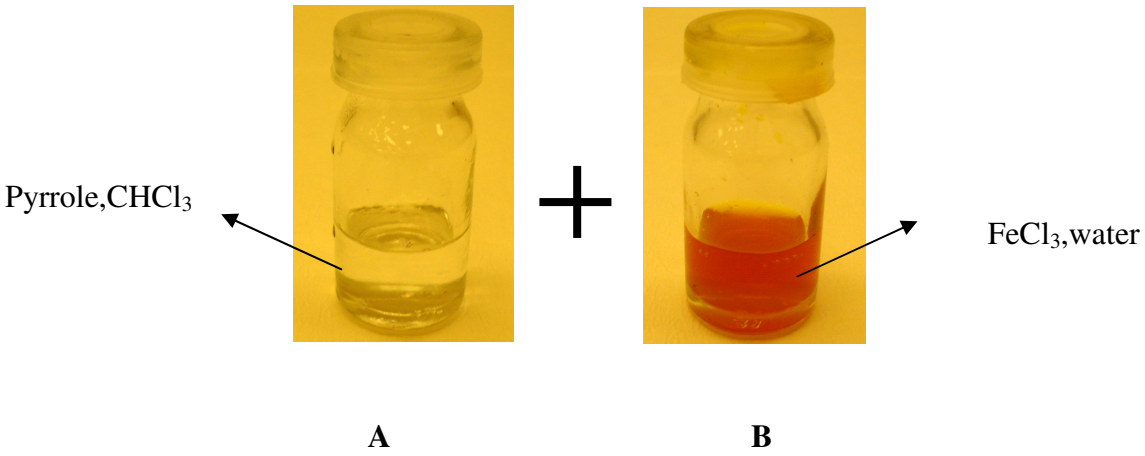

Figure 2.1 Preparation of reaction environment: (A) an organic phase including pyrrole and chloroform and (B) an aqueous phase with iron (III) chloride in water

In progress, in a 10 ml reaction bottle, two separately prepared phases (Figure 2.1) were combined and no disturbance was allowed after mixing (Figure 2.2A). In a few minutes, a thin polymer film started to form at interface. Polymerization was followed at room temperature for 3h (Figure 2.2A-2.2F). 2A was observed that polymerization was initiated at interface of them and formed polymers were carried up by the surfactant present in the water phase (Figure 2.2B-2.2F).

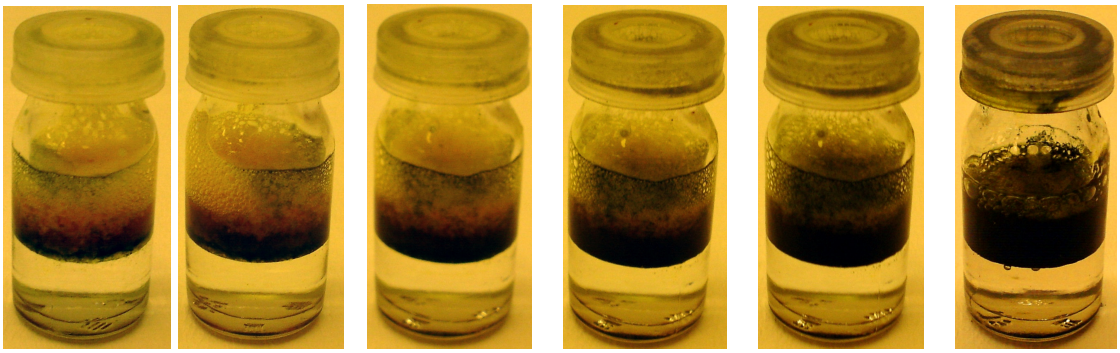

Figure 2.2 Reaction vessels including surfactant inside the organic phase with respect to polymerization time scales: 0 minute (A), 10 minutes (B), 30 minutes (C), 1 hour (D), 2 hours (E), 3 hours (F).

After 3 hours of polymerization, the subphase was removed and polymers were washed with 20 ml of methanol (3 times) to remove excess oxidant and 20 ml of a 30% of ammonia solution (3 times) to neutralize the polymer. Thereafter, the neutral polymer

was centrifuged and dried under vacuum overnight. In further studies, optimum reaction parameters were defined by variations in the mole ratios of monomer, oxidant and surfactant.

2.2.2 Template Polymerization (B)

Both PPy and P(NMPy) nano-arrays have been successfully synthesized by using Millipore PC membrane filters (diameter: 25 mm) (Figure 2.3) with an average pore size of *ca* 220 nm in aqueous medium.

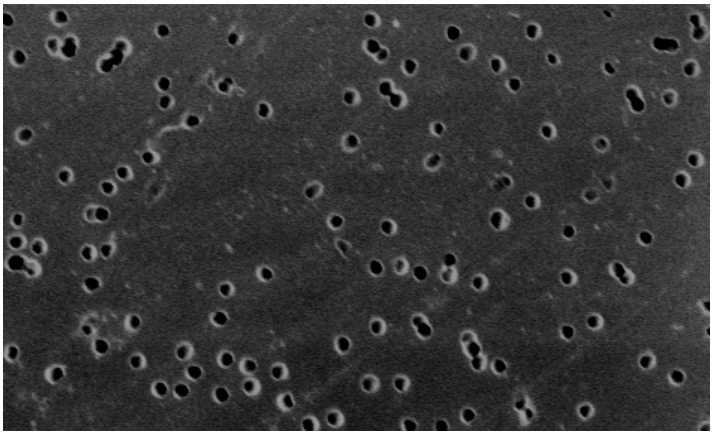

Figure 2.3 SEM picture of a PC membrane of Millipore Corporation with a pore size of *ca* 220 nm

First, PC membrane was sandwiched between two O-rings of a U-shaped glass tube composed of two compartments. One arm of the U-tube had a set-up for holding PC membrane with a clips (Figure 2.4). Monomer and oxidant solutions were separated with this membrane in which they diffuse through each other by the way of the pores that the polycarbonate membrane has.

Next, the reaction medium was prepared by dissolving iron (III) chloride (0.25 M) in aqua and then added from one arm of the U-shaped glass tube at room temperature (Figure 2.4B). Aqueous pyrrole (0.05 M) or N-methylpyrrole (0.05 M) solutions were also poured from another arm of the tube (Figure 2.4A). It is worth noting that both were purified by eluding in a column filled with aluminum oxide and the solutions must be shaked well before pouring into the U-tube. As soon as both monomer and oxidant

solutions contact with each other, the reaction immediately starts by diffusing through the pores of PC membrane filter. After successive polymerization time (3h), PC

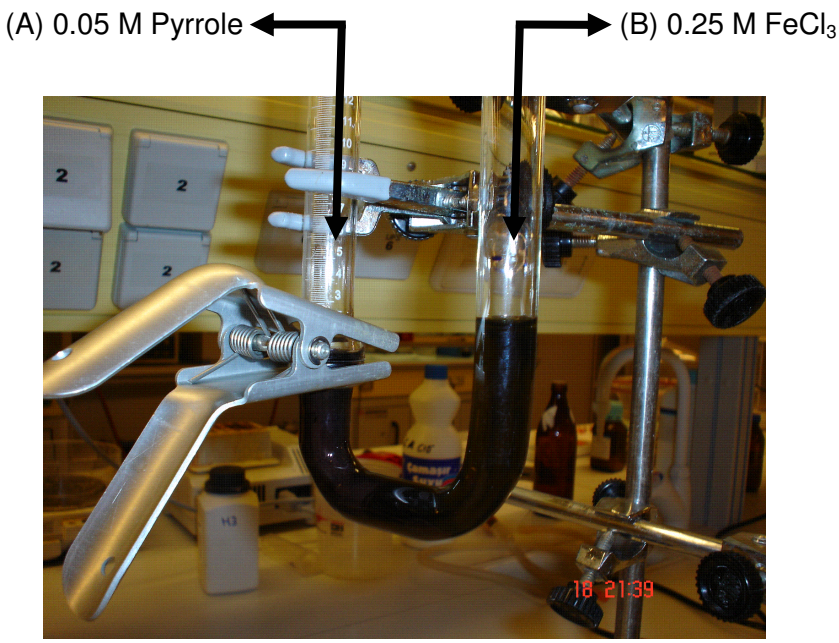

Figure 2.4 Reaction vessel (U-tube) for template synthesis method with two compartments: (A) monomer solution unit, (B) oxidant solution unit

membrane filter including PPy or P(NMPy) nanotubules was taken out by removing two separate parts of the U-tube. In the following step, membrane with its contents was washed with methanol and bidistilled water three times, respectively. After washing step, it was kept under vacuum overnight for drying to prevent any deterioration in tubule structures. Then, chloroform was used to dissolve PC membrane filter so that remaining solid powders were all elongated as PPy nanotubules coming out of PC membrane filter pores.

Above steps were also repeated by using the same experimental set-up in Figure 2.4 in the same order to obtain template synthesis of PTh or PEDOT nanotubules in 1D as well. However, due to high hydrophobicity of these thiophene derivatives, prepared aqueous reaction medium was irresponsive to the synthesis of these nanostructures by using the same type of PC membrane filter. The best solvent system, which increases the rate of oxidation and oxidizes thiophene or 3,4-ethylenedioxythiophene immediately, was found as 0.05 M $LiClO_4$ in acetonitrile (MeCN). It is also important to mention that PC membrane filter does not work in this solvent system because MeCN

was incompatible with PC membrane filter as the pores become slightly occludent. So that, there was no logic to use PC membrane filter due to the pore blocking behaviour of MeCN. The best membrane filter type for this new system suitable to use in MeCN medium was Whatman Anodisc alumina membrane filters (diameter: 25 mm) (Figure 2.5) with an average pore size of *ca* 200 nm, 100 nm or 20 nm.

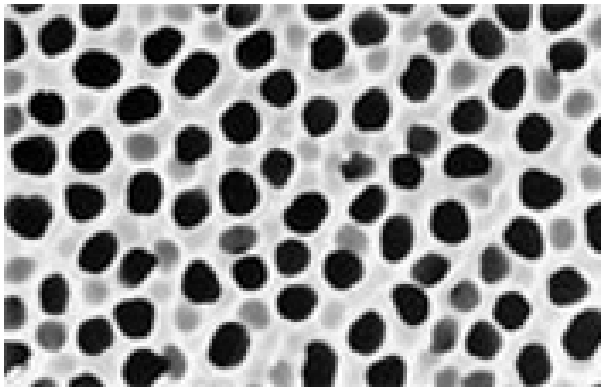

Figure 2.5 SEM image of a commercial anodic alumina membrane of Whatman Corporation with a pore size of 200 nm

Dissolving iron (III) chloride (0.25 M) in 0.1 M $LiClO_4$/MeCN, this prepared solution was quickly transferred into one arm of the U-tube (Figure 2.4B) by also adding thiophene (0.5 M) or EDOT (0.1 M) in 0.1 M $LiClO_4$/MeCN from other side of the U-tube (Figure 2.4A). For the reaction medium of PEDOT, solution of 0.05 M $LiClO_4$/MeCN also worked effectively, while decrease in dopant ion concentration prevented nanotubule formation of PTh. All reactions were performed at room temperature in contact of both monomer and oxidant solutions with alumina membrane filter in the same closed system.

After the polymerization completes itself in 3h, alumina membrane filter with PTh nanotubules grown in its pores was removed and washed with methanol and bidistilled water three times. One quick method to dissolve alumina membrane filter was washing template material with a 20% (v/v) aqueous solution of hydrofluoric acid (HF) until the whole membrane filter was removed. Then, freely separated particulates of PTh nanostructures should be rewashed several times with bidistilled water until the effect of all aqueous HF solution residue was taken away from the medium. For PTh, the whole formation completed itself yielding nanotubules in 1D in 3h, while for PEDOT, the effective reaction time was at least 24 h. One should note that as the reaction time was

so long for whole polymerization of PEDOT, alumina membrane filter was sandwiched between two arms of glass U-tube by stacking two black-lined filter papers to prevent the piles of PEDOT nanostructures on its two sides. Alumina membrane filter should be removed carefully and slowly without giving any disturbance over it as PEDOT bugle-like structures are so delicate to be distorted. Followingly, membrane including polymers was washed with methanol and bidistilled water three times, respectively. In this case, vacuum overnight is necessary to dry all PEDOT nanostructures and to decrease the possibility of distortion in the structures as well. However, it was not necessary to apply vacuum so long not more than 3 hours for PTh as the reaction time was less. After drying, the template was dissolved with a 20% of aqueous hydrofluoric acid (HF) solution.

2.3 Characterization Methods

2.3.1 Electropolymerization

A platinum button electrode (diameter: 1.6 mm; area 0.02 cm^2) or ITO-coated glass slides were performed as working electrodes. In completion of this electrode set-up, a platinum flag or wire were chosen as a counter electrode, and a silver wire or 0.01 M $Ag/AgNO_3$ (Ag/Ag^+) as reference. The electrodeposition was performed from a 0.01 M solution of the monomer in the electrolyte potentiostatically at 50 mV above the oxidation potential of monomer by using an Epsilon EC Potentiostat/Galvanostat. For cyclic voltammetry applications, the same electrode set-up was used with monomer-free electrolyte solution. Here, the electrolyte used was 0.1 M of tetrabutylammonium hexafluorophosphate (Bu_4NPF_6) in water, acetonitrile (MeCN) or mixture of MeCN and water.

2.3.2 Spectroelectrochemistry

A Shimadzu UV 3150 UV-visible-NIR spectrophotometer connected to a computer and an Epsilon EC Potentiostat/Galvanostat was run to collect spectroelectrochemical data. To record the outputs, a three-electrode cell assembly was used. The working electrode was an ITO-coated glass slide (7 x 50 x 0.6 mm, $R_s \leq 10$ Ω /□, Delta Technologies Inc.), and the counter electrode was a platinum wire and a Ag wire as a pseudo-reference electrode. Calibration of the pseudo-reference was performed externally using a 5 mM solution of ferrocene (Fc/Fc^+) in the electrolyte ($E_{1/2}(Fc/Fc^+)$) = +0.130 V *vs.* Ag wire and +0.080 V *vs.* Ag/Ag^+ in 0.1 M (Bu_4NPF_6/MeCN). The potentials were reported versus Ag/Ag^+. Polymer films for spectroelectrochemistry were deposited potentiostatically on ITO-coated glass slides and then, those prepared films were characterized with the spectrophotometer.

2.3.3 Surface Analysis

Surface areas of samples were measured by ASAP 2000 Accelerated Surface Area and Porosimetry system manufactured by Micromeritics Co., USA. Before the analysis was performed, all the samples were vacuumed overnight.

2.3.4 Electrical Conductivity Measurements

The conductivity measurements were performed by using Agilent 34401A 6½ Digit Multimeter and interdigitated microelectrodes at room temperature.

2.3.5 Elemental Analysis

A LECO, CHNS-932 instrument was used for the measurements of elemental analyses. Before analysis, all the samples prepared by interfacial oxidative method were synthesized in large amounts and vacuumed overnight.

2.3.6 SEM Analyses

Morphology of conducting polymer nanotubules was investigated via a high resolution Supra Gemini 35VP Field Emission Scanning Electron Microscope from Leo. Before analysis, all samples were coated with carbon by Emitech, T950x Turbo Evaporate. Imaging was generally operated at 2-5 keV accelerating voltage, using the secondary electron imaging technique.

2.3.7 FTIR-ATR Analyses

FTIR spectra of samples were measured with a Bruker EQUINOX 55 FTIR spectrometer. Samples were vacuumed overnight for drying before analyses. Spectra were obtained with 200 scans at a resolution 2 cm^{-1}.

3. RESULTS AND DISCUSSION (A)

3.1 Optimization of Mole Ratios

To synthesize nano-structured materials made of conducting polymers by interfacial polymerization technique, optimizing reaction conditions is necessary [132]. An immiscible solvent system was used, in which monomer and oxidizing agent were dissolved in two different solvents, namely chloroform and water, respectively. One another reactant was the surfactant, sodium dodecyl (lauryl) sulfonate (DSA), which was the carrier of positively charged polymers. To achieve desired PPy nanostructures by using oxidative interfacial polymerization method, different mole fractions of monomer, oxidizing agent and surfactant were used to optimize experimental conditions.

First, mole ratio of oxidizing agent to the monomer was optimized in an arbitrarily chosen mole ratio range by changing the ratio from 2 to 5 (Table 3.1, A-E).

Table 3.1 Mole ratios of oxidant/monomer and surfactant/monomer as arbitrary trials in a range of 2 to 5 (A-E)

Arbitrary Trials	$n_{oxidant}/n_{monomer}$	$n_{surfactant}/n_{monomer}$
A	3	1
B	2	1.75
C	4	1.75
D	3	0.25
E	5	1.75

Experimantal studies of different arbitrary trials proved that performance of these systems changed with respect to different mole ratios of both oxidant to monomer and surfactant to monomer as soon as two immiscible solvent systems contact with each other (Table 3.1, A-E). In this respect, the system performance also differed surprisingly according to its surfactant to monomer mole ratio change when the mole ratio of oxidant

to monomer was constant in the system. In comparison of the behaviour of these systems after mixing and in the end of 24 hours, it was observed that conditions for case C was the best way to study on to reach to desired optimal environment.

Although PPys were successfully formed at interface or at the upper layer of polymerization solution in all mole ratios of oxidizing agent to the monomer, a complete polymerization of pyrrole was achieved when the ratio was 3 or above. Morphologies of these systems, characterized by SEM imaging, including different mole ratios of oxidant to monomer (Figure 3.1). In comparison of Figure 3.1A with Figure 3.1D, morphology of PPy structures varied when the mole ratio of surfactant to monomer was changed from 1 to 0.25 by keeping mole ratio of oxidant to monomer at 3. As the amount of surfactant was decreased, fiber formation was impossible to be seen in the case of Figure 3.1D.

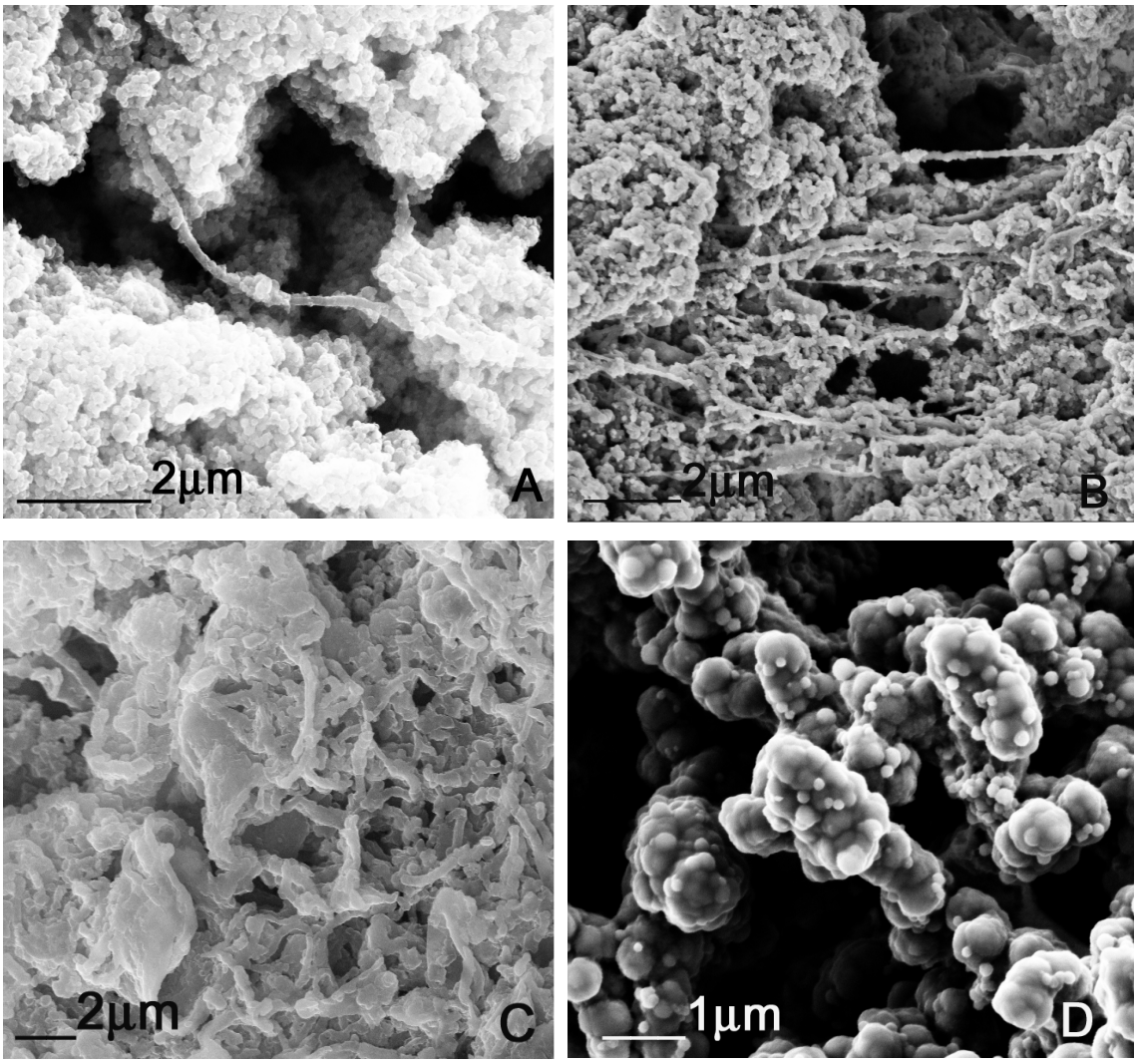

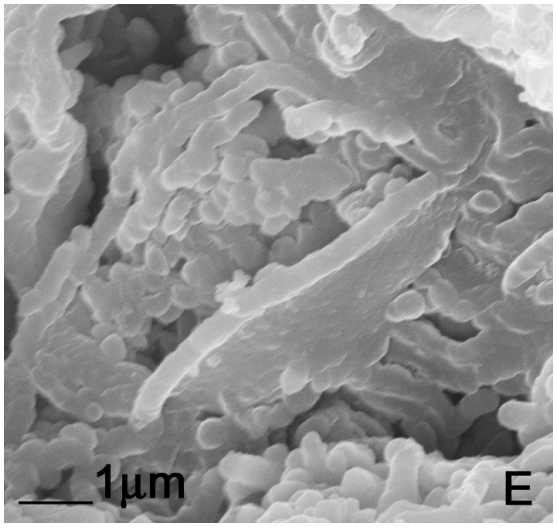

Figure 3.1 SEM images of each samples synthesized as above experimental conditions (A-E)

SEM images of Figure 3.1 were excellent evidences for the effect of surfactant amount onto the system. These figures facilitated the route for the optimization of mole ratios of surfactant to monomer, by keeping mole ratios of oxidant to monomer constant. When the amount of surfactant was unchanged, it was possible to change morphology of PPy structures by playing with the mole ratios of oxidizing agent to monomer (Figure 3.1B, 3.1C, and 3.1D). Clearly, SEM image of 1C indicated that fiber formation could mostly be observed if the mole ratio of oxidant to monomer was kept at 4:1. Although PPy fibers were not in fibrillar morphology in the case of 3.1C, it is noteworthy to state that they could be separated by changing the surfactant amount in the system. According to morphology characterization with SEM images (Figure 3.1), results of first trials illustrated that mole ratio of oxidant to monomer should be kept constant at 4:1 (Table 3.1C).

In the next step, mole ratio of surfactant to monomer was optimized by changing it in a range from 1:1 to 10:1, while keeping the mole ratio of oxidant to monomer constant at 4:1 (Table 3.2, C1-C10).

Table 3.2 Mole ratios of surfactant/monomer in a range from 1 to 10, when mole ratios of oxidant/monomer were set at 4:1 (C1-C10)

Trials	$n_{oxidant}/n_{monomer}$	$n_{surfactant}/n_{monomer}$
C1	4	1
C2		2
C3		3
C4		4
C5		5
C6		6
C7		7
C8		8
C9		9
C10		10

C1 and C2 interpreted that surfactant to monomer mole ratio less than 3:1 was not enough to complete fiber formation (Figure 3.2). Mole ratios from 6:1 to 10:1 resulted nearly the same morphologies with a few fiber formation (Figure 3.2, C6-C10). Although there existed some fibers in a bulk structure in the case of ratio 6:1 and 7:1, mole ratios more than 5:1 yielded undesired PPy structures (Figure 3.2, C6 and C7). Since the amount of surfactant was too much to form fibers, it caused to stick PPy structures. If the mole ratio of surfactant to monomer was increased more than that of C7, fibers inside the bulk structures could not be differentiated (Figure 3.2, C8-C10). This case also confirmed that large amounts of surfactant hindered fiber formation.

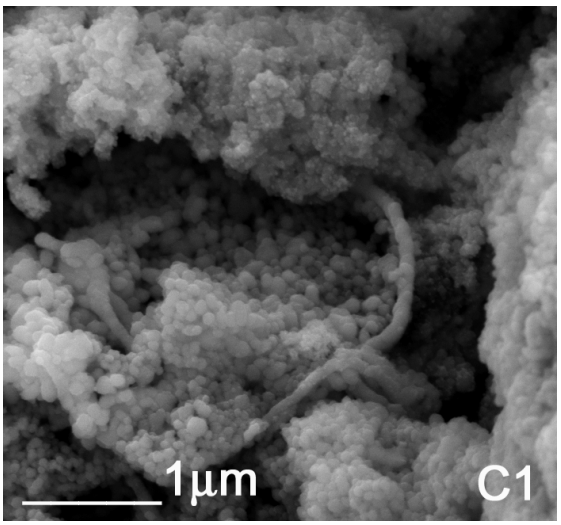

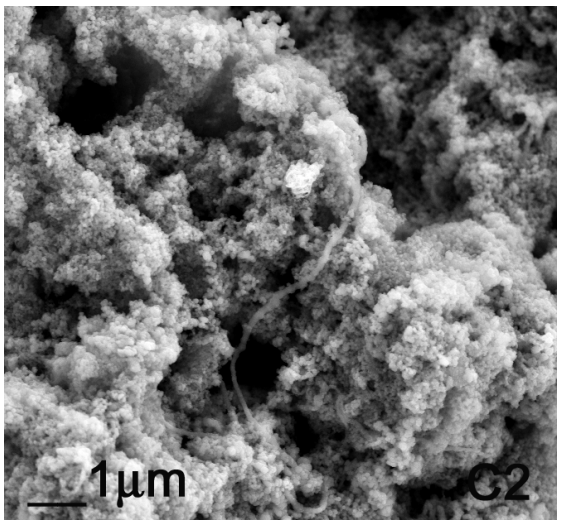

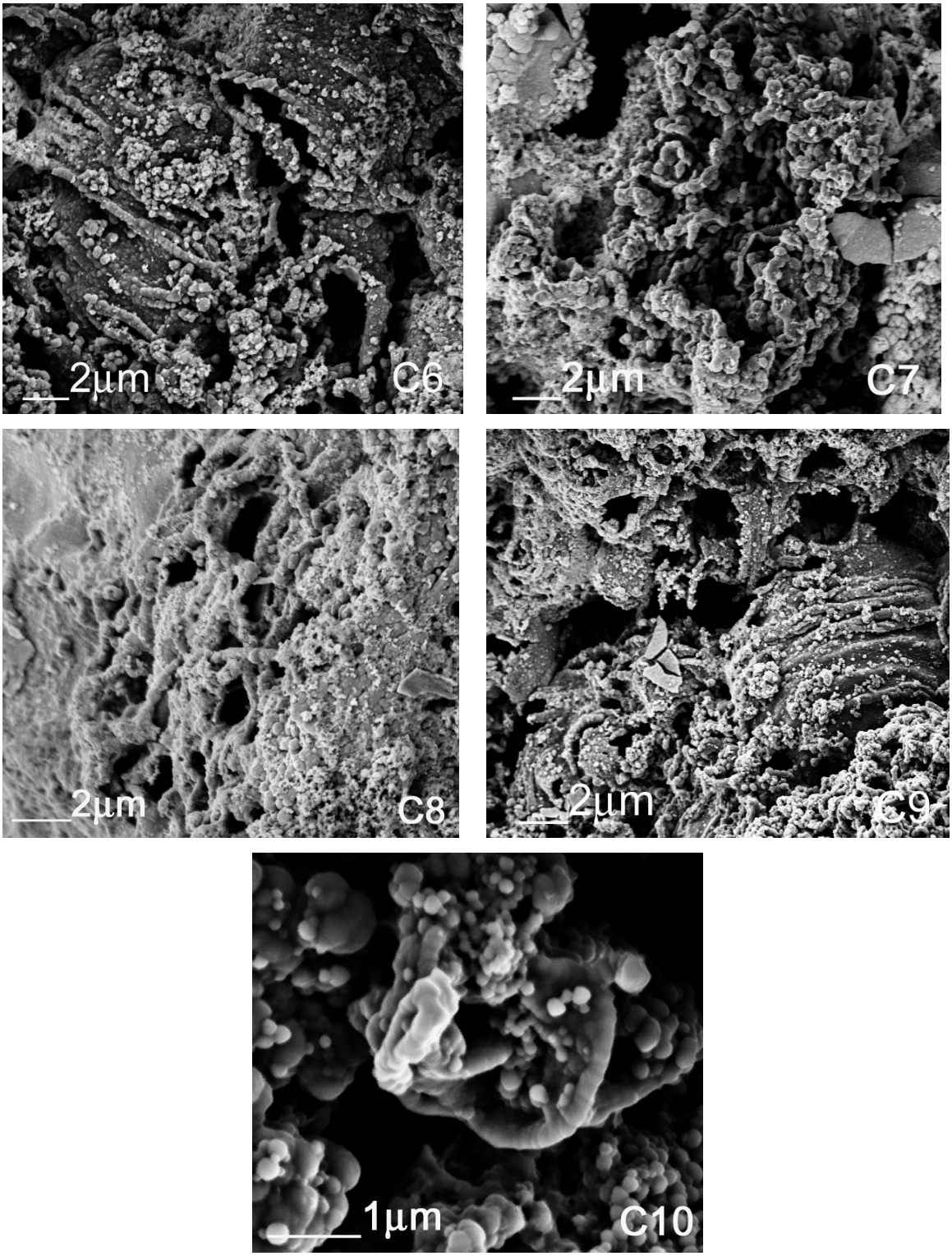

Figure 3.2 SEM micrographs as a result of experimental conditions, which were applied according to Table 2, C1, C2, C5, C6, C7, C8, C9, C10, respectively.

The presence of surfactant helped formation of suspended PPy fibers in all ratios but, the best fibrillar nanostructures were obtained when surfactant to monomer mole ratio was kept between 3:1 and 5:1 (Figure 3.3, C3-C5) [133]. A comparison of the morphology of PPy fibers at different feed ratios of surfactant to monomer was given in Figure 3.3. As can be seen from Figure 3.3, PPy nanofibers were homogeneously aligned in three dimensions and crosslinked after some point forming nano-networks. A homogeneous network formation was clearly seen from the picture of C3, in which PPy was prepared by using the surfactant to monomer ratio as 3:1 (Figure 3.3). As the concentration of surfactant was increased to its ratio of 4 or 5, although same fibrillar structure was observed, a dilution of fibers, in other words an increase in the void spaces among fibers as well as in the fiber lengths was observed.

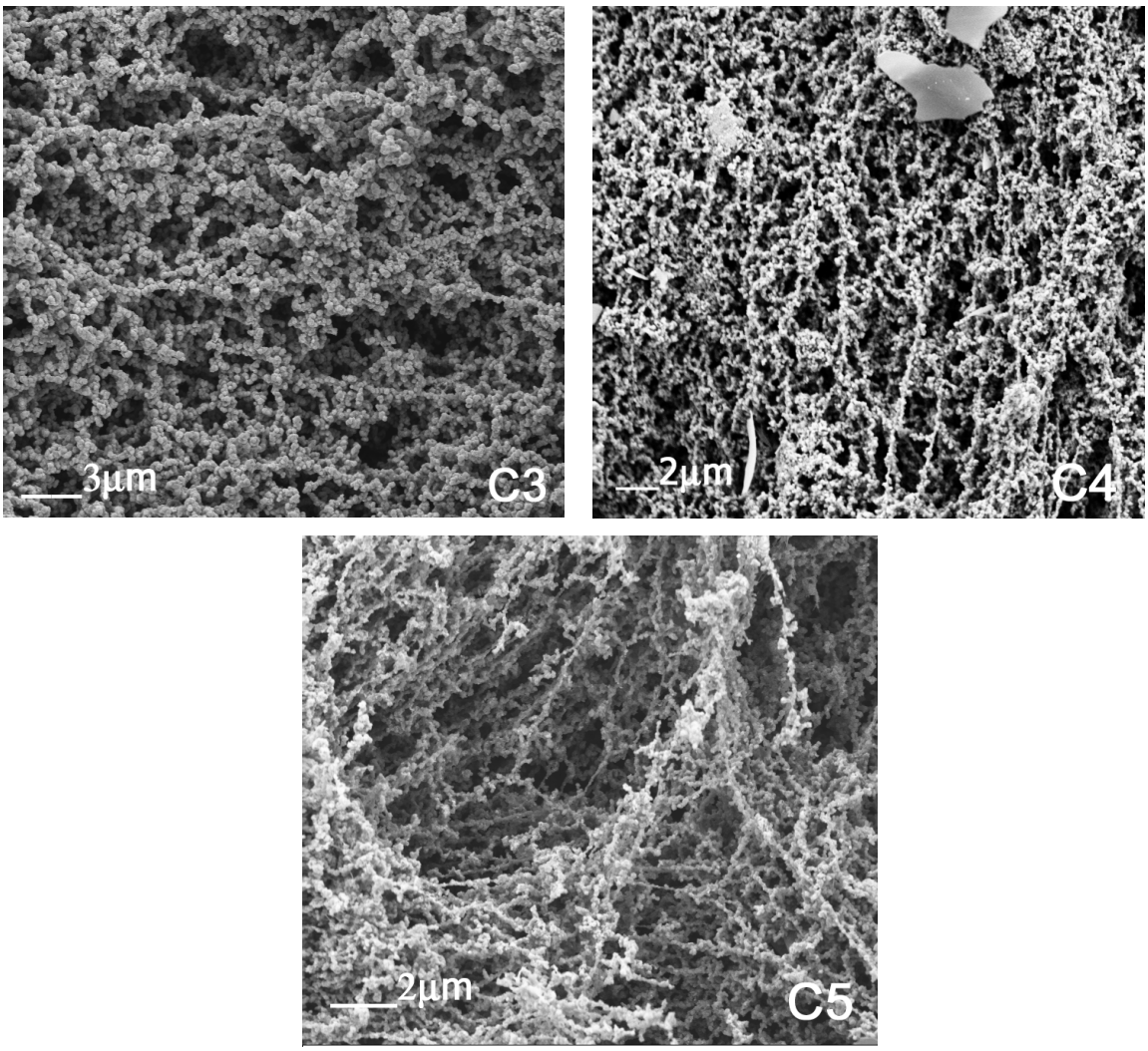

Figure 3.3 SEM micrographs as a result of experimental conditions applied according to Table 2 in conditions of C3 to C5.

Upon focusing on PPy nanostructures from a detailed aspect, PPy nanofibers were lined with beads on it with a pearl necklace structure (Figure 3.4). Average size of fibers and beads was calculated with the help of SEM images as *ca* 150 and 300 nm, respectively. The lengths of fibers, usually in a range of 1-20 μm, and the void spaces among them could be controlled by changing polymerization conditions, such as concentrations of reactants and polymerization time.

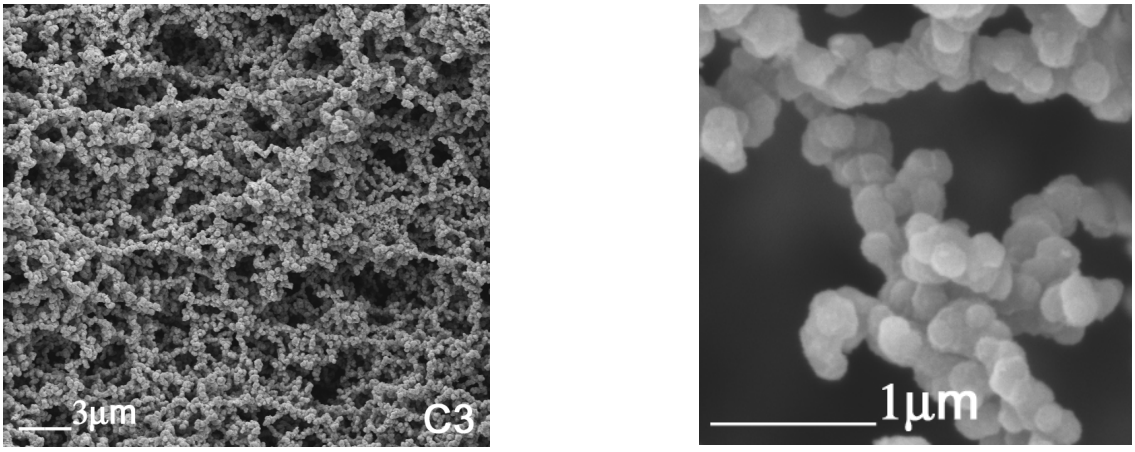

A **B**

Figure 3.4 (A) SEM micrograph of C3 and (B) that of its magnified portion indicating beads with pearl necklaces and void spaces among crosslinked PPy nanofibers

3.2 Optimization of Polymerization Time

Mole ratio optimizations were experimented for 24 hours till this step to be sure that polymerization time was also kept constant to understand the reaction behaviour. After the best optimum conditions from the point of concentrations were clarified, polymers were prepared with the same experimental conditions of C3 (Table 3.2, Figure 3.3) in a different time scales from 10 minutes to 24 hours. Resultantly, effect of time on fiber formation was seemed unimportant from the aspect of morphology change (Figure 3.5, A-E). Then, characterization of each sample with SEM imaging, experimental results and elemental analyses showed that fiber formation completed itself in 3 hours. Since 3 hours was enough to synthesize these polymers in nano-network formation, 24 hours was not applied any more. Results of morphological

studies about determination of polymerization time scale can be easily seen from Figure 3.5.

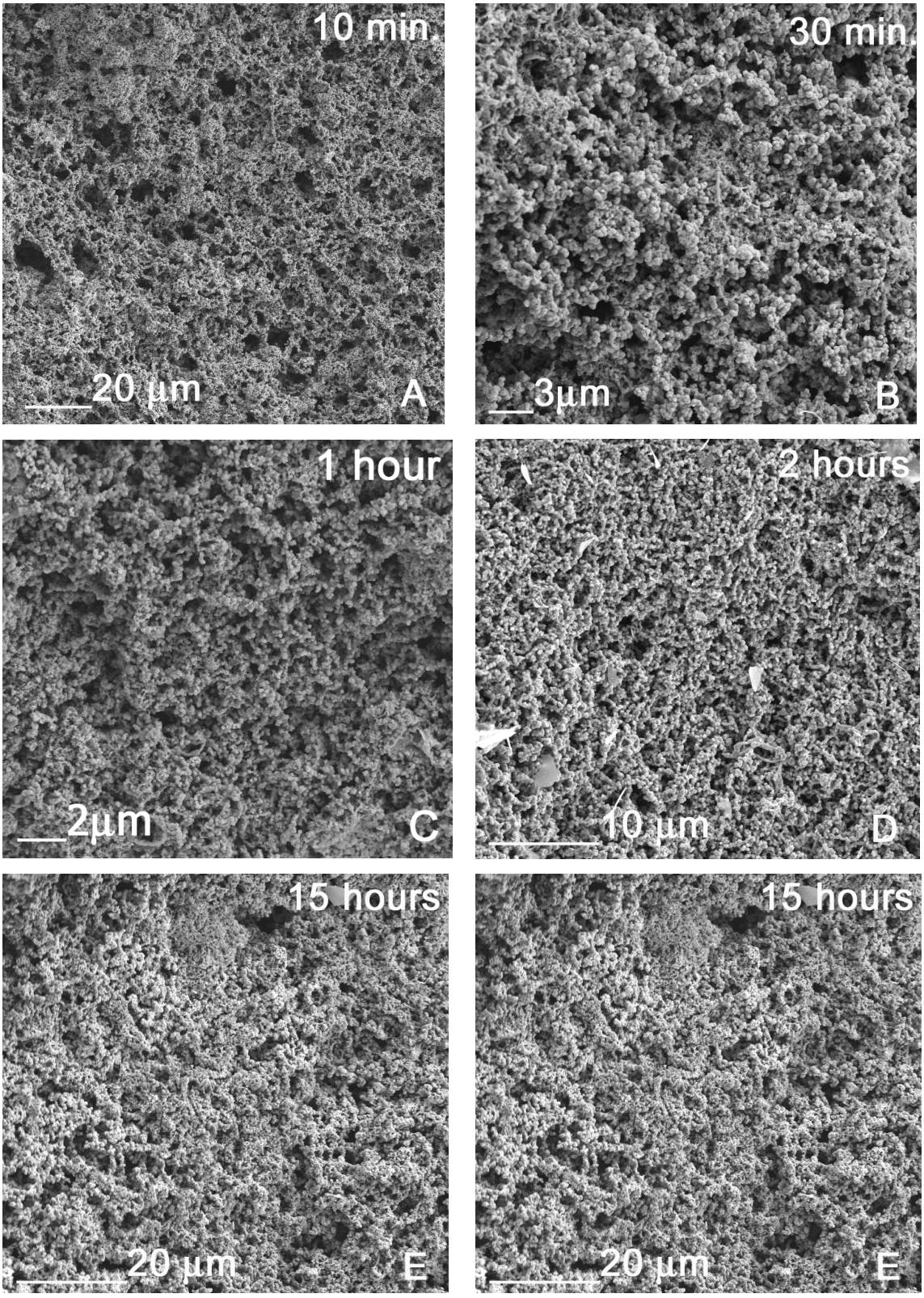

Figure 3.5 SEM micrographs investigating polymerization time in a time scales of 10 minutes, 30 minutes, 1 hour, 2 hours, 15 hours and 24 hours, from A to F, respectively.

3.3 Composition of Polymer

Keeping optimized conditions above in hand, it was also desirable to understand the effect of surfactant on system performance to obtain futuristic nanofibers of PPy from the point of composition of polymers. For this purpose, spectral, chemical and electrochemical methods were applied in both presence and absence of surfactant to clarify its importance for the system.

3.3.1 Roles of Surfactant

This different morphology may stem from the effect of dilution of polymerization solution by surfactant. The presence of DSA helps not only form such a nano-network structure formation with void spaces among fibers, but also carry resulting polymers up in the solution. This fact stemmed from strong electrostatic attractions between positively charged polymer backbone and negatively charged ends of surfactant, namely SO^{3-} end groups (Scheme 3.1).

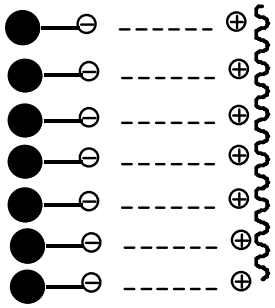

Electrostatic interaction between
polymer backbone and negatively
charged ends of surfactant

surfactant carries polymer

Scheme 3.1 Chart of electrostatic interactions between polymer backbone (〰) and surfactant tail (●—)

In the absence of DSA, positively charged polymer backbone could not be carried in the solution. The only thing that could be observed from the repetitions of experiments without surfactant was PPy film formations covering the walls of reaction bottle and a free-standing film at interface without any PPy nano-network structures. SEM analysis clearly demonstrates that there could exist two morphologically different structures in the absence of DSA (Figure 3.6). Figure 3.6A and 3.6B pointed out morphologies of PPy free standing films as flat layers. Thus, several repetitions of both experiments and morphology characterization works proved that these PPy free standing films were desired if no surfactant was used because impossibility of polymer carriage did not allow the separation of PPy structures in the shape of fibers.

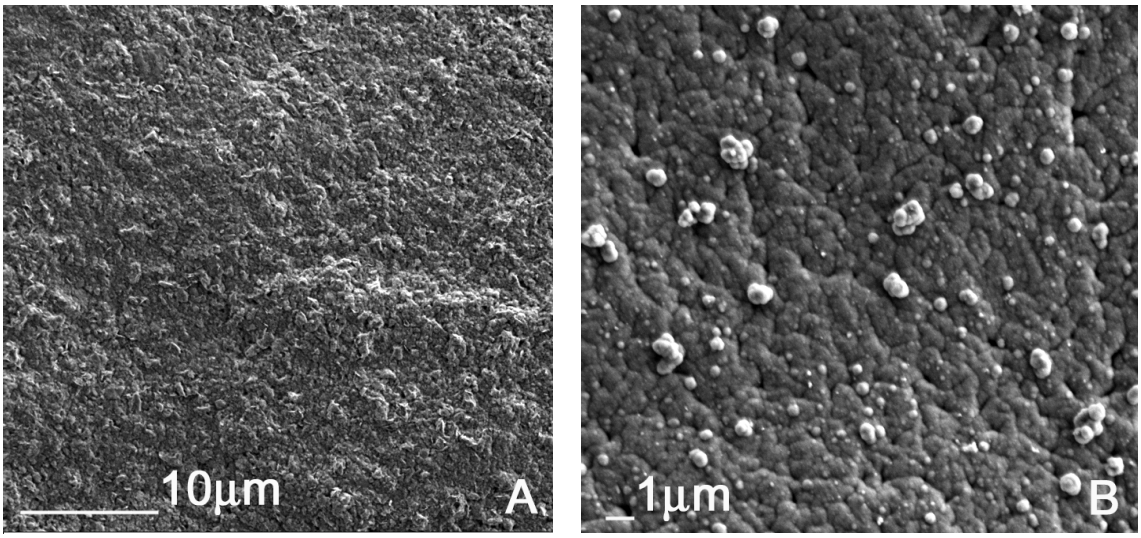

Figure 3.6 (A)-(B) SEM micrographs of PPy free standing films in the absence of surfactant as flat layers

3.3.2 Investigation of Effect of DSA in Reaction Medium

Investigation of morphology change with or without DSA in the reaction medium was also performed by electrochemically prepared PPy and PPy-DSA films. Hence, PPy was potentiostatically deposited on ITO-coated glass slides both in the presence and in the absence of DSA in the solution. First, thin PPy and PPy-DSA films were deposited on ITO coated glass substrates using potentiostatic deposition at a potential of 50 mV above the oxidation potential of pyrrole from 0.01 M monomer solution. The electrolyte used was 0.1 M Bu_4NPF_6/MeCN and a mixture of 0.03 M DSA and 0.1 M Bu_4NPF_6 in a

water/MeCN (20/80) for PPy and PPy-DSA depositions, respectively. Figure 3.7A depicts morphology of PPy structures in the absence of DSA and Figure 3.7B in the presence of DSA. In comparison, results clarify that a three-dimensional nucleation growth could be observed in both cases. Although an irregular three dimensional growth was observed in PPy structures, completely different and such a regular knitting type structure was seen in resulting polymer films that have been grown in the presence of DSA. This different nature of structure presented in Figure 3.7B is very likely resulting from steric effects induced by the long alkyl chain ended with a sulfonate dopant ion, DSA.

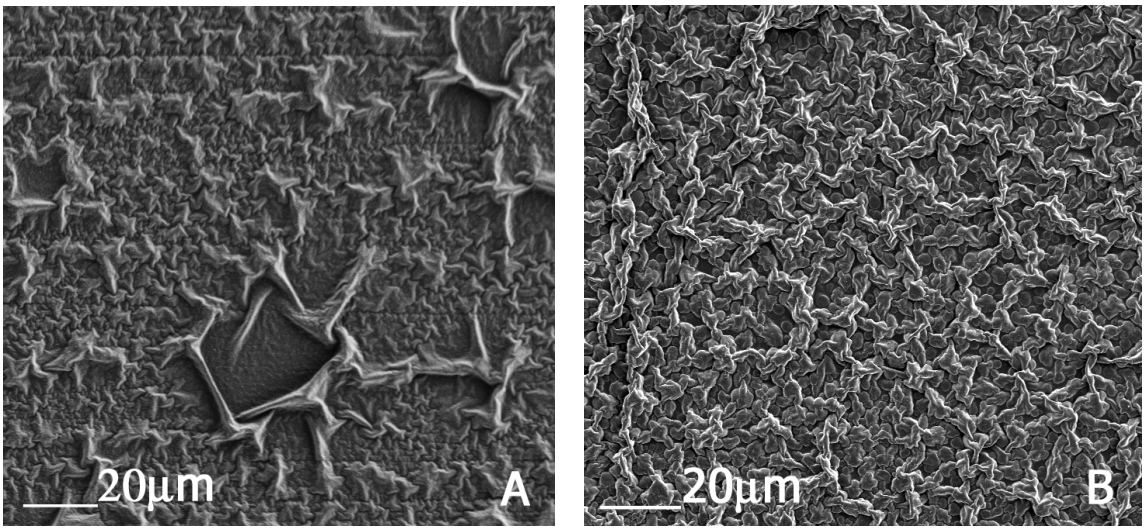

Figure 3.7 SEM images of electrochemically prepared PPy films on ITO-coated glass slides (A) in the absence (B) in the presence of DSA

3.4 Results for Quantitative Analyses

3.4.1 Spectroelectrochemical Analyses Results

In pursue of characterization, the same polymer films shown in Figure 3.7 were also used for spectroelectrochemistry. Spectroelectrochemistry of these polymer films with similar thicknesses was compared in the same plot. Figure 3.8 presents comparison of spectroelectrochemistry of corresponding PPy and PPy-DSA films. In visible region, a maximum absorption peak was observed at 2.95 eV (420 nm) and 3.1 eV (405 nm)

due to π-π* transition of both PPy and PPy-DSA films, respectively. In addition, neutral PPy-DSA had absorption peaks at about 2.2 eV (570 nm) and 1.4 eV (900 nm), which PPy did not have. These two absorption peaks might be associated with incorporation of DSA into the PPy films resulting in an incomplete reduction of polymer. A strong interaction between positive ions present in the electrolyte solution and sulfonates, that DSA has, results in a reflectance below 1.8 eV for the neutral polymer [134]. Upon oxidation, π-π* transitions were depleted at the expense of a broad band at lower energies for both polymers with slight differences. Comparing oxidized PPy and PPy/DSA films, π-π* transition of PPy/DSA film could not be depleted completely and remained a residual absorption at 2.9 eV. In other words, the band corresponding to intermediate energy charge carriers (radical cations or polarons) could not be converted to low energy charge carriers (dications or bipolarons). A remained strong absorption at 1.5 eV might be resulted from the strong interactions of DSA with the PPy backbone.

It was also possible to calculate electronic band gap from the onset of π-π* transition, which is 2.52 eV for PPy films. Since π-π* transition band for PPy-DSA was not very well defined, band gap for this polymer was calculated using isobestic point resulted almost the same value with PPy.

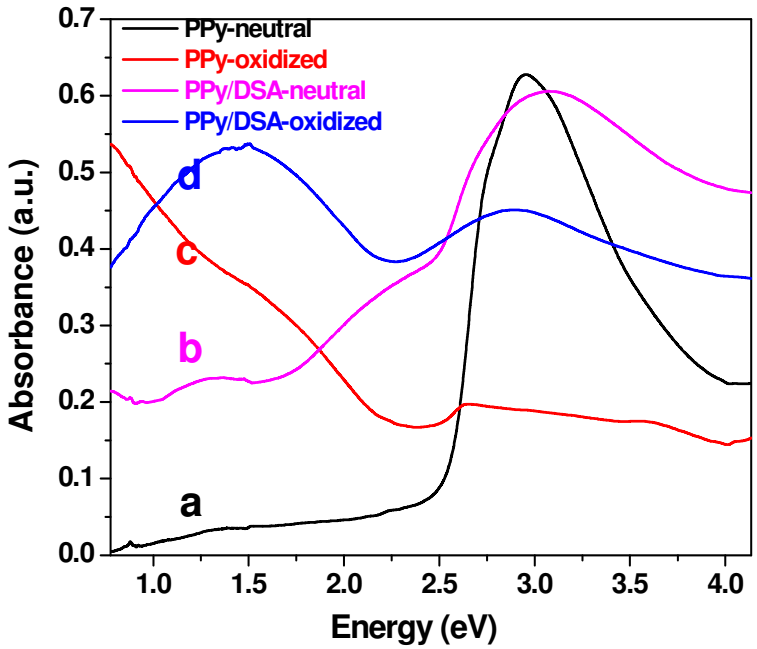

Figure 3.8 Spectroelectrochemistry of PPy and PPy-DSA in 0.1 M Bu_4NPF_6/PC at different oxidation states: (a) neutral PPy, (b) neutral PPy-DSA, (c) oxidized PPy, (d) oxidized PPy-DSA

3.4.2 Percent Yield Results

Optimized experimental condition C3 (Table 3.2, Figure 3.3) was also repeated in larger amounts in order to prove whether the system was still stable when the synthesis was repeated by using huge amounts of reactants. The main purpose was to check whether the system was applicable to industrial applications or not. Experimental results indicated that the larger the amounts of reactants, the longer the polymerization time for reaction to be completed and the thicker the resulting PPy layer at interface. Figure 3.9A clarifies that there was no morphological difference from the points of both network and bead formation if the amounts of reactants are increased. Especially, Figure 3.9B in a larger magnification explicitly confirmed that structural change in morphology could not be observed as a result of use of larger amounts of reactants.

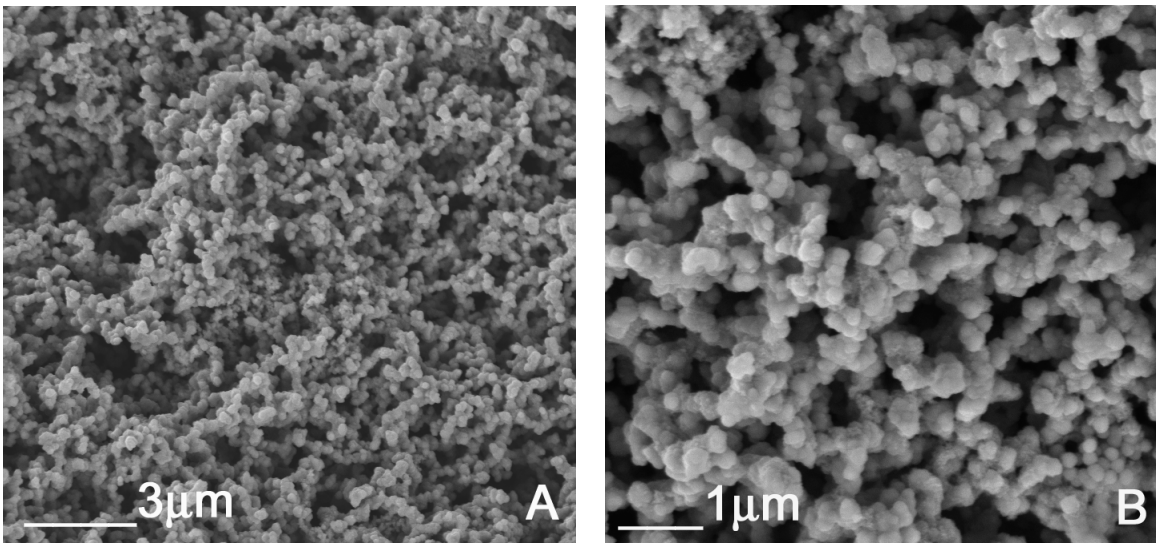

Figure 3.9 SEM images of PPy nano-networks for large amount syntheses in two different magnifications

In this sense, steps of polymer synthesis were repeated several times in the same time scale in larger amounts and samples were vacuumed to dry for two days. Then, dried samples in various amounts were weighed in four significant digits and used for both elemental analyses and percent yield calculations. To calculate yield in percentages, ratio of each amount for polymer to that of monomer (0.081 g) in grams was taken and multiplied with hundred by ignoring dopant effects during

polymerization. Percent yield calculations indicated that the longer the polymerization time, the larger the percent yield (Table 3.3).

Table 3.3 Results of percent yield calculations from weight amounts in grams of synthesized PPy materials in different time scales

TIME (minutes)	WEIGHT AMOUNTS (mg)	PERCENT YIELD %
10	5.4	6.7
20	7.2	9.0
40	7.3	9.0
80	17.0	21.0
150	22.1	27.3
300	24.1	29.8
720	46.3	57.2
1440	81.5	100.6

3.4.3 Elemental Analyses Results

Elemental analyses results yielded efficient information about the percentages of C, H, N, and S in the total amount (Table 3.4).

Table 3.4 C, H, N, S and total element amounts in percentages inside the PPy nanostructures synthesized in various time scales

TIME (min)	C%	H%	N %	S %	TOTAL %
40	58.0	5.3	12.2	3.4	79.0
80	64.2	5.7	14.0	3.6	87.3
300	62.3	5.6	13.3	4.0	85.0
720	60.4	6.1	11.5	4.8	82.8
1440	56.1	6.0	10.0	5.0	77.0

Calculations in Table 3.4 indicated that dopped amounts of surfactant inside the polymer backbone did not allow to yield hundred percentages of total element amounts, which was an ideal case. Therefore, the ratio of percent sulfur to nitrogen was not calculated directly from the results above obtained from instrumental results. The way to determine exact ratios of percent sulfur to nitrogen was recalculated by using the percent total element amounts. The DSA content of polymer was determined using the ratio of S and N atoms obtained from elemental analysis that also gives doping level. A

similar increase in the percent yield and doping level is an evidence for the source of the increase in yield % that is incorporated DSA. Table 3.5 summarizes elemental analyses results for C, H, N and S atoms and the doping level calculated using the ratio of S to N atom for the PPy/DSA system at different polymerization time.

Table 3.5 Results of elemental analyses for percent N and S atoms calculated using the ratio of S to N atoms for the PPy/DSA system at different polymerization time.

TIME (min)	N%	S%	Doping Level %
40	15.5	4.3	28
80	15.9	4.1	26
300	15.7	4.5	29
720	13.9	5.7	41
1440	12.9	6.4	50

3.4.4 Relationship Between Doping Levels (%) and Yields (%)

Doping level (%) and yield (%) was plotted as a function of polymerization time to understand the correlation between them (Figure 3.10). A similar trend of increase was observed in both percent yield and doping level in different time scales between 10 min and 24 h. A sharp increase of *ca* 27% in yield was observed at the initial stages of polymerization. Then, change in the yield was less than 3% between 2.5 h and 5 h, which indicated that tendency of increase slowed down. It is believed that the increase in yield % was resulted from incorporation of DSA into the polymer structure after 5 h, which was confirmed by elemental analyses results. Obviously, plot in Figure 3.10 was a good evidence that incorporation of negatively charged DSA into positively charged polymer backbone existed by starting from the first steps of polymerization in time.

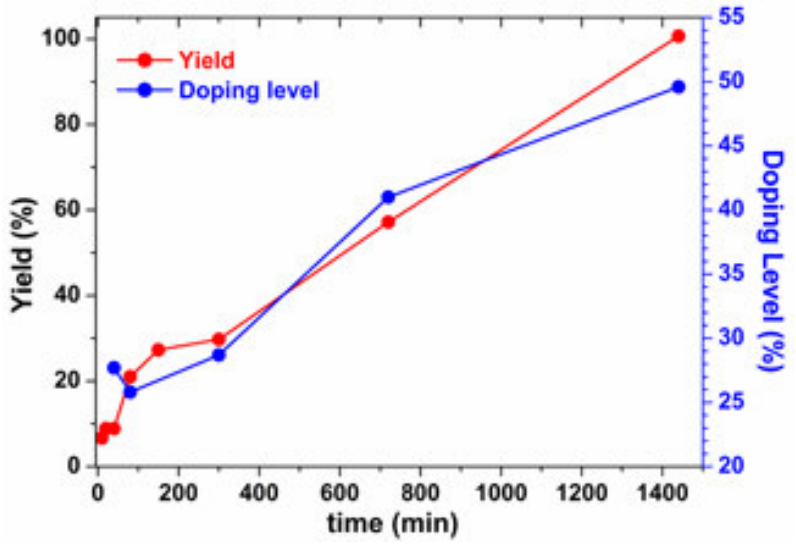

Figure 3.10 Variation of the calculated percent yield and incorporation of DSA to the polymer structure with respect to polymerization time

3.4.5 Electrical Conductivity Measurements

Same type of PPy samples were also synthesized to measure electrical conductivities at room temperature with a multimeter. One sample was prepared by only washing with methanol three times to leave it in its oxidized state. Another sample was also synthesized and washed with both methanol and aqueous ammonium solution for three times, respectively, to leave the sample in its reduced (neutral) state.

$$\sigma = 1/R = (I/V)*(\ln 2/\pi.L) \qquad (3.1)$$

Calculations for electrical conductivity were all based on the formula for conductivity in terms of resistivity and potential, where R: resistance (ohm), I: current (A), V: potential (volt), π: constant, L: thickness of sample layer (cm), σ: electrical conductivity (S/cm), given above. In that case, L value differed in both oxidized and reduced states for each steps as the thickness of sample layer was different in some parts. In other words, distribution of layer was not homogeneous while measuring the resistance. Nonetheless, results of these calculations appeared as reasonable expected values of conductivity for synthesized PPy nanostructures.

Table 3.6 Results of conductivity measurements of PPy nano-structured materials synthesized in both oxidized and reduced states

TRIALS	$R_{(OXIDIZED)}$ kΩ	$R_{(REDUCED)}$ kΩ	$\sigma_{(OXIDIZED)}$ $x10^{-3}$ S/cm	$\sigma_{(REDUCED)}$ $x10^{-5}$ S/cm
A	0.4	6.2	2.3	16.1
B	0.4	11.7	2.3	8.6
C	0.5	16.0	2.0	6.3
D	0.3	6.9	3.8	14.5
E	0.3	8.2	3.0	12.2
F	0.3	7.4	3.6	13.5

Material electrical conductivities in both neutral states and oxidized states with six separate measurements could be compared according to the conductivity calculations from resistivity values in kΩ (Table 3.6). Eventually, calculations simplified that bulk conductivity values of nano-networked PPys in oxidized states differed in a range of 10^{-3}, while those in reduced states of 10^{-5}. It is worth noting that low conductivity values of polymer at the oxidized state may stem from the technique used and could be higher in several magnitudes of order if they were measured on a single fiber as previously reported by Martin *et al.* [135].

3.4.6 Surface Area Evaluation

3.4.6.1 BET Analyses Results

The surface area measured using BET technique for such structures was greater than 500 m^2/g. This very high surface area with an additional nano-network structure made these materials excellent candidates for applications including gas or ion sensors [136], electrode materials for batteries, supercapacitors and fuel cells [137].

3.4.6.2 Response Surface Methodology Results

Reliability of BET analyses was also checked with response surface analyses. In this respect, maximum surface area of oxidatively polymerized PPy nanofibers in nano-networks was determined once more by response surface methodology. Quadratic response surface function described variations in surface area properties with related correlation coefficients by mapping a response surface over a particular region of interest. In this study, 9 data points were chosen to design a response surface by using two variables (Table 3.7). One variable was the mole ratio of oxidant to monomer, X1 and the other was the mole ratio of surfactant to monomer, X2 in their original units and in their coded units as X1' and X2'.

Table 3.7 Ranges and parameters of two variables between boundaries of (-0.95, 0.95)

Run	Variables in Original Units		Variables in Coded Units		Response (Surface Area)
	X1	X2	X1	X2	
A	2.1	5.9	-0.95	+0.95	642.7
B	4.0	5.9	0.00	+0.95	1049.2
C	5.9	5.9	+0.95	+0.95	802.4
D	5.9	2.1	+0.95	-0.95	572.1
E	4.0	2.1	0.00	-0.95	1046.3
F	2.1	2.1	-0.95	-0.95	422.6
G	5.9	4.0	+0.95	0.00	745.7
H	4.0	4.0	0.00	0.00	958.7
I	2.1	4.0	-0.95	0.00	487.5

$$X_i = \{ [V_i - (V_i^L + V_i^U)/2] \} / \{ [V_i^U - V_i^L]/2 \} \quad (3.2)$$

As optimized conditions proved that the most suitable design of PPy nano-network structures could be obtained when mole ratio of oxidant to monomer was 4:1 while that of surfactant to monomer 3:1, 4:1 and 5:1. Therefore, $V_i^L = 2$ and $V_i^U = 6$ were chosen as lower and upper boundaries in original units. The coded variable boundaries were also calculated in the range of (-0.95, 0.95) by using the formula above to express coded variable boundaries to determine response surfaces, where V_i^L is the lower bound and V_i^U is the upper bound. It was necessary to choose that range by taking

known ratios in a large range to minimize errors in the result. Thereafter, those data points were plotted as central composite design (Figure 3.11).

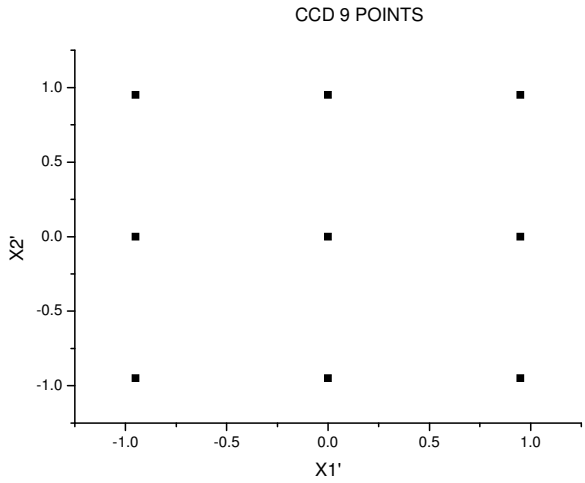

Figure 3.11 Central Composite Design Plot including 9 experimented data points.

To fit data on a response surface model, JMP by SAS software program was used. This operation developed a prediction formula below as a result of least square method via response surface analyses.

$$732.64556 + 27.311667\,\mathbf{X1} - 93.98833\,\mathbf{X2} + 148.195\,\mathbf{X1X2} + 270.10167\,\mathbf{X1X1} - 247.8783\,\mathbf{X2X2} = 0 \quad (3.3)$$

Then, maximum surface area was calculated from the formula as a result of JMP by SAS operated least square method given above. Therefore, 9 data points were maximized by using the equation above with MAT-LAB operation program (Figure 3.12).

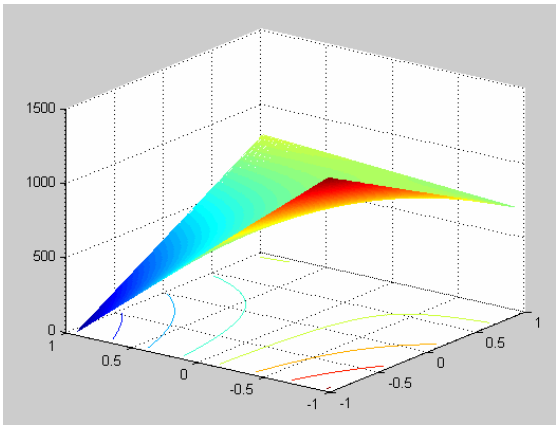

Figure 3.12. Maximized data points via MAT-LAB

According to the result of maximizing data points, maximum point has been detected at (-0.95, 0.95) as 642.7 m^2/g by JMP, which was higher than 500 m^2/g.

3.4.7 Electrochemistry

PPy-DSA films were potentiostatically deposited on a Pt button electrode from a solution of 0.1 M Bu_4NPF_6 in a water/MeCN (20/80) containing 0.03 M DSA and 0.01 M pyrrole. Then, polymer films were characterized by cyclic voltammetry in the monomer free electrolyte solution (Figure 3.13). A linear increase in anodic and cathodic peak currents as a function of scan rate indicated that an electroactive layer was deposited on the electrode surface and the oxidation/reduction processes were not diffusion limited. Therefore, electrochemical analyses confirmed that prepared materials including PPy nanofibers in nano-network structures were all electroactive. The half-wave potential ($E_{1/2}$) of the polymer was about 0.0 V *vs* Ag/Ag^+.

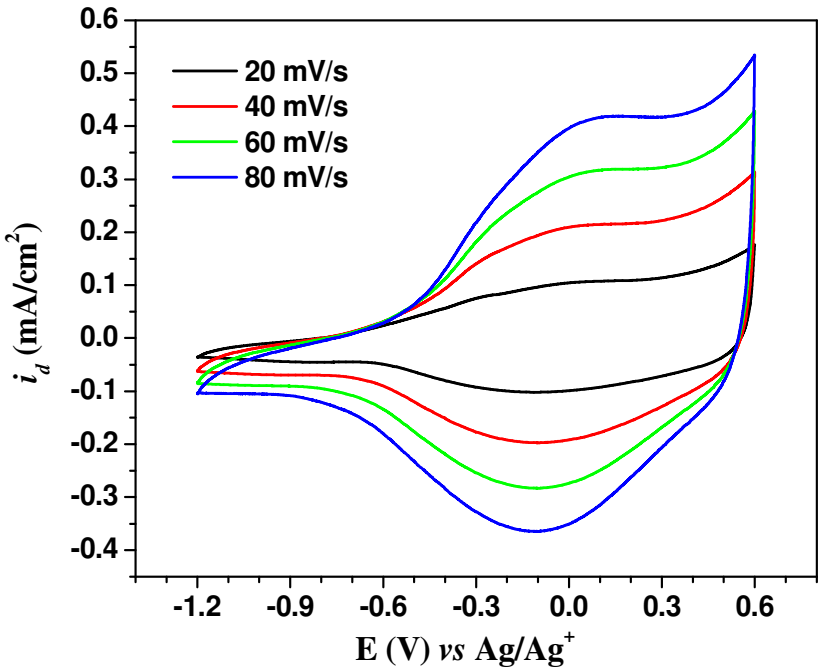

Figure 3.13 Cyclic voltammetry of PPy-DSA films in 0.1 M Bu_4NPF_6/MeCN at different scan rates; 20, 40, 60, 80 mV/s.

4. RESULTS AND DISCUSSION (B)

Advancement in modification of chemical synthesis using membranes as templates for both polypyrrole **(1-2)** and polythiophene **(3-4)** derivatives was successfully achieved. Application of suitable procedures by choosing right membrane types (Table 4.1) was responsive to assembling of nano-scaled structures in 1D. Investigation of morphology with SEM images resulted that any kinds of conducting polymers could be designed if the exact reaction medium is prepared. To accomplish desired nanostructures, appropriate experimental conditions were originated and some parameters like the outcome of membrane type, solvent type, set-up design, washing and membrane dissolution efficiency, concentration diversity, membrane pore size variation, layer construction mechanism on fiber compositions were all investigated step by step. Besides, there was a number of different aspects in terms of regularity, dissipation, orientation and geometrical design to compare all resulting nanostructures.

Table 4.1 Chemical compatibility of polycarbonate and alumina membranes;
R: Recommended NR: Not Recommended T: Prior Testing Recommended

Solvent Types	Polycarbonate Membrane	Alumina Membrane
Acetonitrile	T	R
Water	R	R
Hydrofluoric Acid	NR	NR
Toluene	T	R
Chloroform	NR	NR
Ethers	T	R
Ethyl Acetate	T	R
Hexane	R	R
Hydrochloric Acid	R	R
Hydrofluoric Acid	T	R
Isobutyl Alcohol	R	R
Nitric Acid	R	R
Petroleum Ether	R	R
Pentane	R	R
Sulfuric Acid	NR	R
Tetrahydrofuran	T	R
Toluene	T	R

4.1 One Dimensional (1D) Alignment of Polypyrrole (PPy) Nanotubules

4.1.1 Results for Optimization of Experimental Conditions

Commercially available PC membrane was started to be used for the research so that the solvent system, which was compatible with it, was tried to be optimized. All solvents in Table 4.1 was experimented except not recommended ones in terms of membrane compatibility. As a result, the most efficient system was established in an aqueous medium using PC membrane. In taking into account of iron (III) chloride dissolution, water was best, on the other hand, it was not desirable due to the 1% aqueous solubility of pyrrole. Though, communication between solvent and monomer was able to be raised by shaking aqueous solution of them well by using pyrrole monomer in its low concentrations.

It was observed that any selected solvent from Table 4.1 (except water) was evaporated if the arms of U-tube set-up was not sealed completely. Although water was used as the solvent, unsealed ends of U-tube caused a significant amount decrease in aqueous pyrrole solution as soon as the reaction was set at long hours. This effect in the set-up design was investigated by SEM imaging of products and yielded that dried ends of fibers were blocked as little solvent existed on top of the upper layer due to the lack of solvent diffusion (Figure 4.1). Figure 4.1A and its greater magnification, Figure 4.1B, revealed that formation of upper layer was impossible without any solvent in the upper arm of U-tube.

SEM images revealed that PPy nanofibers were supported with two layers. Bottom layer was made of PPy bulky structures and it covered bottom ends of PPy nanofibers as a support material. That supportive layer could be successfully observed as a landscape from top by SEM images seen in Figure 4.1A. Other side layer could also be imaged as a similar structure (Figure 4.1B).

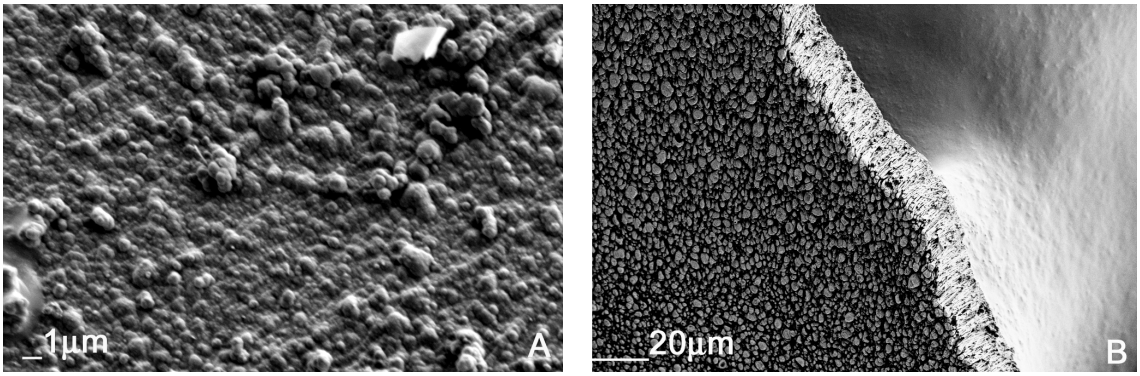

Figure 4.1 SEM image of supportive layer (A) at the bottom of PPy nanofibers (B) morphology of top layer

Strength of PPy nanofibers sandwiched between two whole layers was searched by disturbing this system with sonification technique. A 10 ml acetonitrile solution including a miniature amount of PPy sample was exposed to sonification during 20 seconds, 40 seconds, 5 minutes, 10 minutes and 30 minutes, respectively. Morphologies of these sonified particles taken at the end of each duration was imaged by SEM (Figure 4.2). PPy nanofibers could be observed after 20 seconds exposition to sonification as again undisturbed systems. In other words, PPy nanofibers could not be separated out of top and bottom layers in 20 seconds sonification.

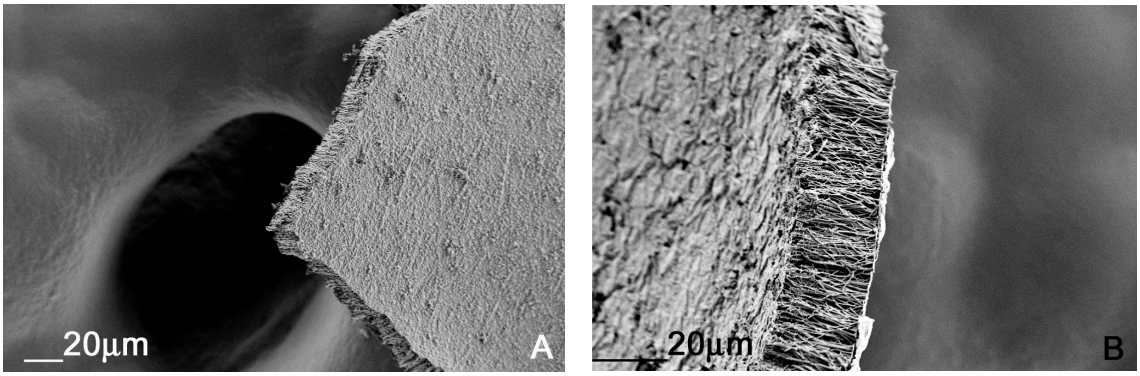

Figure 4.2 (A) SEM image of sonified PPy nanofibers during 20 seconds (B) in larger magnification

Next, PPy nanofibers were applied to 40 seconds sonification. SEM images pointed out they could not be damaged with such a short time sonification as seen in Figure 4.3A. The only distortion was peeling of one side layer so that PPy nanofibers embedded between two layers could be imaged in Figure 4.3B.

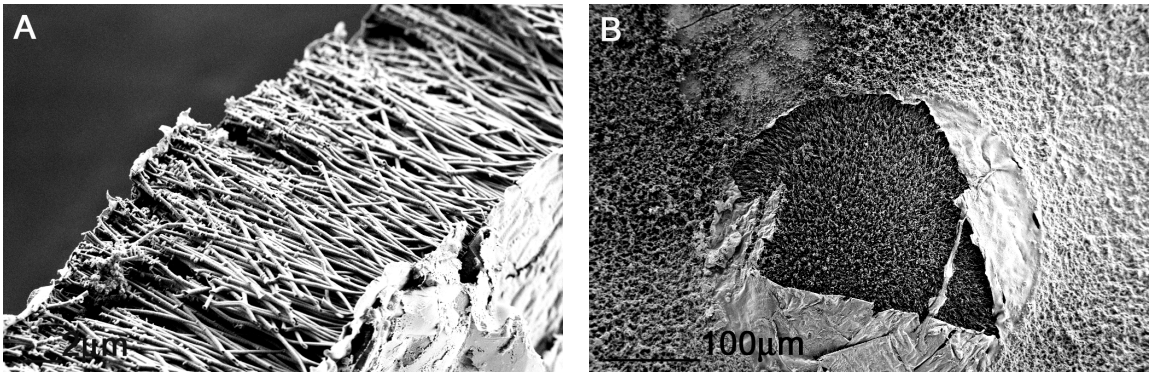

Figure 4.3 (A) SEM image of sonified PPy nanofibers during 40 seconds (B) morphology of peeling of one side layer

In 5 minutes application of sonification, some cracks among PPy layers were observed in Figure 4.4A. Moreover, some other pictures, in which peelings of one side layer were much more in the system in a longer time exposition, were also taken. One example to those layer cracks could be seen in Figure 4.4B.

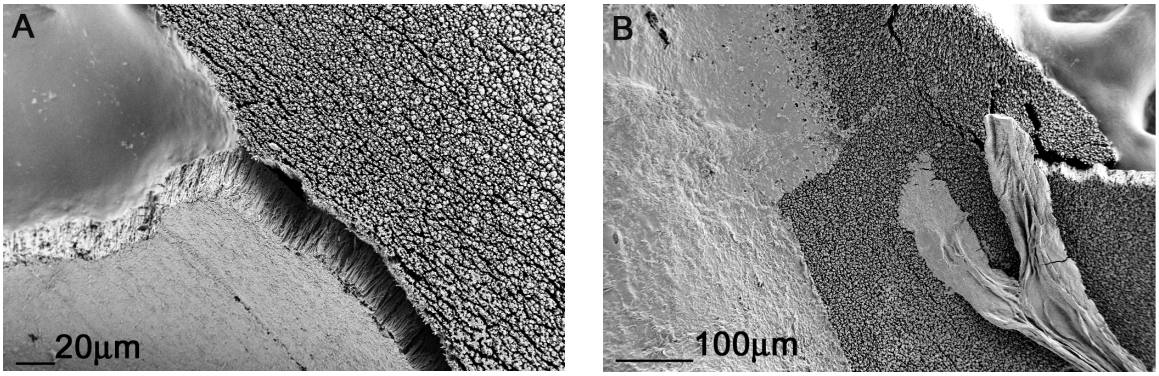

Figure 4.4 SEM image of sonified PPy nanofibers during 5 minutes (A) crack formation (B) peeling of one side layer after crack formation

After 10 minutes exposition, bottom layer separation was observed (Figure 4.5). Though, PPy nanofibers could not be separated, they all still kept their tendency to align through the layers. Their tendency could easily be seen in a larger magnification (Figure 4.5B).

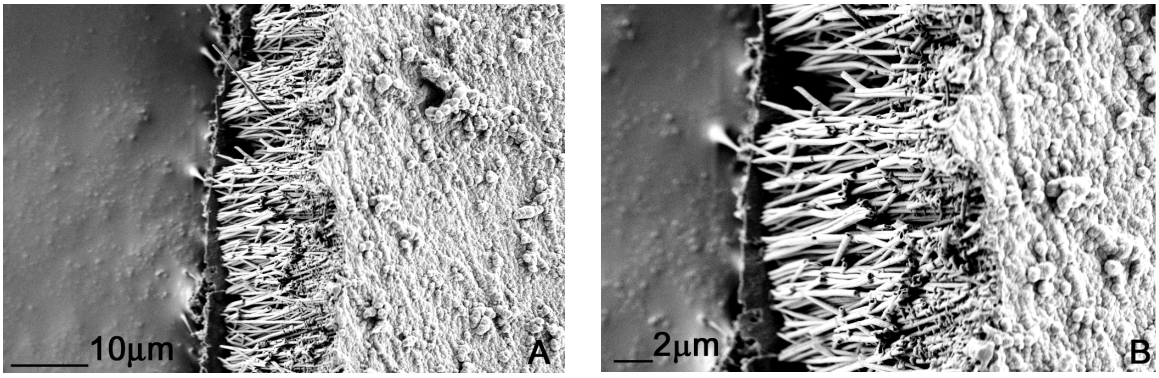

Figure 4.5 SEM image of sonified PPy nanofibers during 10 minutes (A) bottom layer separation (B) magnified portion of (A)

In 30 minutes, 1D alignment of PPy nanofibers was still kept between two layers (Figure 4.6A). However, sonification increased the layer cracks more than in 10 minutes. Additionally, some more peelings of those bottom and top layers were observed (Figure 4.6B).

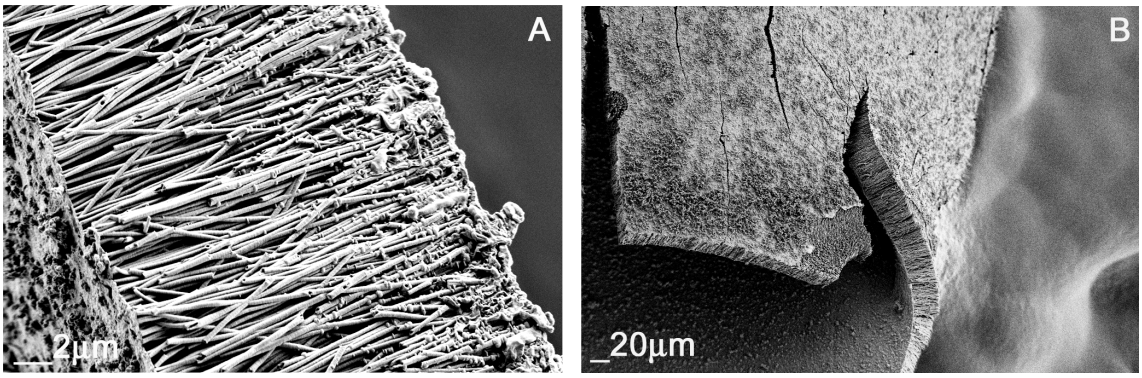

Figure 4.6 (A) SEM image of sonified PPy nanofibers during 30 minutes (B) SEM picture of a layer crack

Although some more disturbance on the system caused refractions of layers, PPy nanofibers still kept their tendency to deterioration (Figure 4.7). This last step resulted that it was not easy to separate those aligned PPy nanofibers due to the strong interactions as a consequence of secondary bond attractions in both PPy nanofibers and between them and the two supportive layers.

Figure 4.7 SEM image of sonified PPy nanofibers during long hours

Fiber formation mechanism was supplied by observations done by SEM images to understand their behavior between layers. When zoomed, it was seen that PPy nanofibers could be aligned without any separation, though, they were not all laid from one layer to the other side layer as whole fibers (Figure 4.8A). If magnified to larger scales, then the image could easily prove that there existed a mixture of PPy nanofibers in various lengths (Figure 4.8B).

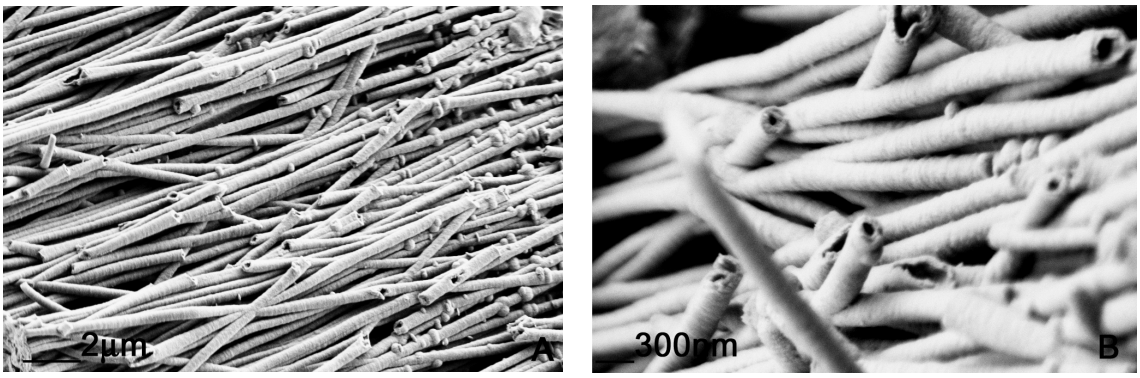

Figure 4.8 (A) SEM imaging of PPy nanofiber alignment between two layers (B) in larger magnification of (A)

It was also confirmed by SEM images that those aligned PPy nanofibers were tubule like nanostructures, namely, PPy nanotubules (Figure 4.9A). As aimed, it was important to check the fiber structures in terms of morphology. Those hollow tubes include one outside layer, one another inside layer and an additional thick, bulky coating sandwiched between outside and inside layers (Figure 4.9B).

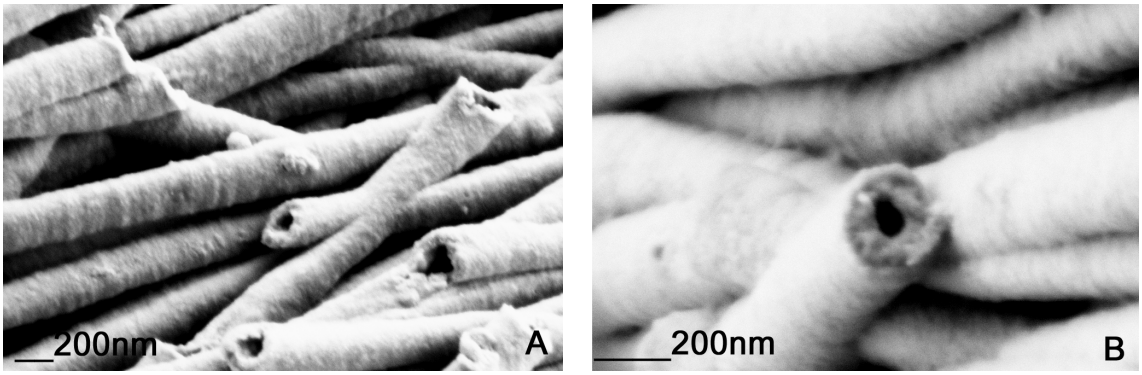

Figure 4.9 (A) SEM picture of PPy nanofibers as tubule like nanostructures (B) One selected PPy nanotubule in larger magnification

The approximate whole diameters of PPy nanotubules and also of inside hallow tubes could be easily determined by SEM imaging. One example of this measurement could be detailed in Figure 4.10. In this image, one of the arbitrarily chosen fiber's outside diameter was measured as ca. 286 nm, whereas the inside diameter was ca. 115 nm. In the leading of those measurements, the overall average approximation for diameters of PPy nanotubules could be taken in a range of 110 nm to 350 nm.

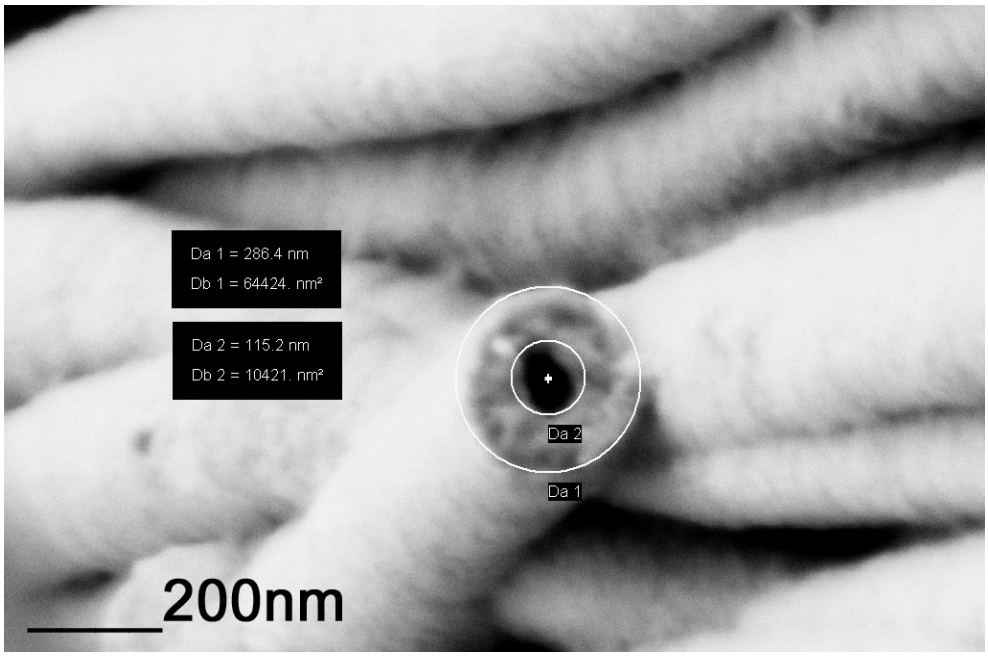

Figure 4.10 SEM image of one PPy nanotubule showing outside and inside tubule diameter measurement

As a result, polymerization of pyrrole produced well-ordered threadlike structures between double-sheet layers. Figure 4.11 depicts elongation of PPy nanofibers that is clearly packed between sheets after dissolution of PC membrane with chloroform.

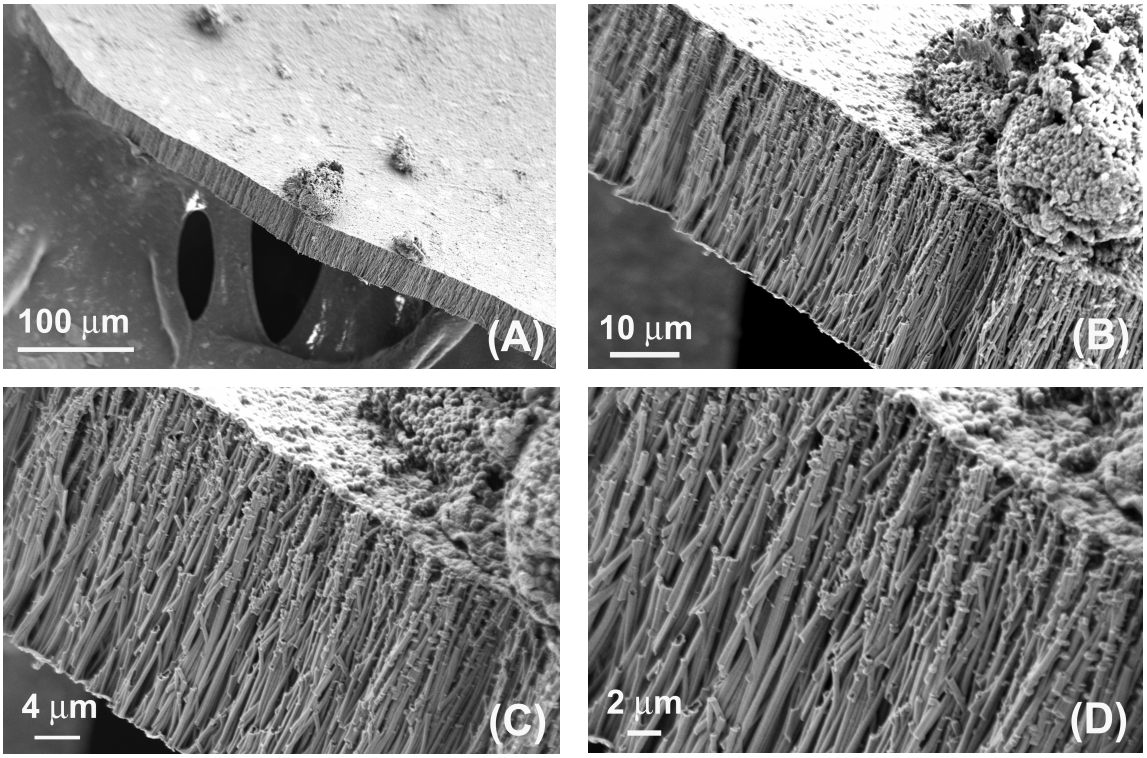

Figure 4.11 SEM images of threadlike nanostructures of PPy in different magnifications.

4.2 One Dimensional (1D) Alignment of Poly(N-Methylpyrrole) (P(NMPy)) Nanotubules

4.2.1 Results for Optimization of Experimental Conditions

It was clarified that no P(NMPy) nanofiber formation could be observed if alumina membrane was chosen as a template instead of PC membrane in the same optimized experimental conditions. Images taken via SEM displayed that three different structures could be seen when alumina membrane was used (Figure 4.12). Figure 4.12A and Figure 4.12B indicated formation of beads connecting to each other including

branches made of P(NMPy). One other type of structure was also a thin layer formation placed among these branches, but no fiber formation was observed (Figure 4.12C). A few of short P(NMPy) nanofibers could be observed, which were embedded into the system (Figure 4.12D). Though, whole P(NMPy) nanofiber alignment could not be noticed from those images, which proved alumina membrane was not applicable to this environment. However, one thing should be mentioned here that suitable environment can allow fiber formation using alumina membrane if a different system can be prepared.

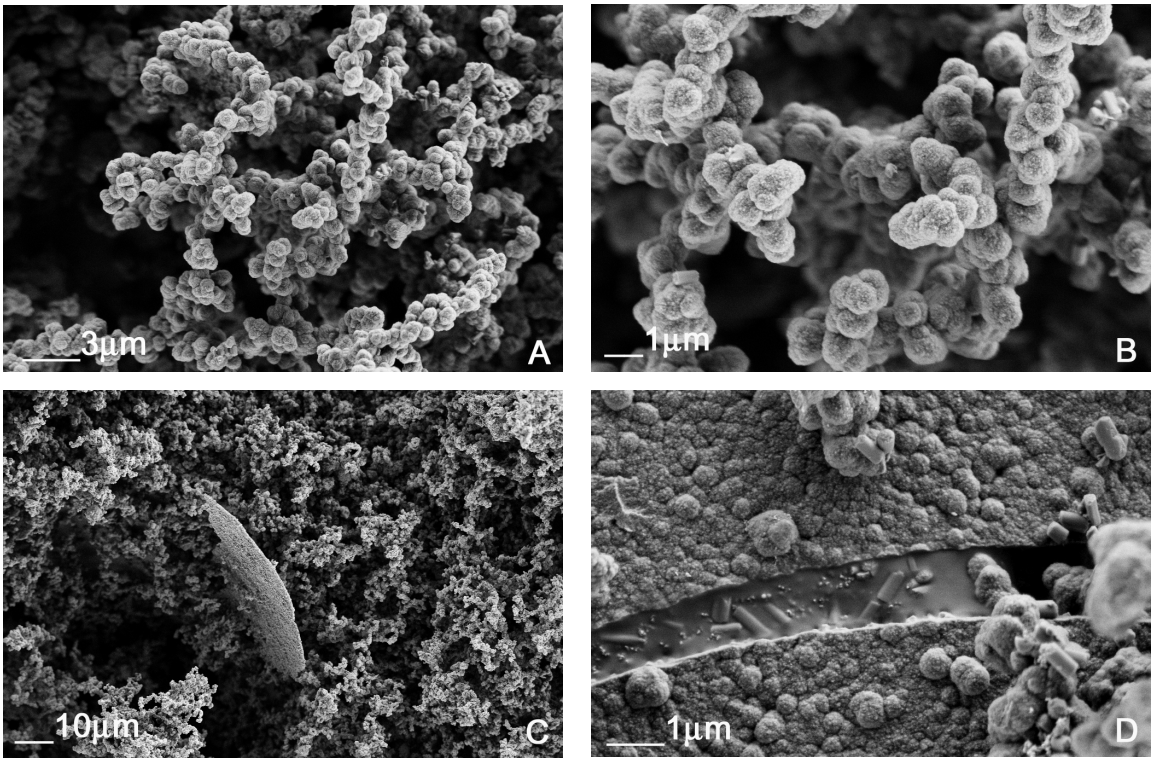

Figure 4.12 SEM images of P(NMPy) structures if alumina membrane is used instead of PC membrane

Desired bottom and top layer formations were observed in the case of P(NMPy) nanofiber alignment in 1D. The only difference was that layers were made of P(NMPy) when compared with those of supportive layers of PPy nanotubules. This was again confirmed with SEM images (Figure 4.13).

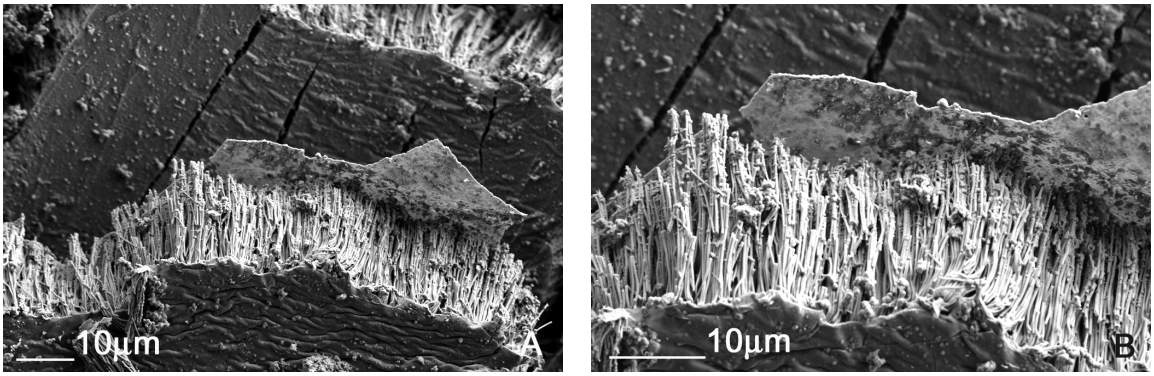

Figure 4.13 SEM images of P(NMPy) nanofibers showing layer formations in different magnifications

P(NMPy) nanofibers were all aligned between two layers, though, one layer was enough to support fibers without any deformation in the system (Figure 4.14).

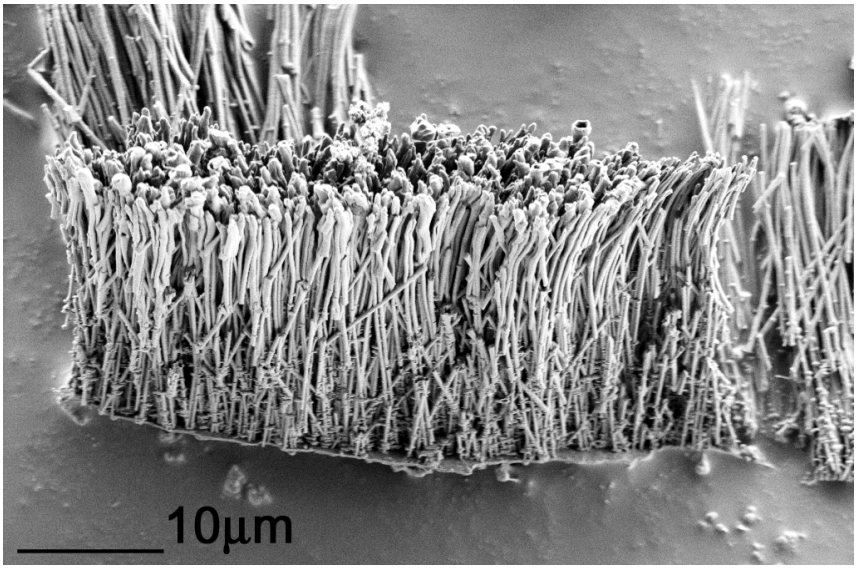

Figure 4.14 SEM image of P(NMPy) nanofibers supported by only one layer

Horizontal alignment of P(NMPy) nanofibers could be imaged, which gave some information about variety in fiber lengths between two layers (Figure 4.15A). Therefore, the same type packing behaviour with PPy nanotubules was observed in the case of P(NMPy) nanofiber alignment in 1D. Although they all were dispersed between two panels, they still had a strong correlation with the layers (Figure 4.15B).

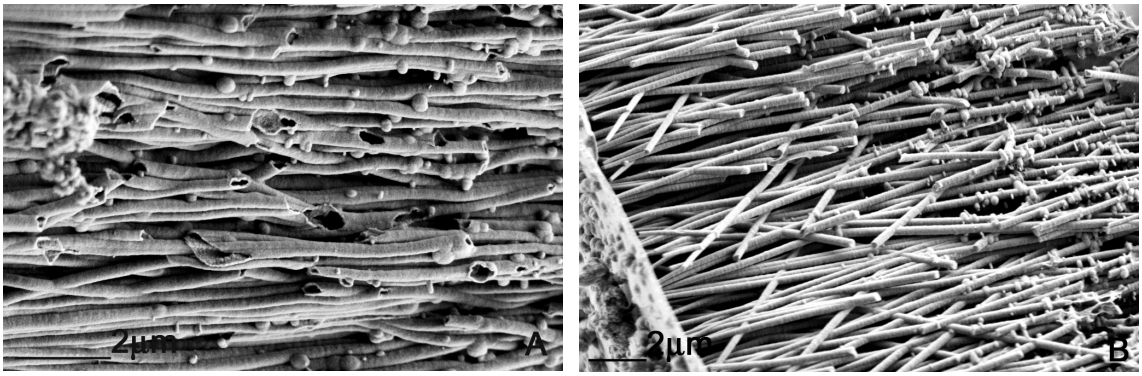

Figure 4.15 (A) SEM image of P(NMPy) nanofibers showing variety in fiber lengths (B) dispersion of P(NMPy) nanofibers between two layers

Figure 4.16A indicates whole layer packaging including a crack, and a magnified image of this crack including P(NMPy) nanofibers coming out of it is in Figure 4.16B. One of a layer crack from bottom was easy to see from Figure 4.16B, which confirmed that only one layer was also sufficient to align them in 1D.

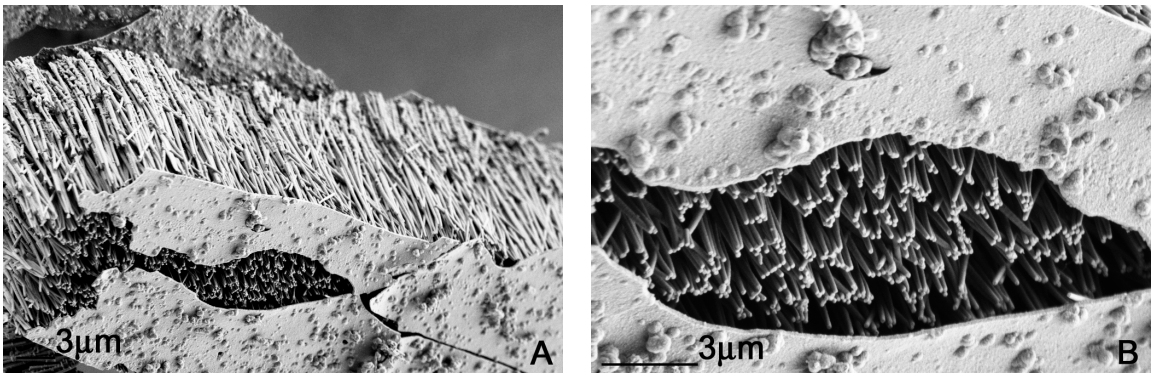

Figure 4.16 (A) SEM picture showing packing behaviour of P(NMPy) nanofibers (B) in larger magnification

The image of Figure 4.17A belongs to P(NMPy) nanofiber formation in case of the only difference in synthetic method was the molarity of NMPy change to 0.1 M. This study resulted that ends of P(NMPy) nanofibers were closed due to the increase in molarity of NMPy, while 0.05 M of NMPy use allowed open-ended P(NMPy) nanofibers because of dilute medium (Figure 4.17B). Figure 4.17B also proved that all P(NMPy) nanofibers were in the shape of tubes including outside and inside layers together with a thick bulky part between them, the same as PPy nanotubules. In other words, the more the concentration of monomer in this environment, the less the possibility of hollow formation with open-ends. Decrease in amount of NMPy was

allowed less interaction between NMPy and PC membrane in the reaction medium. Thereafter, no dissolution of PC membrane was observed.

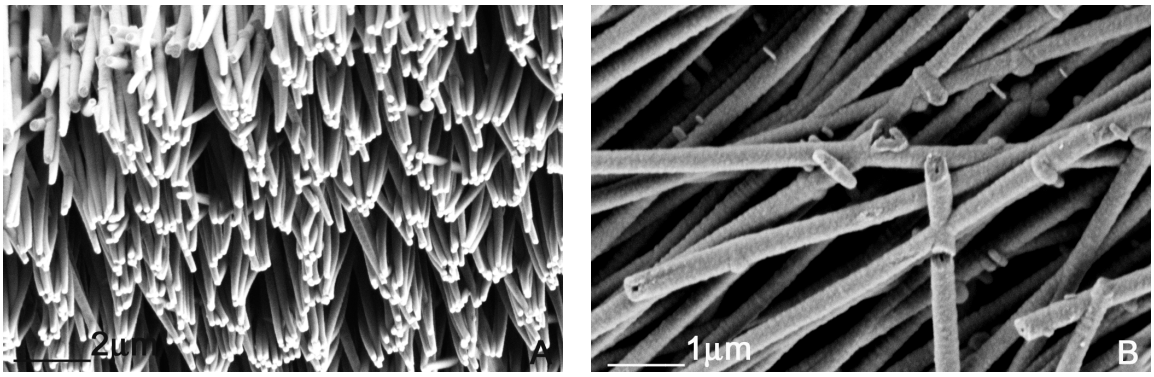

Figure 4.17 SEM pictures of (A) P(NMPy) nanofibers with close ends (B) open-ended P(NMPy) nanofibers

Figure 4.18 shows one example for one-side layer formation including some P(NMPy) network type structures in different magnifications. SEM images prove there exist some other network type P(NMPy) structures in the sample.

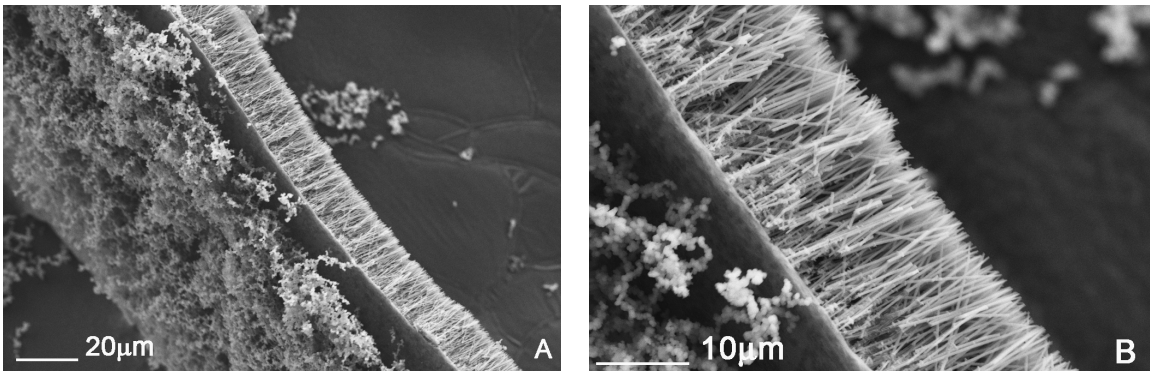

Figure 4.18 SEM images of (A) network type P(NMPy) structures on one-side layers (B) in larger magnification

It is evident from Figure 4.19 that effective polymerization of NMPy produced well-ordered tubule like P(NMPy) nanotubules elongated between double-sheet layers after dissolution of PC membrane with chloroform. Figure 4.19 illustrates SEM images of these resulting P(NMPy) nanotubules with a successful 1D design in four different magnifications.

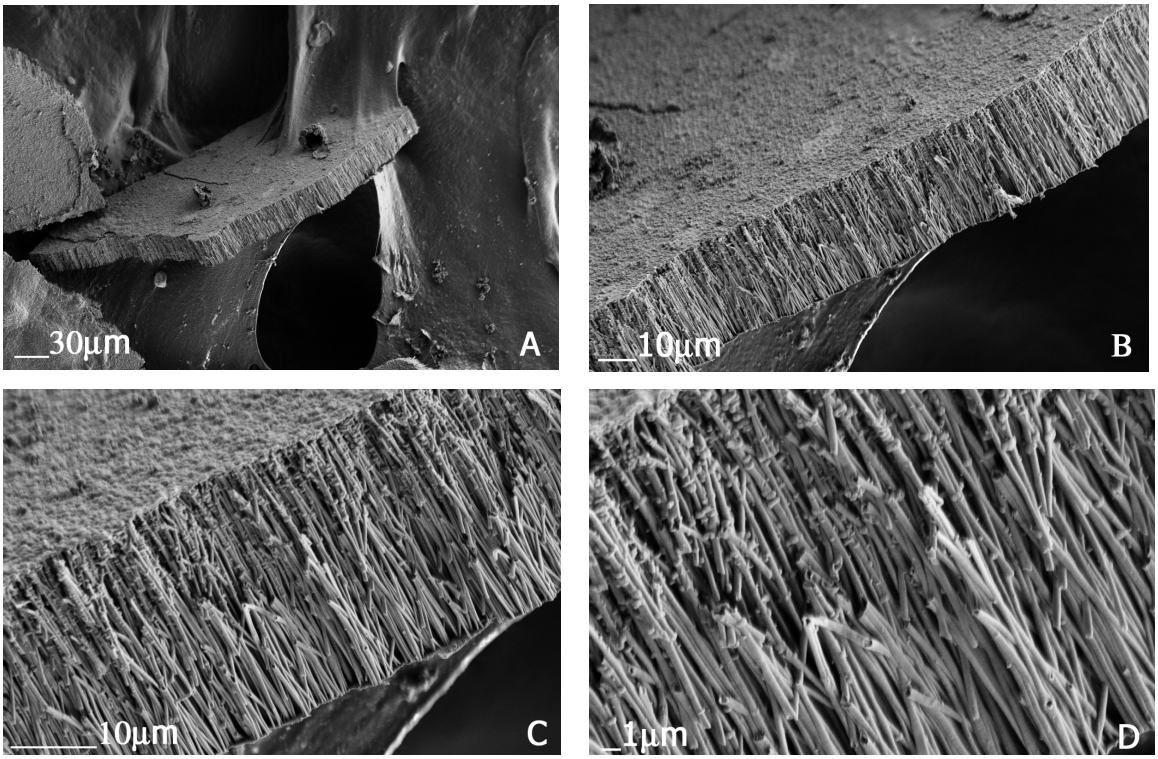

Figure 4.19 SEM pictures of P(NMPy) 1D nanotubule structures in four different magnifications

4.3 One Dimensional (1D) Alignment of Poly(thiophene) (PTh) Nanotubules

4.3.1 Results for Optimization of Experimental Conditions

At initial stages of optimization, as thiophene and its derivatives are immiscible with water, another type of solvent system was tried to be found by working with PC membrane. As experimented, acetonitrile itself was not enough to prepare a solution, where iron (III) chloride could oxidize thiophene. Although the color turned into black, a sign for oxidation of monomer, PTh nanotubule formation could not be observed. Therefore, solvents like isooctane or toluene, of which oxidation rate were greater than acetonitrile, were tried to be used. On the other hand, both solvents were tested and test results indicated that iron (III) chloride could not be dissolved in toluene although thiophene was miscible with toluene. Then, in the following investigation, suitable solvent type for both membrane and monomer was detected. There was a chance for

ethanol to prepare such an efficient system to obtain nanotubule formation. However, no oxidation was observed when the system was prepared by using iron (III) chloride, ethanol and thiophene. A mixture of miscible solvent system by mixing toluene and ethanol was also studied, but the result was insufficient. Propylene carbonate could also dissolve iron (III) chloride, which was miscible with thiophene and was recommended with PC membrane. Nonetheless, morphology studies confirmed that prepared environment could not build nanostructures of PTh (Figure 4.20). Experimental repetitions using propylene carbonate as the solvent resulted in almost same type of morphologies seen in Figure 4.20A and Figure 4.20B.

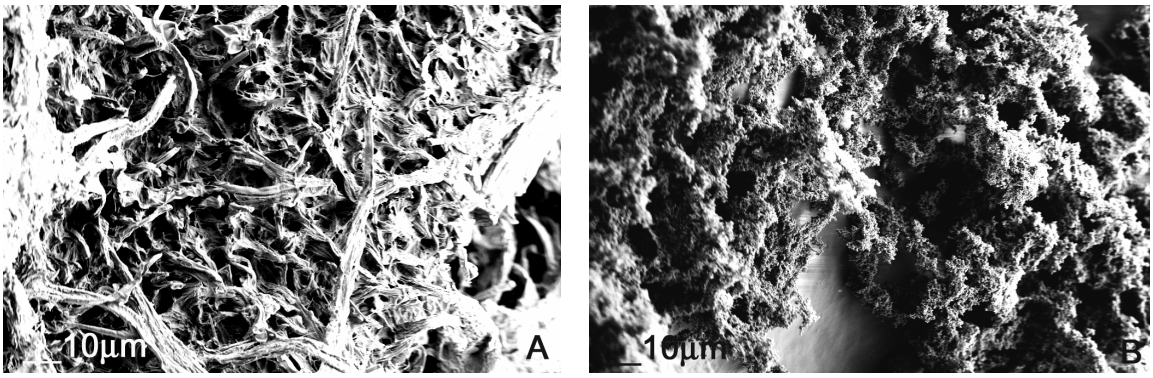

Figure 4.20 SEM images of resulting PTh structures in a reaction medium prepared with propylene carbonate

Based on the fact that, PC membrane was not so compatible with acetonitrile, investigations were turned towards finding another type of membrane. Alumina membrane was known with its compatibility in so many solvent systems. First, acetonitrile environment was repeated by using iron (III) chloride as one of the strongest oxidizing agent in the presence of thiophene. As desired nanostructures could not be obtained, eventually, any other effects, for instance salt effect, were also investigated. In the end, it was discovered that the system worked by using additional dopant ion as $LiClO_4$, which supplied much more negative charges to the system so that polymerization occurred through the pores of alumina membrane resulting PTh nanotubules.

The optimized solvent system for 1D alignment of PTh nanotubules was 0.1 M $LiClO_4$/ACN. It was detected with SEM images that PTh nanotubule alignment was not observed if the molarity of thiophene was decreased to 0.05 M (Figure 4.21). Although observations could not detect any difference in the system, morphology changes could

be imaged. The rest was bulky structures with PTh beads connecting to each other as branches seen more clearly in Figure 4.21B.

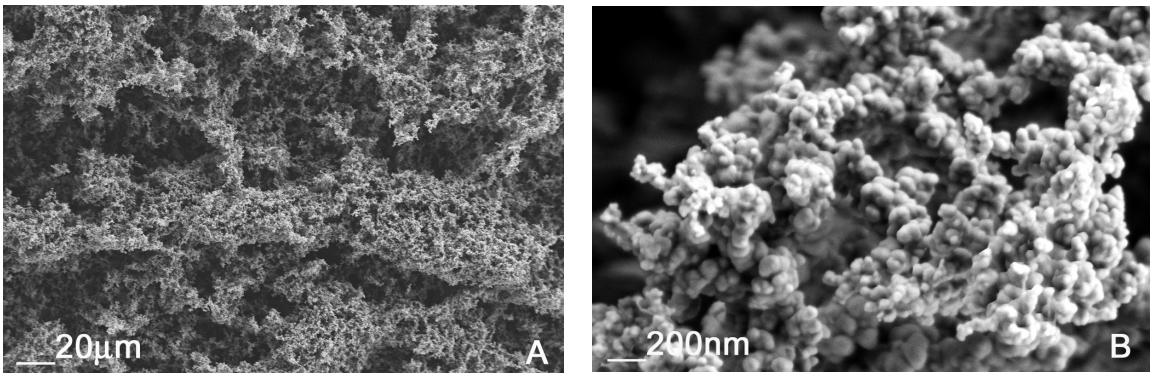

Figure 4.21 (A) SEM micrograph of synthesized PTh structures when the molarity of thiophene was reduced in amount (B) larger magnified micrograph of (A)

An evidence for PTh nanotubule formation including holes can be clearly seen from Figure 4.22A, which was a result of different commercial alumina membrane use. This may be due to poor electrostatic interactions between positively charged PTh backbone and less negatively charged pore walls of alumina membrane. Another case was the use of suitable alumina membrane, about which was thought as including some more negative charges on pore walls so that the electrostatic interaction was stronger (Figure 4.22B).

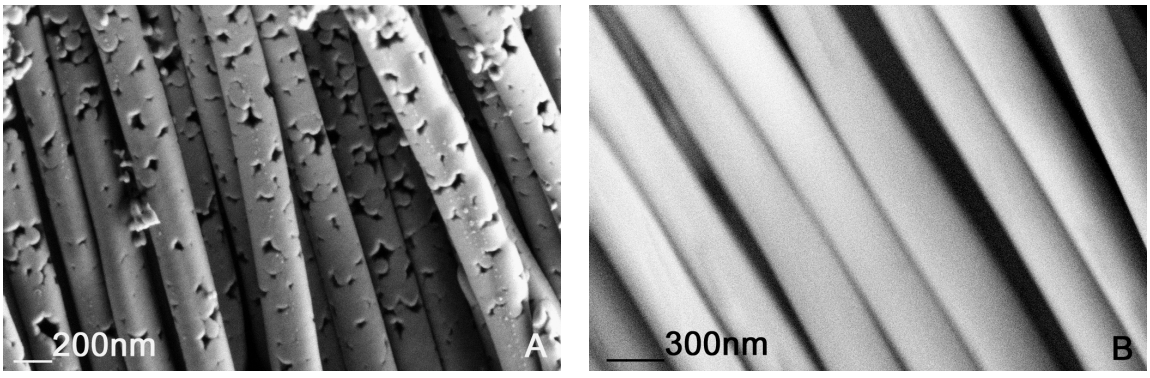

Figure 4.22 SEM images of PTh nanotubules synthesized with two different types of alumina membranes: (A) poor interaction (B) strong interaction

When pore size of alumina membrane was decreased to 0.1 microns, diameter ranges of PThs could not be decreased to around 100 nm as in theory. One case for diameter measurement of synthesized PTh nanotubules by using alumina membrane with pore sizes of 0.1 microns can be seen below (Figure 4.23). The diameter ranges of

PTh nanotubules were determined in two measurements like ca. 280 nm and 300 nm as an example. Therefore, overall average diameter range was detected between 200 nm and 350 nm.

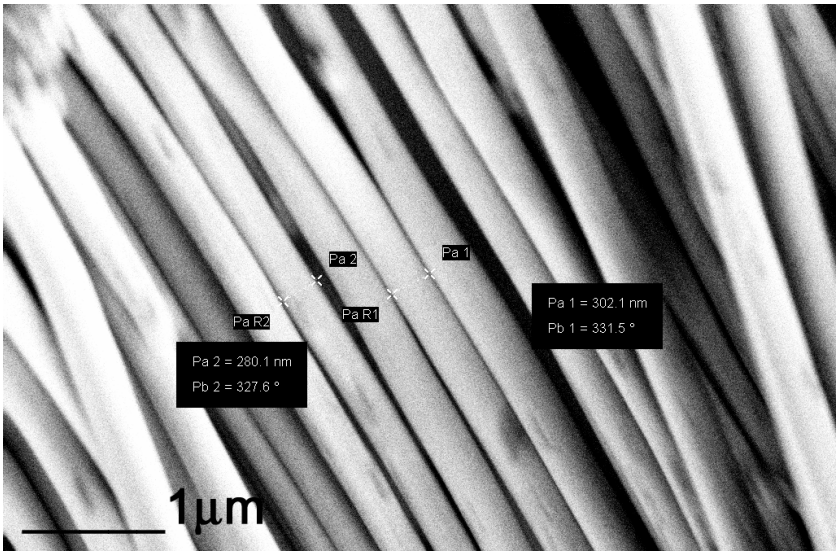

Figure 4.23 SEM image showing diameter measurement of arbitrarily chosen PTh nanotubules

Observations from SEM images of PTh nanotubules confirmed that bottom layer had stronger electrostatic attractions with bottom ends of fibers than the top layer. Thus, PTh nanotubules were packed in groups and separated from each other on a bottom layer (Figure 4.24B). It was such a powerful attraction among fibers and bottom layer that it did not allow them to separate from bottom. PTh nanotubules were aligned in such a way that they could be separated as groups seen from top view in Figure 4.24A.

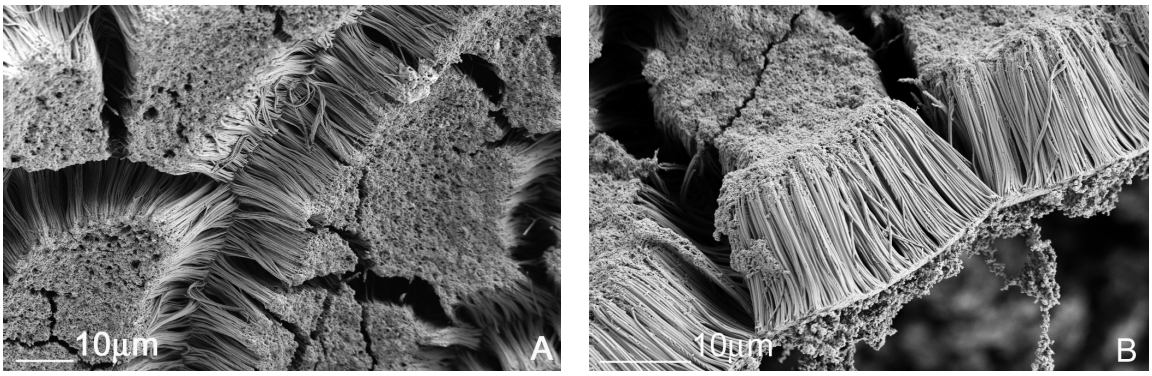

Figure 4.24 SEM pictures of PTh nanotubules attached on a bottom layer (A) strong combination of ends of nanotubules (B) group behaviour

When the molarity of thiophene in optimized conditions was decreased below 0.05 M, materials taken out of membrane pores could not be handled. It was observed that all materials were dissolved together with membrane, which was an unusual behaviour. This might be based on incomplete polymerization, where a mixture of low molecular weight soluble oligomers like dimers, trimers, etc. was generated in the system. On the other hand, although membrane together with its contents could be separated after dissolution, PTh nanotubule formation could not be observed when 0.1 M or 0.3 M of thiophene was used. Morphologies of these structures were similar to those SEM pictures in Figure 4.21. Eventually, the best molarity to be used for PTh nanotubule synthesis was determined as 0.5 M.

Success in 1D alignment of PTh nanotubules was revealed with an effective template polymerization of thiophene, which produced well-ordered PTh nanotubules attached to a sheet. Figure 4.25 depicts SEM images of these aligned PTh nanotubules after dissolution of alumina membrane in four different magnifications.

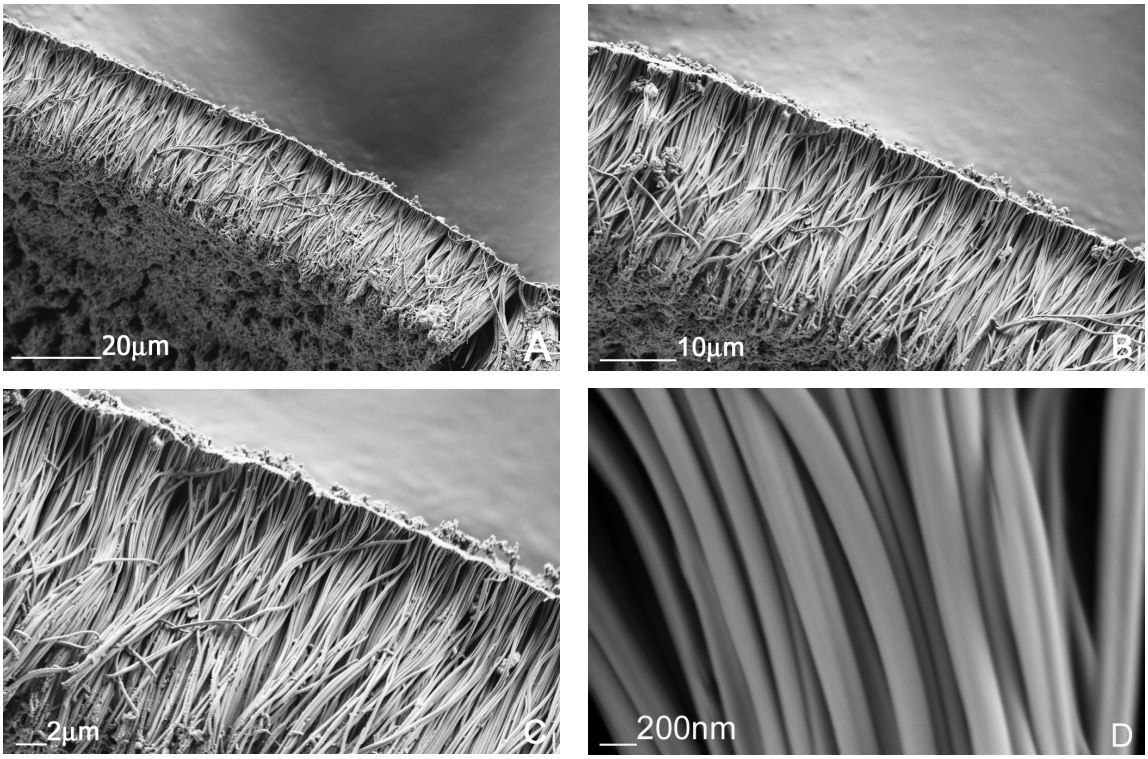

Figure 4.25 SEM pictures of PTh 1D nanotubule structures in four different magnifications

4.4 One Dimensional (1D) Alignment of Poly(3,4-ethylenedioxythiophene) (PEDOT) Nanopipes

4.4.1 Results for Optimization of Experimental Conditions

After discovering right membrane type for thiophene and its derivative- EDOT (3, 4-ethylenedioxythiophene) as alumina membrane, an appropriate solvent system was investigated for EDOT. Hence, two separate systems without using membranes were prepared. First, EDOT and iron (III) chloride were dissolved in acetonitrile separately, then they were mixed. At initial stages of oxidation, dark green color was observed. After one hour mixing, no color change was observed. However, when the same system was prepared with additional use of $LiClO_4$ as dopant, color change from dark green to dark blue was observed (Scheme 4.1). One another result of this work was that agglomeration occurred in the first system, while well-dispersed homogeneous solution was resulted in the latter. All these observations indicated that oxidation rate of the latter case was greater than the first due to the dopant ion effect. This might depend on the amount of radicals, which was less than amount of polarons or bipolarons in the first case.

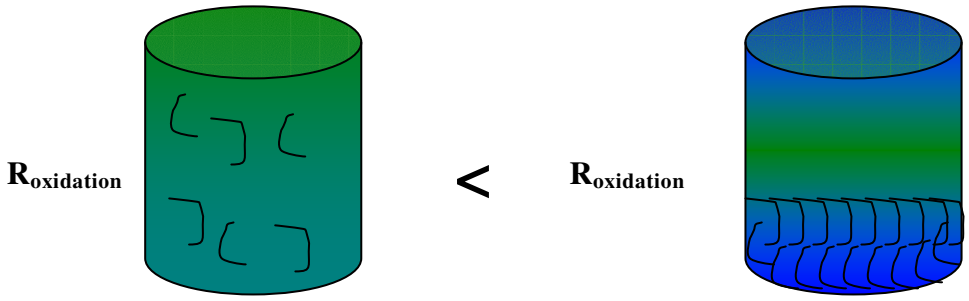

Scheme 4.1 Change in rate of oxidation (R) in a reaction medium prepared with EDOT (I) in the absence of $LiClO_4$ as dopant (II) in its presence

Since effective dissolution of alumina membrane produced separately aligned PEDOT nanotubules, it was explicitly understood from SEM micrographs that lack of membrane dissolution prevents separation of these tubules. Resulting PEDOT nanotubules were all obtained as structures stuck on each other including undissolved parts of alumina membrane among them. Therefore, this sticky behaviour may occur not only between tubules seen in Figure 4.26A, 4.26C and 4.26D but also it may stand on top of tubules as a new layer, which causes unseparation again (Figure 4.26B).

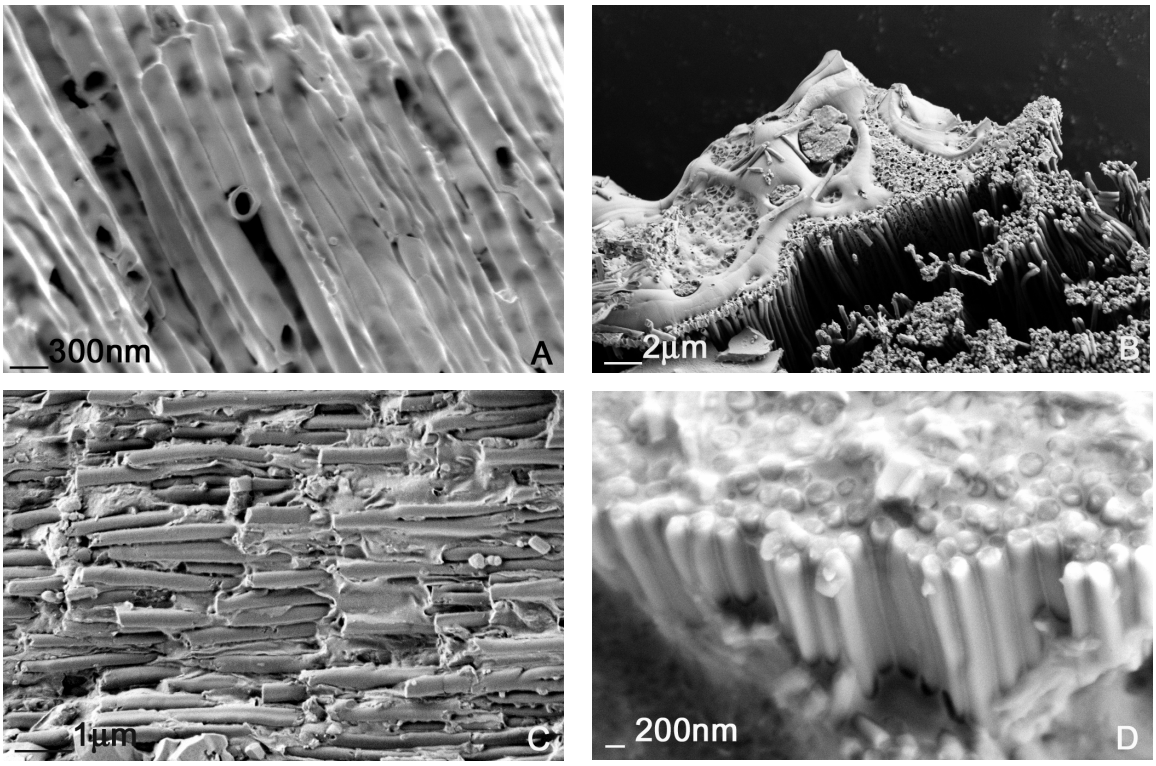

Figure 4.26 SEM images of PEDOT nanotubules including some portions of undissolved alumina membrane: (A), (C), (D) between tubules (B) collection on top

In order to understand the effect of filtering style on the formation of PEDOT nanopipes in desired diameters and shapes, different types of filtering techniques were experimented. One alternative was filtering out these PEDOT nanopipes using a filter paper, but it was observed that these filter papers were affected by aqueous hydrofluoric acid solution, which was interpreted from SEM images (Figure 4.27A). It was clear that fibers of filter papers were disorganized with PEDOT nanopipes so that pipes could not be separated from filter papers seen in Figure 4.27B.

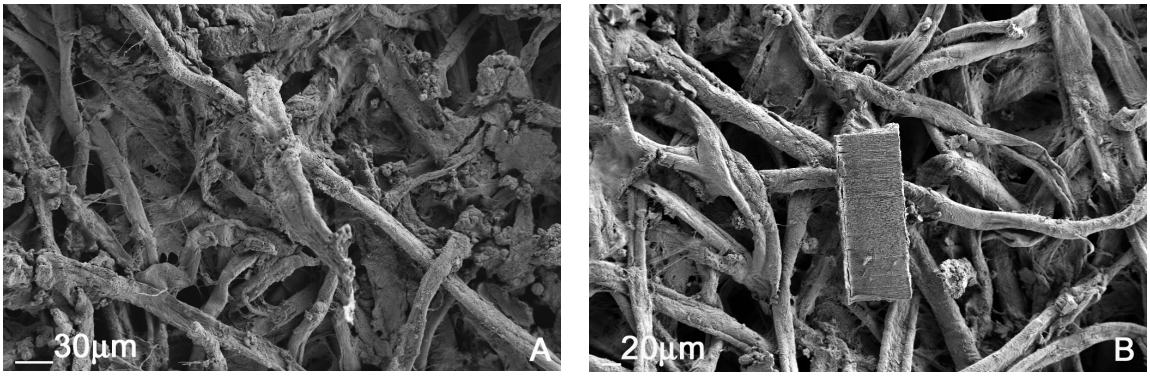

Figure 4.27 SEM images depicting embedded PEDOT structures inside fibers of filter paper

One portion of cross-sectional view of supportive layers was also observed with SEM imaging. SEM images in Figure 4.28 interprets that hollow-like structures of these PEDOT nanopipes can be clearly observed from their open-sided ends when a layer was separated from a bunch of tubules. These structures were magnified in Figure 4.28B to provide clear landscape view of pipes attached from one ends onto one supportive layer.

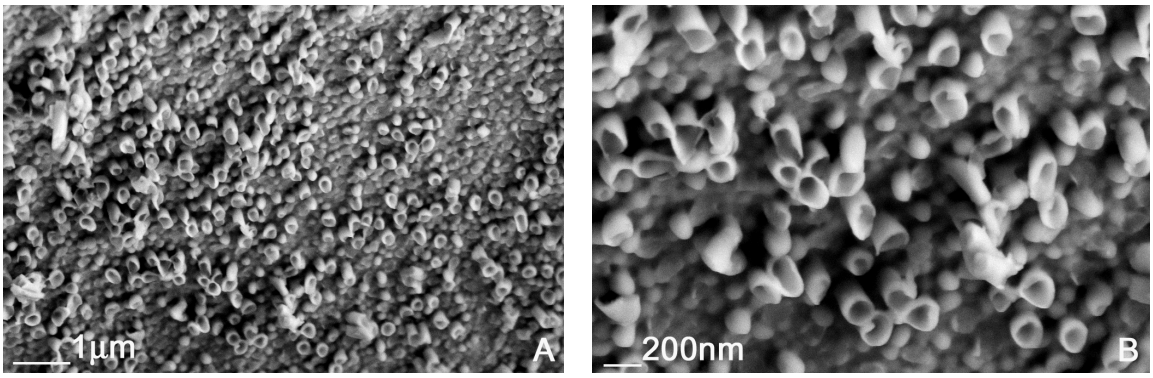

Figure 4.28 (A) SEM image showing a landscape of embedded PEDOT nanopipes in a supportive layer (B) in larger magnification

Figure 4.29 illustrates that PEDOT nanopipes can be packed as a whole layer in 1D due to strong intermolecular interactions between pipes, or created as units of packed structures, which may be categorized according to package properties of these tubules: bunches with packing all pipes including no unfilled spaces among them in a hazelnut-like shaped unit (Figure 4.29A), bunches with one-way oriented PEDOT nanopipes including voids among units (Figure 4.29B), or self-organized pipes in all directions with some voids among units (Figure 4.29B, 4.29D). However, they also behave as separate bunches with huge voids among those units (Figure 4.29B), though

growth of PEDOT nanopipes may be self-organized one directionally with a one-sided sheet from their one ends like in Figure 4.29C.

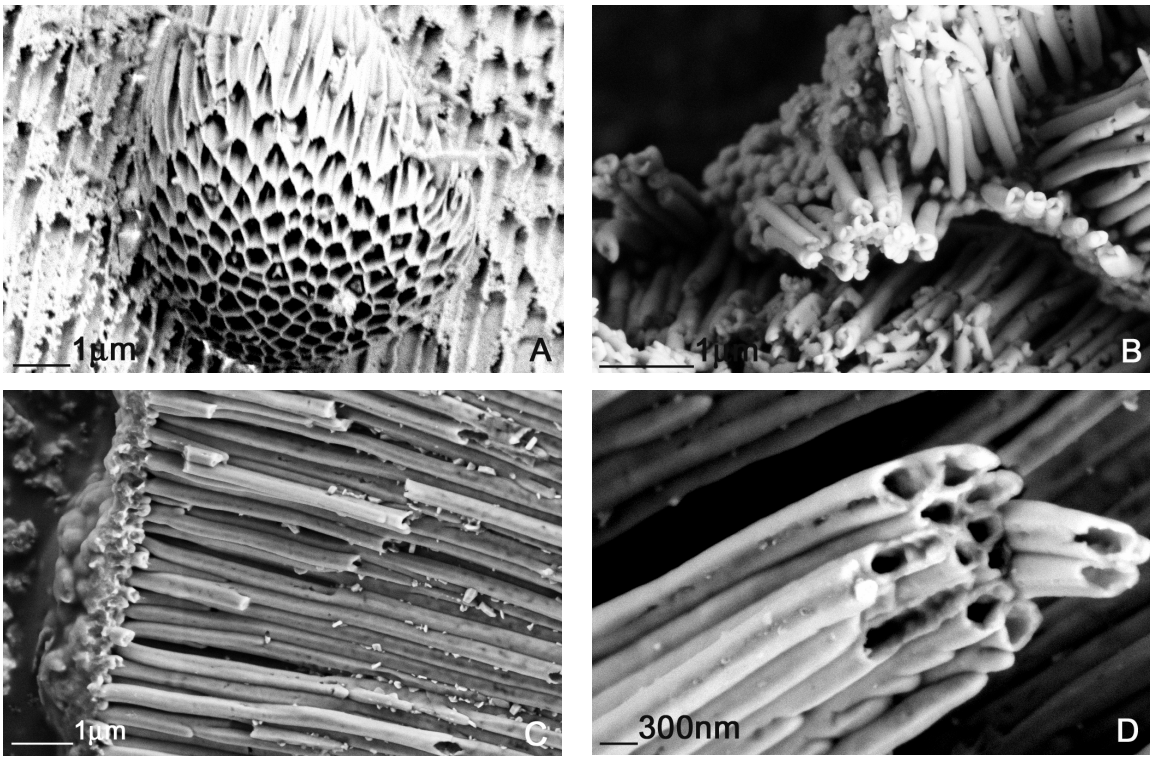

Figure 4.29 SEM pictures of PEDOT nanopipes illustrating different packaging behaviours

One unsupportive portion of layers could be imaged by SEM micrographs, in which some of ends of PEDOT nanopipes were attached stronger than the rest so that a bulk image of this supported part of one layer was such a good evidence for the existence of layers on their both upper and bottom ends (Figure 4.30).

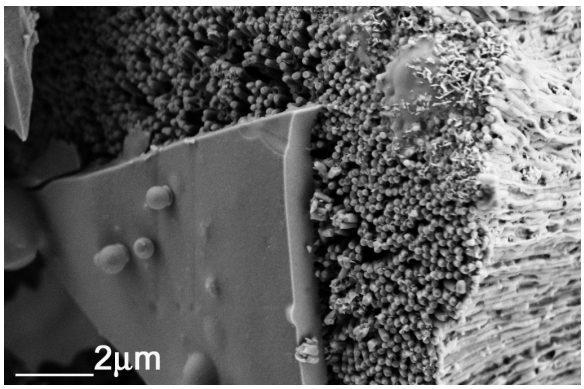

Figure 4.30 SEM picture of a portion of supportive layer with unsupportive ends of PEDOT nanopipes

So many repetitions of experiments resulted two type end behaviors of PEDOT nanopipes. Some were produced with open ends, one example given in Figure 4.31A, and some were close-ended PEDOT nanopipes like in Figure 4.31B or in Figure 4.30. It was understood from these SEM images that ends of tubules were enclosed as soon as the concentration of EDOT is raised or the polymerization time is extended.

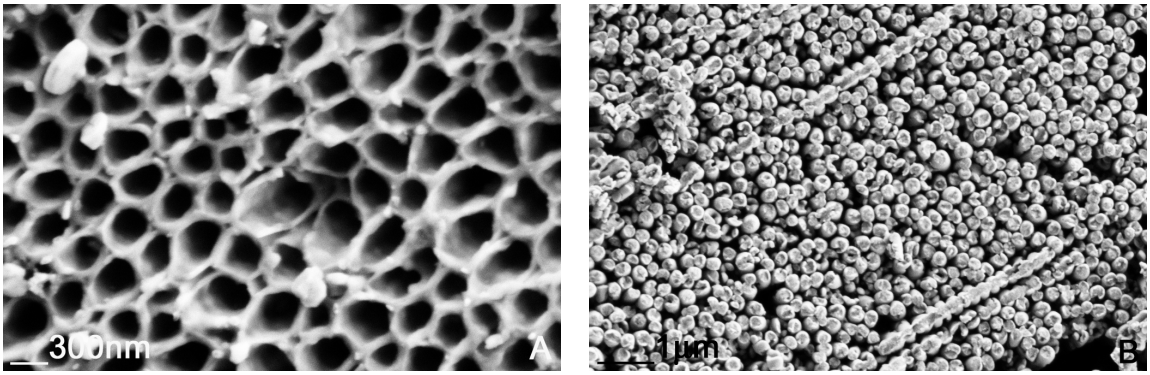

Figure 4.31 SEM images of PEDOT nanopipes with (A) open ends (B) close ends

SEM imaging confirmed the effect of membrane pore type on the shapes of synthesized PEDOT nanopipes. If membranes composed of hexagonally-etched pore sizes are used for the synthesis of these PEDOT nanopipes, resulting pipes could organize themselves by packing hexagonally (Figure 4.32A and 4.32B). When membrane pores are all round, cylindrical type PEDOT nanopipes could be aligned (Figure 4.28B and Figure 4.31).

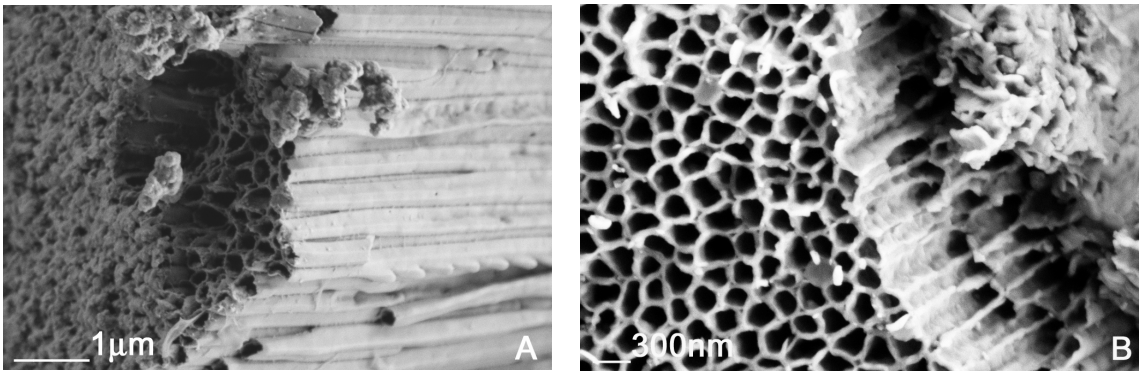

Figure 4.32 Hexagonal packing behaviour of PEDOT nanopipes

When it was focused on synthesized PEDOT nanopipes using hexagonal pore units by magnifying on a bunch of pipes in the image below, hexagonally ordered thick walls of pipes were available to be clarified (Figure 4.33).

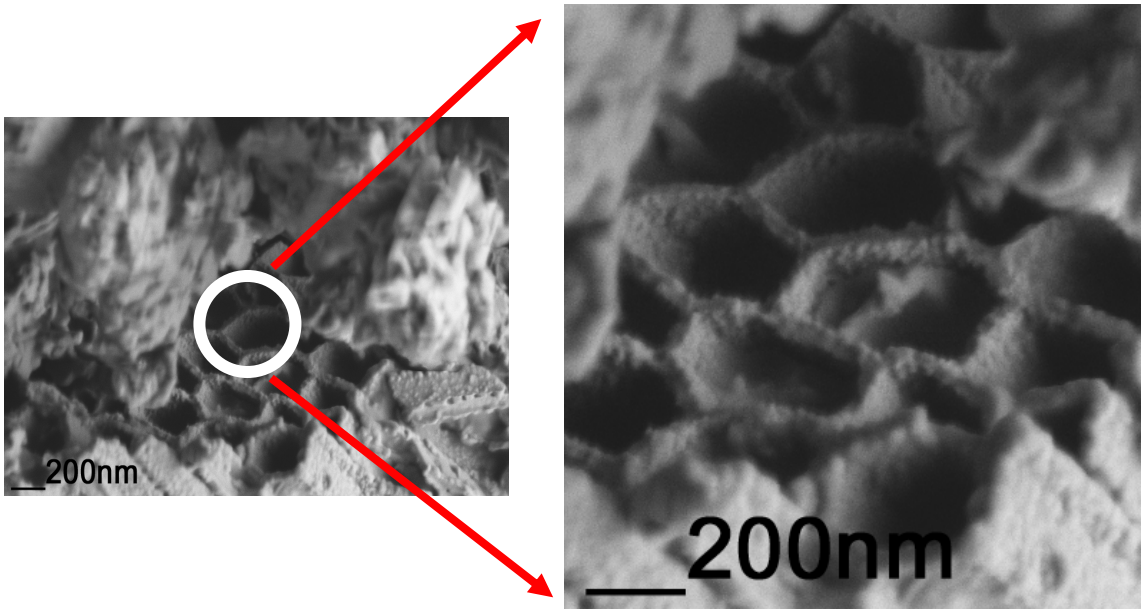

Figure 4.33 SEM image zoomed in to illustrate a more clear PEDOT nanopipes in hexagonal shapes

Alignment of PEDOT nanopipes with well-defined structures was a subject of fundamental as well as practical importance. In this respect, control of pipe diameters as well as their geometrical shapes was desirable. Upon exploring such perfect systems, it was intended to decrease pipe diameters, in theory, by using alumina membranes with smaller pore sizes. Such a purpose, membranes with pore sizes of 0.1 µm and 0.02 µm were applied to the same experimental procedure. SEM images of these synthesized PEDOT nanopipes resulted that diameter range was decreased to 160 nm at least with 0.1 µm pore sized alumina membrane. However, use of alumina membrane including 0.02 µm pore sizes produced pipes with diameters in a range of 88 nm to 300 nm. One example of these analyses is given in Figure 4.34. As a result of various arbitrary measurements from SEM images, it was concluded that diameter of inner hollow structure was ca. 180 nm with an outside pipe diameter of ca. 270 nm. For this case, wall thickness of this pipe was ca. 90 nm, which was also another indication for hollow type PEDOT nanopipes.

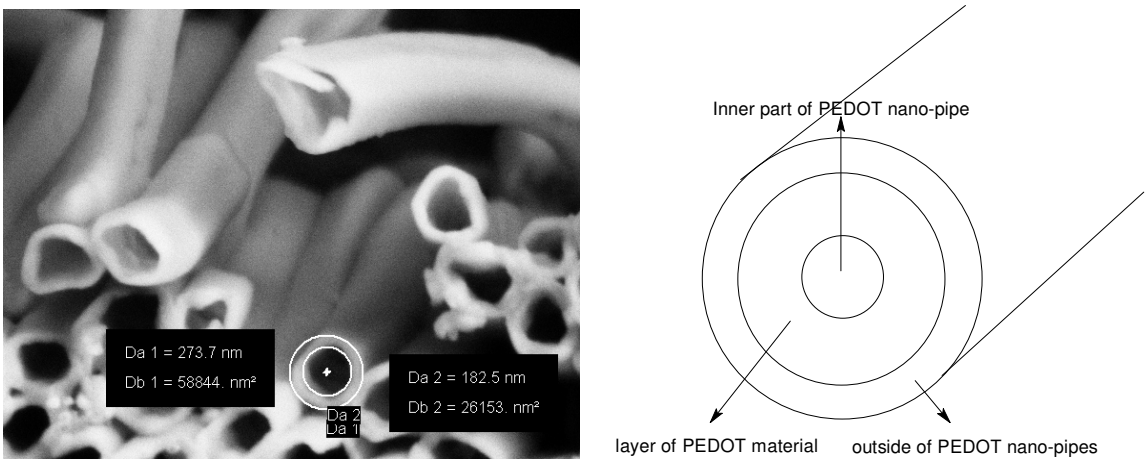

Figure 4.34 (A) SEM picture illustrating diameter measurement of arbitrarily chosen PEDOT nanopipe (B) including both outside and inside diameters of hallow tubules

SEM images of resulting template synthesized PEDOT nanopipes within a success after the optimization of reaction parameters are given in Figure 4.35. Effective polymerization of EDOT produced well-aligned PEDOT tubule like nanostructures after dissolution of alumina membrane. Figure 4.35 depicts SEM images of 1D alignment of PEDOT nanopipes in groups or standing alone in four different magnifications.

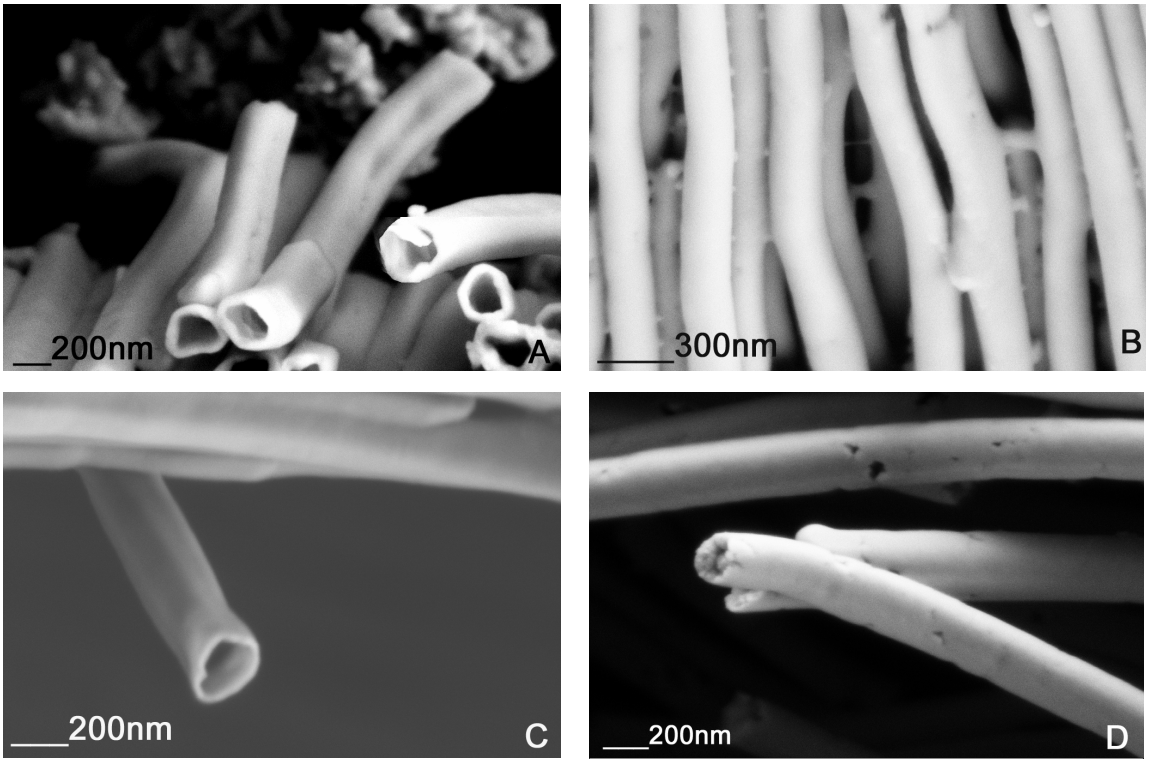

Figure 4.35 SEM pictures of PEDOT 1D nanopipes as hallow like tubules in four different magnifications

4.5 Results of FTIR-ATR Measurements

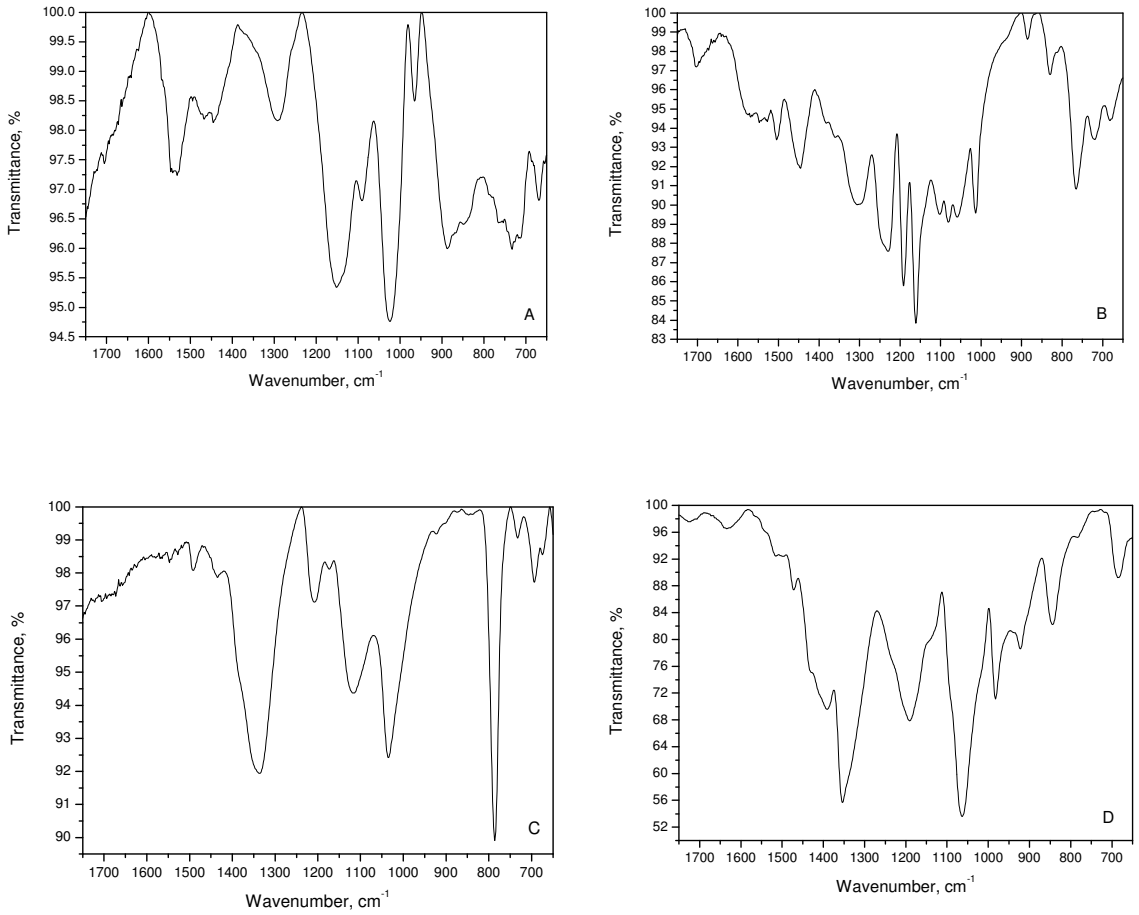

Figure 4.36 FTIR-ATR spectra of (A) PPy, (B) P(NMPy), (C) PTh and (D) PEDOT nanotubules in a range of 1750-600 cm^{-1}

Figure 4.36 demonstrates FTIR-ATR spectra of PPy, P(NMPy), PTh and PEDOT samples including nanotubules prepared by template synthesis. Based on the fact that polar solvents reduce the frequency of absorption, aforementioned peaks were all red-shifted as acetonitrile and water were used. In addition, in all these spectra, blue-shifts (shifting to left) and red shifts (shifting to right) of peaks could be observed, which may be dependent on Cl^- anion and ClO_4^- incorporation of these successfully synthesized

tubule-shaped polymers. In PTh and PEDOT molecular chains, ClO_4^- ions are inserted into a certain number of Th or EDOT units. The characteristic peak of ClO_4^- can be seen at around 1100 cm^{-1} in Figure 4.36C and 4.36D, which proves successful ClO_4^- incorporation. Other vibrational modes of each peak in all spectra are given below in details.

4.5.1 FTIR-ATR Studies of PPy Nanotubules

An overlapping of N-H band due to ring stretchings was assigned to a broad region of 1480-1540 cm^{-1} with a defined small peak at around 1540 cm^{-1}, where N-H wagging vibrations could additionally be observed [138]. This red shift of wavenumber of the N-H band resulted from N-H bonds on Pyrrole ring, which P(NMPy) does not have. The conjugated C=C stretchings of pyrrole ring at around 1100 cm^{-1} were splitted into three peaks (1050 cm^{-1}, 1080 cm^{-1}, 1150 cm^{-1}), which also corresponds to C-H in-plane vibrations [139]. An overlapping characteristic of N-H bending vibration in pyrrole ring absorbs broadly around 1650-1700 cm^{-1}. This situation was usually observed at 1680 cm^{-1} P(NMPy) has no such characteristic peak in this range as the N-H stretchings could not be observed due to aliphatic methyl (CH_3) groups attached to the nitrogen atom. There also exist two shoulders of =C-N stretching vibrations at1150 cm^{-1} and 1250 cm^{-1}. The peaks at 830 cm^{-1} and 710 cm^{-1} are undoubtedly attributable to the out-of-plane deformation of the C-H bond vibrations in the heterocyclic ring. The strongest N-H stretchings could be observed at around 1300 cm^{-1}.

4.5.2 FTIR-ATR Studies of P(NMPy) Nanotubules

Peaks at around 1700 cm^{-1} are characteristics of the stretching vibration of carbonyl groups, which belongs to CO_3^{2-} groups of inefficient dissolving of PC membrane. There is another possibility for these carbonyl groups, which may exist at all P(NMPy) prepared from aqueous medium. The OH groups are introduced in the ring by the nucleophilic attack of water molecules on cation radicals resulting carbonyl groups

by keto-enol tautomerism [140,141]. Bands in the range from 1000 cm^{-1} to 1100 cm^{-1} originate from ring C-H out-of-plane bendings. Peak at approximately 1160 cm^{-1} could correspond to ring out-of-plane bendings of C=C-N, C=C-C and C-N-C. In addition, ring C-H out-of-plane bendings could be observed in the range of 600 cm^{-1} to 800 cm^{-1}. Vibration at approximately 1450 cm^{-1} may originate from ring C-N, C=C, C=C-N, C=C-C and C-H out-of-plane bendings. The characteristic bands of P(NMPy) samples were consistent with those in [141], the C=C and C-C in-plane bendings in a broad range of 1500-1600 cm^{-1} and the C-C in-plane bending vibrations at 1300 cm^{-1}.

4.5.3 FTIR-ATR Studies of PTh Nanotubules

The vibration modes from the C=C stretchings in the thiophene ring can be seen at approximately 1350 cm^{-1}, C=C weak conjugated or C-C stretchings at around 1500 cm^{-1}, bands of C-S stretchings in the thiophene ring 600 cm^{-1} to 800 cm^{-1} [138].

4.5.4 FTIR-ATR Studies of PEDOT Nanotubules

Bands ascribable to CH_2 twisting and wagging vibrations at 1400 cm^{-1}, C=C stretchings at 1350 cm^{-1}, small peaks of C=C weak conjugated or C-C stretchings were observed in the range of 1400 cm^{-1} to 1600 cm^{-1} [138]. Characteristic bands of C-S stretchings in the thiophene ring correspond to the peaks in the range from 1000 cm^{-1} to 600 cm^{-1}. The bands at approximately 1050 cm^{-1} and 1180 cm^{-1} are assigned to the stretching modes of the C-O-C bonds in ethylene oxide groups [142]. As well, vibration at around 900 cm^{-1} is due to the ethylenedioxy ring deformation mode.

4.6 Electrochemistry Results

Electroactivity of P(NMPy) nanotubules as solid particles were characterized with cyclic voltammetry between -1.75 and 1.75 V (vs. Ag/Ag^+ reference electrode) at a scan rate of 150 mV/s in 0.1 M TBAP/MeCN. A very small amount of template-synthesized P(NMPy) material was attached onto the surface of a Pt button electrode including a little amount of silver paint. After half an hour, the characterization was done using multi-scan function under argon environment. The cyclic voltammograms were obtained for both silver paint itself on a Pt button electrode and then by sticking P(NMPy) nanotubules on this Pt button electrode. Overlayed cyclic voltammograms of P(NMPy) nanotubules and silver paint are shown in Figure 4.37. The existence of anodic and cathodic peak currents gave information about the electroactivity of P(NMPy) nanotubules compared to cyclic voltammogram of the silver paint as a background. This figure is an evidence that template-synthesized conducting polymers will produce electroactive materials.

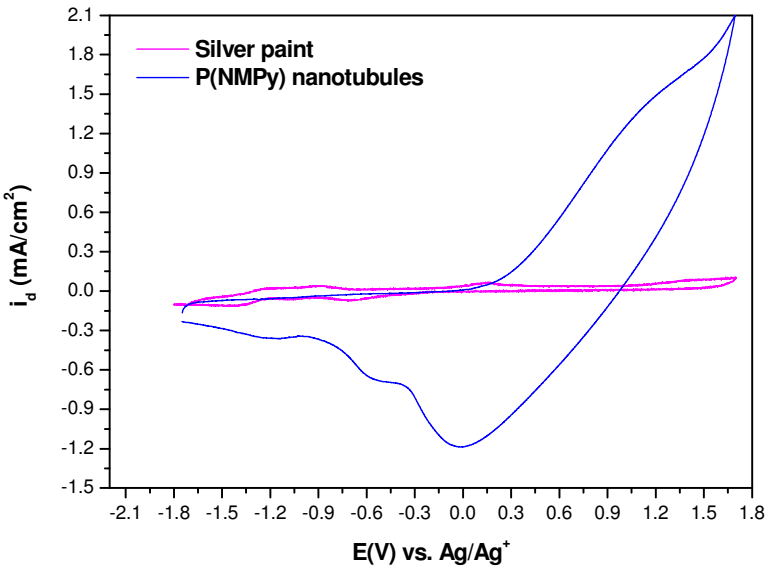

Figure 4.37 Cyclic voltammetry obtained during characterization of both silver paint and silver paint with P(NMPy) nanotubules on top of it in 0.1 M TBAP/MeCN at a scan rate of 150 mV/s.

CONCLUSIONS

A preliminary objective of this study was to envisage highly-surfaced, nano-scaled, electroactive, conductive polymers for supercapacitor applications, which was reasonably fulfilled with two useful synthetic approaches. Both interfacial oxidative polymerization method and template synthesis techniques were successfully applied to obtain PPy nano-networks and PPy, P(NMPy), PTh and PEDOT nanotubules. The scanning electron micrographs showed that both nano-networks and nanotubules of conducting polymers could be arranged in a diameter range of ca. 80-350 nm. Existence of a surfactant in an interfacial oxidative synthesis environment resulted in PPy nanofibers as a network structure. SEM images of potentiostatically deposited PPy in the presence of a surfactant produced a morphology of PPy that had knitting type structures due to the electrostatic interactions between polymer backbone and surfactant.

High regularity of PPy and P(NMPy) nanotubules differentiates in build of fibrillar structures when compared with PTh and PEDOT nanotubules in 1D. Although their appearance are similar, P(NMPy) nanotubules are not as much uniform as PPy nanotubules. However, below and upper films that support nanotubules of P(NMPy) have much more smooth surfaces than those of PPy nanotubules. The smoothness of PEDOT bucky-like structures is similar to PTh case and they have mostly cylindrical, freely separated structures like PThs.

General overview of PTh nanotubules indicates similar arrangement in 1D like in PPy and P(NMPy) cases. Since one side of PTh nanostructures are not protected by a layer, dispersity in layer arrangement may decrease stiffness of PTh nanotubules. Therefore, PTh nanotubules show more free-standing property as a result of their self-dispersion with the lackness of one end coating. As well, PTh nanotubules have smoother surfaces but they are as delicate as pyrrole derivated nanostructures. Although

PTh nanotubules lack in having two end films, this does not alter their adjustment in 1D. In this respect, voids among fibers are clearly observable that large gaps may increase surface area as the proximity of one fiber to another is not so little. In comparison of all nanostructures, PEDOT nanopipes indicate the most dissipative behaviour among other conducting polymers studied.

PPy and P(NMPy) nanotubules yield more densed nanostructures as arrays with small holes among their fibers while those PPy and PEDOT nanostructures indicate more dilution in self-organization. Distribution of PTh nanotubules is likely to P(NMPy) environment, which tells inhomogenity in their orientations. Since one ends of PTh and PEDOT's nanotubules are open-sided, their tendency to stand freely should be much more than that of PPy and P(NMPy) nanotubules. Additionally, PEDOT nanopipes may have more unoccupied spaces among them that increases the surface area of the whole material or not if they are densely formed.

Taking geometrical structures of all PEDOT nanopipes themselves into account, some pipes may be self-structured as hollow-type nanostructures, some can shape as hexagonal arrays. Moreover, those hollow-type PEDOT nanopipes should be categorized as: well-ordered elongated, irregularly ordered structures. Nevertheless, all types of PEDOT nanopipes have smooth surfaces. Though, PPy, P(NMPy) nanotubules and PTh nanotubules are more cylindrical in their structures.

Other than SEM micrographs, FTIR-ATR analyses also confirmed that desired polymer structures in nano-scales could be clearly reached and engineered. More importantly, characterization of P(NMPy) nanotubules and PPy nano-networks with cyclic voltammetry indicated that synthesized conducting polymers using interfacial and template methods are electroactive, which revealed that these materials are promising for supercapacitor applications.

REFERENCES

[1] Shirakawa, H., Louis, E., McDiarmid, A., Chiang, C., Heeger, A. J. Synthesis electrically conducting organic polymers-halogen derivatives of of polyacetylene, (CH)X. *J. Chem. Soc., Chem. Commun.* 1977, 578.

[2] Diaz, A. F. and Castillo, J. I. A polymer electrode with variable conductivity-polypyrrole. *J. Chem. Soc., Chem. Commun.* 1980, 397.

[3] Ivory, D. M., Miller, G. G., Sowa, J. M., Shacklette, L. W., Chance, R. R., Baughman, R. H. Highly conducting charge-transfer complexes of poly(p-phenylene). *J. Chem. Phys.* 1979, 71, 1506.

[4] Wnek, G. E., Chien, J. C. W., Karasz, F. E., Lillja, C. P. Electrically conducting derivative of poly(*p*-phenylene vinylene). *Polymer.* 1979, 20, 1441.

[5] Rabolt, J. F., Clarke, T. C., Kanazawa, K. K., Reynolds, J. R., Street, G. B. Organic metals: Polyparaphenylene sulfide hexafluoroarsenate. *J. Chem. Soc., Chem. Commun.*, 1980, 347.

[6] Diaz, A. F., Logan, J. A. Electroactive polyaniline films. *J. Electroanal. Chem.* 1980, 111, 111.

[7] Tourillon, G., Garnier, F. New electrochemically generated organic conducting polymers. *J. Electroanal. Chem.* 1981, 135, 173.

[8] Guenther, H., Bezoari, M. D., Kovacic, P., Gronowitz, S., Hoernfeldt, A. B. Conductivity of doped poly(2,5-selenienylene). *J. Polym. Sci., Polym. Lett. Ed.* 1984, 22, 65.

[9] Bargon, J., Mohmand, S., Waltman, R. Polyazulene, a member of a new class of polymers. *J. Mol. Cryst. Liq. Cryst.* 1983, 93, 279.

[10] Roncali, J. Conjugated poly(thiophenes): synthesis, functionalization and applications. *Chem. Rev.* 1992, 92, 711.

[11] Science and Applications of Conducting Polymers (Eds: Salaneck, W. R., Clark, D. T., Samuelsen, E. J.), Norway 1990.

[12] Paoli, M. D., Gazotti, W.A. Conductive polymer blends: preparation, properties and applications. *Macromol. Symp.* 2002, 189, 83.

[13] Handbook of Conducting Polymers, 2nd ed. (Eds: Skotheim, T., Reynolds, J. R., Elsenbaumer, R. L.), Marcel Dekker, New York 1997.

[14] Garnier, F. Functionalized conducting polymers-towards intelligent materials. *Adv. Mater.* 1989, 4, 117.

[15] Molecular Engineering of π-Conjugated Polymers (Reddinger, J. R., Reynolds, J. R.), Berlin Heildelberg 1999.

[16] Cho, S. I., Choi, D. H., Kim, S.-H., Lee, S. B., Electrochemical Synthesis and Fast Electrochromics of Poly(3,4-ethylenedioxythiophene) Nanotubes in Flexible Substrate. *Chem. Mater.* 2005, 17, 4564.

[17] (a) Gosch, J., Electronics, July 9, 1987, p. 41. Lithium-Polymer Knopfzelle 2025 product information sheet. H. Naarmann, BASF Kunststoffe, "Forschung und Entwicklung", Nov. 1986, p. 40. D. Naegele, R. Bittihn, Solid State Ionics 1988, 983, 28. (b) Hostaphan Priliminary data sheet (June, 1992). K. –H. Kochem, H. – U. Ter Meer, H. Millauer, Kunststoffe 1992, 82, 575. Kunststoffe Ger. Plast. 1992, 82, 13.

[18] Sanghvi, A. B., Miller, K. P.-H., Belcher, A. M., Schmidt, C. E. Biomaterials functionalization using a novel peptide that selectively binds to a conducting polymer. *Nat. Mater.* 2005, 4, 496.

[19] Johnson, B. J. S., Wolf, J. H., Zalusky, A. S., Hillmyer, M. A. Template syntheses of polypyrrole nanowires and CdS nanoparticles in porous polymer monoliths. *Chem. Mater.* 2004, 16, 2909.

[20] (a) Yang, H., Ozin, G. A., Kresge, C. T. The role of defects in the formation of mesoporous silica fibers, films, and curved shapes. *Adv. Mater.* 1998, 10, 883. (b) Shim, M., Guyot-Sionnest, P. Organic-capped ZnO nanocrystals: Synthesis and n-type character. *J. Am. Chem. Soc.* 2001, 123, 11651.

[21] An, K. H., Kim, W. S., Park, Y. S., Choi, Y. C., Lee, S. M., Chung, D. C., Bae, D. J., Lim, S. C., Lee, Y. H. Supercapacitors using single-walled carbon nanotube electrodes. *Adv. Mater.* 2001, 13, 497.

[22] Shukla, A. K., Sampath, S., Vijayamohanan, K. Electrochemical supercapacitors: Energy storage beyond batteries. *Curr. Sci. India.* 79, No. 12, 2000.

[23] Hughes, M., Chen, G. Z., Shaffer, M. S. P., Fray, D. J., Windle, A. H. Electrochemical capacitance of a nanoporous composite of carbon nanotubes and polypyrrole. *Chem. Mater.* 2002, 14, 1610.

[24] Ingram, M. D., Staesche, H., Ryder, K.S. 'Ladder-doped' polypyrrole: a possible electrode material for inclusion in electrochemical supercapacitors? *J. Power Sources.* 2004, 129 107.

[25] Ingrama, M. D., Staeschea, H., Ryderb, K. S. 'Activated' polypyrrole electrodes for high-power supercapacitor applications. *Solid State Ionics.* 2004, 169, 51.

[26] Heywang, G., Jonas, F. Poly(alkylenedioxythiophene)s-new, very stable conducting polymers. *Adv. Mater.* 1992, 4, 116.

[27] Wu, A., Kolla, H., Manohar, S. K. Chemical synthesis of highly conducting polypyrrole nanofiber film. *Macromolecules*. 2005, 38, 7873.

[28] Grunden, B. and Iroh, J. O. Formation of graphite fibre-polypyrrole coatings by aqueous electrochemical polymerization. *Polymer.* 1995, 36, 559.

[29] Zhou, M. and Heinze. Electropolymerization of pyrrole and electrochemical study of polypyrrole: 1. Evidence for structural diversity of polypyrrole. J. *Electrochim. Acta.* 1999, 44, 1733.

[30] Ramanathan, K., Bangar, M. A., Yun, M., Chen, W., Myung, N. V., Mulchandani, A. Bioaffinity sensing using biologically functionalized conducting-polymer nanowire. *J. Am. Chem. Soc.* 2005, 127, 496.

[31] Motheo, A. J., Santos, J. R., Venancio, E. C., Mattoso, L. H. C. Influence of different types of acidic dopant on the electrodeposition and properties of polyaniline films. *Polymer.* 1998, 39, 6977.

[32] Rodriguez, J., Grande, H. J., Otero, T. F in "Handbook of Organic Conductive Molecules and Polymers" edited by H. S. Nalwa (John Wiley & Sons, New York, 1997).

[33] Sakkopoulos, S., Vitoratos, E., Dalas, E. Conductivity degradation due to thermal aging in conducting polyaniline and polypyrrole. *Synth Met*. 1998, 92, 63.

[34] Simonet, J., Berhelot, J. R. Electrochemistry: A technique to form, to modify and to characterize organic conducting polymers. *Prog. Solid State Ch.* 1991, 21, 1.

[35] Diaz, A. F., Bargon, J. in "Handbook of Conducting Polymers," edited by T. A. Skotheim (Dekker, New York, 1986) Vol. I, p. 81.

[36] (a) Bjorklund, R. B. and Liedberg, B. Electrically conducting composites of colloidal polypyrrole and methylcellulose. *J. Chem. Soc. Chem. Commun.* 1986, 1293. (b) Sarac, A. S., Sonmez, G., Ustamehmetoglu, B., Mustafaev, M. I., Water-soluble polypyrroles by matrix polymerization: Interpolymer complexes. *J. Polym. Sci. Part A: Polym. Chem.* 1996, 35, 1255.

[37] Sonmez, G., Schottland, P., Zong, K., Reynolds, J.R. Highly transmissive and conductive poly[(3,4-alkylenedioxy)pyrrole-2,5-diyl] (PXDOP) films prepared by air or transition metal catalyzed chemical oxidation. *J. Mater. Chem*. 2001,11, 289.

[38] Orgzall, I., Lorenz, B., Ting, S. T., Hor, P. H., Menon, V. P., Martin, C. R., Hochheimer, H. D. Thermopower and high-pressure electrical conductivity measurements of template synthesized polypyrrole. *Phys. Rev. B*. 1996, 54, 16654.

[39] Oh, K. W., Park, H. J., Kim, S. H. Electrical property and stability of electrochemically synthesized polypyrrole films. *J. Appl. Polym. Sci*. 2004, 91, 3659.

[40] Arbizzani, C., Mastragostino, M., Meneghello, L., Paraventi, R. Electronically conducting polymers and activated carbon: Electrode materials in supercapacitor technology. *Adv. Mater.* 1996, 8, 331.

[41] Kros, A., Nolte, R. J. M., Sommerdijk, N. A. J. M. Conducting polymers with confined dimensions: Track-etch membranes for amperometric biosensor applications. *Adv. Mater.* 2002, 14, 1779.

[42] Ramanathan, K., Sundaresan, N. S., Malhotra, B. D. Ion exchanged polypyrrole-based glucose biosensor: Enhanced loading and response. *Electroanal.* 1995, 7, 579.

[43] An, K. H., Jeong, S. Y., Hwang, H. R., Lee, Y. H. Enhanced sensitivity of a gas sensor incorporating single-walled carbon nanotube-polypyrrole nanocomposites . *Adv. Mater.* 2004, 16, 1005.

[44] Hosono, K., Matsubara, I., Murayama, N., Woosuck, S., Izu, N. Synthesis of polypyrrole/MoO_3 hybrid thin films and their volatile organic compound gas-sensing properties. *Chem. Mater.* 2005, 17, 349.

[45] Kros, A., Linhardt, J. G., Bowman, H. K., Tirrell, D. A. From giant vesicles to filaments and wires: Templates for conducting polymers. *Adv. Mater.* 2004, 16, 723.

[46] Guo, R., Li, G., Zhang, W., Shen, G., Shen, D. Superlong polypyrrole nanowires aligned within ordered mesoporous silica channels. *ChemPhysChem.* 2005, 6, 2025.

[47] Jager, E. W. H., Inganäs, O., Lundström, I. Perpendicular actuation with individually controlled polymer microactuators. *Adv. Mater.* 2001, 13, 76.

[48] Faverolle, F., Attias, A. J., Bloch, B., Audebert, P., Andrieux, C. P. Highly conducting and strongly adhering polypyrrole coating layers deposited on glass substrates by a chemical process. *Chem. Mater.* 1998, 10, 740.

[49] Gregory, R. V., Kimbrell, W. C., Kuhn, H. H. Conductive textiles. *Synth. Met.* 1989, 28, C823.

[50] White, A., Slade, R. Carbon papers with conductive polymer coatings for use in solid-state supercapacitors. *Macromol. Symp.* 2004, 212, 275.

[51] Rowley, N. M., Mortimer, R. J. New electrochromic materials. *Science Progress*. 2002, 85, 243.

[52] Sides, C. R. and Martin, C. R. Nanostructured electrodes and the low-temperature performance of Li-ion batteries. *Adv. Mater.* 2005, 17, 1.

[53] Leclerc, M. Optical and electrochemical transducers based on functionalized conjugated polymers. *Adv. Mater.* 1999, 11, 1491.

[54] Hermsdorf, N., Stamm, M., Forster, S., Cunis, S., Funari, S. S., Gehrke, R., Muller-Buschbaum, P. Self-Supported particle-track-etched polycarbonate membranes as templates for cylindrical polypyrrole nanotubes and nanowires: An x-ray scattering and scanning force microscopy investigation. *Langmuir.* 2005, 21, 11987.

[55] Reece, D. A., Pringle, J. M., Ralph, S. F., Wallace, G. G. Autopolymerization of pyrrole in the presence of a host/guest calixarene. *Macromolecules.* 2005, 38, 1616.

[56] Pernaut, J. M., Reynolds, J. R. Use of conducting electroactive polymers for drug delivery and sensing of bioactive molecules. A redox chemistry approach. *J. Phys. Chem. B.* 2000, 104, 4080.

[57] Hien, N. T. L., Garcia, B., Pailleret, A., Deslouis, C. Role of doping ions in the corrosion protection of iron by polypyrrole films. *Electrochim. Acta.* 2005, 50, 1747.

[58] Iroh, J. O. and Su, W. Adhesion of electrochemically formed polypyrrole coatings to low carbon steel. *J. Appl. Polym. Sci.* 2002, 85, 2757.

[59] Zhou, X. J., Leung, K. T. Modification of electronic structure of mesoscopic perchlorate-doped polypyrrole films by ion irradiation. *Macromolecules.* 2003, 36, 2882.

[60] Mecerreyes, D., Alvaro, V., Cantero, I., Bengoetxea, M., Calvo, P. A., Grande, H., Rodriguez, J., Pomposo, J. A. Low surface energy conducting polypyrrole doped with a fluorinated counterion. *Adv. Mater.* 2002, 14, 749.

[61] Masalles, C., Llop, J., Viñas, C., Teixidor, F. Extraordinary overoxidation resistance increase in self-doped polypyrroles by using non-conventional low charge-density anions. *Adv. Mater.* 2002, 14, 826.

[62] Ikegame, M., Tajima, K., Aida, T. Template synthesis of polypyrrole nanofibers insulated within one-dimensional silicate channels: Hexagonal versus lamellar for recombination of polarons into bipolarons. *Angew. Chem., Int. Ed.* 2003, 42, 2154.

[63] He, J., Chen, W., Xu, N., Li, L., Li, X., Xue, G. SERS studies on the ordered structure of the surface of polypyrrole nanotubules. *Appl. Surf. Sci.* 2004, 221, 87.

[64] Martin, C. R. Nanomaterials- A membrane-based synthetic approach. *Science.* 1994, 266, 1961.

[65] Mishra, S. P., Krishnamoorthy, K., Sahoo, R., Kumar, A. Synthesis and characterization of monosubstituted and disubstituted poly(3,4-propylenedioxythiophene) derivatives with high electrochromic contrast in the visible region. *J. Polym. Sci. Part A: Polym. Chem.* 2005, 43, 419.

[66] Jonas, F., Heywang, G., Schmidtberg, W., Heinze, J. Dietrich, M. EP 339 (BAYER AG), Prior: 1988-04-22.

[67] Argun, A. A., Berard, M., Aubert, P. H., Reynolds, J. R. Back-side electrical contacts for patterned electrochromic devices on porous substrates. *Adv. Mater.* 2005, 17, 422.

[68] Jang, J., Chang, M., Yoon, H. Chemical sensors based on highly conductive poly(3,4-ethylene-dioxythiophene) nanorods. *Adv. Mater.* 2005, 17, 1616.

[69] Zhang, F., Nyberg, T., Inganäs, O. Conducting polymer nanowires and nanodots made with soft lithography. *Nano Lett.* 2002, 2, 1373.

[70] Meng, H., Perepichka, D.F., Wudl, F. Facile solid-state synthesis of highly conducting poly(ethylenedioxythiophene). *Angew. Chem.* 2003, 115, 682.

[71] Doherty, W. J., Armstrong, N. R., Saavedra, S. S. Conducting polymer growth in porous sol-gel thin films: Formation of nanoelectrode arrays and mediated electron transfer to sequestered macromolecules. *Chem. Mater.* 2005, 17, 3652.

[72] Li, X., Lu, M., Li, H. Electrochemical copolymerization of pyrrole and thiophene nanofibrils using template-synthesis method. *J. Appl. Polym. Sci.* 2002, 86, 2403.

[73] Duvail, J.L., Rétho, P., Garreau, S., Louarn, G., Godon, C., Demoustier-Champagne, S. Transport and vibrational properties of poly(3,4-ethylenedioxythiophene) nanofibers. *Synth. Met.* 2002, 131, 123.

[74] Cho, S. I., Kwon, W. J., Choi, S., Kim, P., Park, S., Kim, J., Son, S. J., Xiao, R., Kim, S., Lee, S. B. Nanotube-based ultrafast electrochromic display. *Adv. Mater.* 2005, 17, 171.

[75] Kim, B.H., Park, D.H., Joo, J., Yu, S.G., Lee, S.H. Synthesis, characteristics, and field emission of doped and de-doped polypyrrole, polyaniline, poly(3,4-ethylenedioxythiophene) nanotubes and nanowires. Synth. Met., 2005, 150, 279.

[76] Joo, J., Kim, B. H., Park, D. H., Kim, H. S., Seo, D. S., Shim, J. H., Lee, S. J., Ryu, K. S., Kim, K., Jin, J. -I., Lee, T. J., Lee, C. J. Fabrication and applications of conducting polymer nanotube, nanowire, nanohole, and double wall nanotube. *Synth. Met.* 2005, 153, 313.

[77] Kros, A., Van Hövell, S. W. F. M., Sommerdijk, N. A. J. M., Nolte, R. J. M. Poly(3,4-ethylenedioxythiophene)-based glucose biosensors. *Adv. Mater.* 2001, 13, 1555.

[78] Trivedi, D.C. in: H. S. Nalwa (Ed.), Handbook of Organic Conductive Molecules and Polymers, John Wiley & Sons, New York, 1997.

[79] Groenendaal, L. B., Zotti, G., Aubert, P., Waybright, S. M., Reynolds, J. R. *Adv. Mater.* 2003, 15, 855.

[80] Zhang, X., Chan-Yu-King, R., Jose, A., Manohara, S. K. Nanofibers of polyaniline synthesized by interfacial polymerization. *Synth. Met.* 2004, 145, 23.

[81] Gao, H., Jiang, T., Han, B., Wang, Y., Du, J., Liu, Z., Zhang, J. Aqueous/ionic liquid interfacial polymerization for preparing polyaniline nanoparticles. *Polymer*. 2004, 45, 3017.

[82] Lu, Y., Shi, G., Li, C., Liang, Y. Thin polypyrrole films prepared by chemical oxidative polymerization. *J. Appl. Polym. Sci.* 1998, 70, 2169.

[83] Zhang, X. and Manohar, S. K. Bulk Synthesis of Polypyrrole Nanofibers by a Seeding Approach. *J. Am. Chem. Soc.* 2004, 126, 12714.

[84] Yang, Y., Liu, J., Wan, M. High-yield production of quasi-aligned carbon nanotubes by catalytic decomposition of benzene. *Nanotechnology.* 2002, 13, 771.

[85] Tai, Y.-L., Teng, H. Template synthesis and electrochemical characterization of nickel-based tubule electrode arrays. *Chem. Mater.* 2004, 16, 338.

[86] Hou, S., Harrell, C. C., Trofin, L., Kohli, P., Martin, C. R. Layer-by-Layer nanotube template synthesis. *J. Am. Chem. Soc.* 2004, 126, 5674.

[87] Kohli, P., Wirtz, M., Martin, C. R. Nanotube membrane based biosensors. *Electroanal.* 2004, 16, 9.

[88] Wallace, G. G., Innis, P. C. Inherently conducting polymer nanostructures. *J. Nanosci. Nanotech.* 2002, 2, 441.

[89] Xia, Y., Yang, P., Sun, Y., Wu, Y., Mayers, B., Gates, B., Yin, Y., Kim, F., Yan, H. One-Dimensional nanostructures: Synthesis, characterization, and applications. *Adv. Mater.* 2003, 15, 353.

[90] Martin, C. R., Penner, R. M., Van Dyke, L. S. "Electrochemical investigation of electronically conductive polymers" in Bergbreiter, D. E.; Martin C. R., Eds. Functional Polymers, Plenum Press, New York, 1989 pp. 119-139.

[91] (a) Wu, C. G. and Bein, T. Conducting polyaniline filaments in a mesoporous channel host. *Science.* 1994, 264, 1757. (b) Martin, C. R. Template synthesis of electronically conductive polymer nanostructures. *Acc. Chem. Res.* 1995, 28, 61. (c) Parthasarathy, R. V. and Martin, C. R. Synthesis of polymeric microcapsule arrays and their use for enzyme immobilization. *Nature.* 1994, 369, 298.

[92] (a) Jang, J. and Yoon, H. Facile fabrication of polypyrrole nanotubes using reverse microemulsion polymerization. *Chem. Commun.* 2003, (6), 720. (b) Huang, K. and Wan, M. Self-assembled polyaniline nanostructures with photoisomerization function. *Chem. Mater.* 2002, 14, 3486. (c) Zhang, L., Long, Y., Chen, Z., Wan, M. The effect of hydrogen bonding on self-assembled polyaniline nanostructures. *Adv. Funct. Mater.* 2004, 14, 693.

[93] Moon, J.-M., Wei, A. Uniform gold nanorod arrays from polyethylenimine-coated alumina templates. *J. Phys. Chem. B.* 2005, 109, 23336.

[94] Martin, C.R., Dyke, L. S. V., Cai, Z., Liang, W. Template synthesis of organic microtubules. *J. Am. Chem. Soc.* 1990, 112, 8976.

[95] Martin, C. R. Membrane-based synthesis of nanomaterials. *Chem. Mater.* 1996, 8, 1739.

[96] Marinakos, S. M., Shultz, D. A., Feldheim, D. L. Gold nanoparticles as templates for the synthesis of hollow nanometer-sized conductive polymer capsules. *Adv. Mater.* 1999, 11, 34.

[97] Mativetsky, J. M. and Datars, W. R. Properties of alumina membrane-templated polypyrrole nanostructures. *Solid State Commun.* 2002, 122, 151.

[98] Mativetsky, J. M. and Datars, W. R. Morphology and electrical properties of template-synthesized polypyrrole nanocylinders. *Physica B.* 2002, 324, 191.

[99] Dyke, L. S. V., Martin, C. R. Electrochemical investigations of electronically conductive polymers. 4. Controlling the supermolecular structure allows charge transport rates to be enhanced. *Langmuir.* 1990, 6, 1118.

[100] Rajesh, B., Thampi, K. R., Bonard, J. M., Xanthopoulos, N., Mathieu, H. J., Viswanathan, B. Template synthesis of conducting polymeric nanocones of poly(3-methylthiophene). *J. Phys. Chem. B.* 2004, 108, 10640.

[101] Cai, Z., Lei, J., Liang, W., Menon, V., Martin, C. R. Molecular and supermolecular origins of enhanced electric conductivity in template-synthesized polyheterocyclic fibrils. 1. Supermolecular effects. *Chem. Mater.* 1991, 3, 960.

[102] Hong, S., Zhu, J. Multiple ink nanolithography: Toward a multiple-pen nano-plotter. *Science*. 1999, 286, 523.

[103] Levenson, M. D. Welcome to the dev revolution. *Solid State Technol*. 1995, 38, 81.

[104] Harrell, C. C., Lee, S. B., Martin, C. R. Synthetic single-nanopore and nanotube membranes. *Anal. Chem.* 2003, 75, 6861.

[105] Hornyak, G. L., Patrissi, C. J., Martin, C. R. Fabrication, characterization, and optical properties of gold nanoparticle/porous alumina composites: The nonscattering maxwell-garnett limit. *J. Phys. Chem. B.* 1997, 101, 1548.

[106] Davis, M. E., Katz, A., Ahmad, W. R. Rational catalyst design via imprinted nanostructured materials. *Chem. Mater.* 1996, 8, 1820.

[107] Wang, H., Holmberg, B. A., Yan, Y. Synthesis of template-free zeolite nanocrystals by using in situ thermoreversible polymer hydrogels. *J. Am. Chem. Soc.* 2003, 125, 9928.

[108] Feldheim, D. L., Grabar, K. C., Natan, M. J., Mallouk, T. E. Electron transfer in self-assembled inorganic polyelectrolyte/metal nanoparticle heterostructures. *J. Am. Chem. Soc.* 1996, 118, 7640.

[109] Lu, G., Ai, S., Li, J. Layer-by-Layer assembly of human serum albumin and phospholipid nanotubes based on a template. *Langmuir.* 2005, 21, 1679.

[110] Sun, L., Crooks, R. M. Single Carbon Nanotube Membranes: A well-defined model for studying mass transport through nanoporous materials. *J. Am. Chem. Soc.* 2000, 122, 12340.

[111] Li, J., Stein, D., McMullan, C., Branton, D., Aziz, M. J., Golovchenko, J. A. Ion-beam sculpting at nanometer length scales. *Nature.* 2001, 412, 166.

[112] Martin, C. R., Nishizawa, M., Jirage, K., Kang, M. Investigations of the transport properties of gold nanotubule membranes. *J. Phys. Chem. B.* 2001, 73, 768.

[113] Kang, M., Martin, C. R. Investigations of potential-dependent fluxes of ionic permeates in gold nanotubule membranes prepared via the template method. *Langmuir*. 2001, 17, 2753.

[114] (a) Ozin, G. A. Nanochemistry: Synthesis in diminishing dimensions. *Adv. Mater.* 1992, 4, 612. (b) Davis, M. E., Saldarrige, C., Montes, C., Garces, J., Crowder, C. A molecular sieve with eighteen-membered rings. *Nature.* 1988, 331, 698.

[115] (a) Cepak, V. M., Hulteen, J. C., Che, G., Jirage, K. B., Lakshmi, B. B., Fisher, E. R., Martin, C. R. Chemical strategies for template syntheses of composite micro- and nanostructures. *Chem. Mater.* 1997, 9, 1065. (b) Pontifex, G. H., Zhang, P., Wang, Z., Haslett, T. L., Al-Mawlawi, D., Moskovits, M. Effect of inert supports for titanium dioxide loading on enhancement of photodecomposition rate of gaseous propionaldehyde**.** *J. Phys. Chem.* 1991, 95, 9989. (c) Almawlawi, D., Liu, C. Z., Moskovits, M. Nanowires formed in anodic oxide nanotemplates. *J. Mater. Res.* 1994, 9, 1014. (d) Zelenski, C. M., Dorhout, P. K. Template synthesis of near-monodisperse microscale nanofibers and nanotubules of MoS_2. *J. Am. Chem. Soc.* 1998, 120, 734.

[116] (a) Cao, G., Hong, H. -G., Mallouk, T. E. Layered metal phosphates and phosphonates: from crystals to monolayers. *Acc. Chem. Res.* 1992, 25, 420. (b) Cao, G., Rabenberg, L. K., Nunn, C. M., Mallouk, T. E. Formation of quantum-size semiconductor particles in a layered metal phosphonate host lattice. *Chem. Mater.* 1991, 3, 149. (c) Feldheim, D. L., Mallouk, T. E. Layer-by-Layer assembly and intercalation reactions of iron (III) and iron (II) alkanebisphosphonates on gold surfaces. *J. Chem. Soc., Chem. Commun.* 1996, 2591.

[117] (a) Fendler, J. H., Meldrum, F. C. The colloid chemical approach to nanostructured materials. *Adv. Mater.* 1995, 7, 607. (b) Fendler, J. H. Membrane-mimetic approach to advanced materials. *Adv. Polym. Sci.* 1994, 113, 1.

[118] (a) Mehrotra, V., Giannelis, E. P. Metal-insulator molecular multilayers of electroactive polymers: Intercalation of polyaniline in mica-type layered silicates. *Solid State Commun.* 1991, 77, 155. (b) Kleinfeld, E. R., Ferguson, G. S. Stepwise formation of multilayered nanostructural films from macromolecular precursors. *Science*. 1994, 265, 370. (c) Pyo, M., Reynolds, J. R. Potential dependent dual ion transport of conducting polymer: Redox polymer bilayers. *J. Phys. Chem.* 1995, 99, 8249. (d) Torres, W., Fox, M.A. Rectifying bi-layer electrodes: layered conducting polymers on platinum. *Chem. Mater.* 1990, 2, 306. (e) Araki, K., Wagner, M. J., Wrighton, M. S. Layer-by-Layer growth of electrostatically assembled multilayer porphyrin films. *Langmuir.* 1996, 12, 5393.

[119] Han, M. G. and Foulger, S.H. 1-Dimensional structures of poly(3,4-ethylenedioxythiophene) (PEDOT): a chemical route to tubes, rods, thimbles, and belts. *Chem. Commun.* 2005, 1, 3092.

[120] MacDiarmid, A. G. Nobel Lecture: "Synthetic metals": A novel role for organic polymers. *Rev. Mod. Phys.* 2001, 73, 701.

[121] Liu, J., Lin, Y., Liang, L., Voigt, J. A., Huber, D. L., Tian, Z. R., Coker, E., Mckenzie, B., Mcdermott, M. J. Templateless assembly of molecularly aligned conductive polymer nanowires: A new approach for oriented nanostructures. *Chem-Eur. J.* 2003, 9, 604.

[122] Goren, M., Lennox, R. B. Nanoscale polypyrrole patterns using block copolymer surface micelles as templates**.** *Nano Lett*. 2001, 1, 735.

[123] (a) Wang, D., Caruso, F. Fabrication of polyaniline inverse opals via templating ordered colloidal assemblies. *Adv. Mater.* 2001, 13, 350. (b) Cassagneau, T., Caruso, F. Semiconducting polymer inverse opals prepared by electropolymerization. *Adv. Mater.* 2002, 14, 34.

[124] (a) Jerome, C., Labaye, D., Bodart, I., Jerome, R. Electrosynthesis of polyacrylic/polypyrrole composites: Formation of polypyrrole wires. *Synth. Met.* 1999, 101, 3. (b) Jerome, C., Ierome, R. Electrochemical synthesis of polypyrrole nanowires. *Angew. Chem. Int. Ed.* 1998, 37, 2488.

[125] McCarthy, P. A., Huang, J., Yang, S. -Z., Wang, H. –L. Synthesis and characterization of water-soluble chiral conducting polymer nanocomposites. *Langmuir.* 2002, 18, 259.

[126] Suri, K., Annapoorni, S., Sakar, A. K., Tandon, R. P. Gas and humidity sensors based on iron oxide–polypyrrole nanocomposites. *Sensors and Actuat. B-Chem.* 2002, 81, 277.

[127] He, H., Zhu, J., Tao, J., Nagahara, L. A., Amlani, I., Tsui, R. A conducting polymer nanojunction switch. *J. Am.Chem. Soc.* 2001, 123, 7730.

[128] Demoustier-Champagne, S, Duchet, J, Legras, R. Chemical and electrochemical synthesis of polypyrrole nanotubules. *Synth. Met.* 1999, 101, 20.

[129] Fu, M., Zhu, Y., Tan, R., Shi, G. Aligned polythiophene micro- and nanotubules. *Adv. Mater.* 2001, 24, 1874.

[130] Kaiser, A. B. Systematic conductivity behavior in conducting polymers: effects of heterogeneous disorder. *Adv. Mater.* 2001, 13, 927.

[131] J. Huang, R. B. Kaner. A general chemical route to polyaniline nanofibers. *J. Am. Chem. Soc.* 2004, 126, 851.

[132] J. Huang, R. B. Kaner. Nanofiber formation in the chemical polymerization of aniline: A mechanistic study. *Angew. Chem.* 2004, 116, 5941.

[133] Acik, M., Baristiran, C., Sonmez, G. Highly-surfaced polypyrrole nano-networks and nanofibers. *J. Mater. Sci.* 2005, *in press.*

[134] Sonmez, G., Sarac, A. S. In situ spectroelectrochemistry and colorimetry of poly(pyrrole-acrylamide)s. *J. Mater. Sci.* 2002, 37, 4609.

[135] Martin, C. R. Template synthesis of polymeric and metal microtubules. *Adv. Mater.* 1991, 3, 457.

[136] J. Huang, S. Virgi, B. H. Weiller, R. B. Kaner. Polyaniline nanofibers: Facile synthesis and chemical sensors. *J. Am. Chem. Soc.* 2003, 125, 314.

[137] Soudan, P., Gaudet, J., Guay, D., Bélanger, D., Schulz, R. Electrochemical properties of ruthenium-based nanocrystalline materials as electrodes for supercapacitors. *Chem. Mater.* 2002, 14, 1210.

[138] He, C., Yang, C., Li, Y. Chemical synthesis of coral-like nanowires and nanowire networks of conducting polypyrrole. *Synth. Met.* 2003, 139, 539.

[139] Kumru, M. E., Springer, J., Sarac, A. S., Bismarck, A. Electrografting of thiophene, carbazole, pyrrole and their copolymers onto carbon fibers: electrokinetic measurements, surface composition and morphology. *Synth. Met*. 2001, 123, 391.

[140] Larraz, E., Redondo, M. I., Gonzaléz-Tejera, M. J., Raso, M. A., Tortajada, J., Sánchez de la Blanca, E., Garcia, M. V. Influence of pH on poly-(N-methylpyrrole) electrochemically synthesized in aqueous solution: an infrared study. *Synth. Met.* 2001, 122, 413.

[141] Redondo, M. I., Sánchez de la Blanca, E., Garcia, M. V., Raso, M. A., Tortajada, J., Gonzaléz-Tejera, M. J. FTIR study of chemically synthesized poly-(N-methylpyrrole). *Synth. Met.* 2001, 122, 431.

[142] Meng, H., Perepichka, D. F., Bendikov, M., Wudl, F., Pan, G. Z., Yu, W., Dong, W., Brown, S. Solid-State synthesis of a conducting polythiophene via an unprecedented heterocyclic coupling reaction. *J. Am. Chem. Soc.* 2003, 125, 15151.